UILU-ENG 87-3603

Report No. 137

ANALYSIS OF ION PLATED Cu/CORDIERITE FILM AND INTERFACE STRUCTURE AND CHEMISTRY

by

Philip A. Scott and J. M. Rigsbee
Department of Materials Science and Engineering

A Report of the

MATERIALS ENGINEERING - MECHANICAL BEHAVIOR

College of Engineering, University of Illinois at Urbana-Champaign

October 1987

ABSTRACT

This research is a fundamental study which uses ion plating, a plasma-assisted physical vapor deposition process (PAPVD), to deposit Cu films onto cordierite glass ceramic substrates. The primary goal of this project is to characterize the ion plated film/substrate interfaces produced using hgh resolution analytical tools such as transmission electron microscopy (TEM). The observed structure and chemistry of the interface is then related to the ion plating process parameters, such as applied substrate voltage, and the interface mechanical properties, such as adhesion failure strength. Some of the results of this study include the following:

1) Films deposited under low substrate bias conditions exhibited open-boundary columnar structures while films deposited under higher bias conditions are of an equiaxed type morphology.

2) Evaporated films exhibited nearly abrupt metal/ceramic interfaces while ion plated films were spatially graded both chemically and structurally.

3) The adhesion failure strength was found to increase significantly with applied substrate bias (voltage). The analytical tools used in this project include SIMS, AES, TEM, and SEM.

ACKNOWLEDGEMENT

The author would like to thank Professor J. M. Rigsbee for his foresight and assistance throughout this study.

The support of the U.S. Army Construction Engineering Research Laboratory is acknowledged for use of the ion plating facility. Mr. V. F. Hock is acknowledged for his assistance as a principal investigator of the ion plater.

The use of the facilities of the Center for Microanalysis of Materials in the Materials Research Laboratory is acknowledged as well as the Center for Electron Microscopy.

The support of the Ion Plating Group at the University of Illinois is acknowledged for assistance regarding vacuum technology and materials microanalysis.

The invaluable assistance of Professor W. H. Mischo and his support staff is acknowledged for their outstanding performance in the areas of library science.

TABLE OF CONTENTS

TABLE OF CONTENTS (Continued)

TABLE OF CONTENTS (Continued)

LIST OF TABLES

LIST OF FIGURES

LIST OF FIGURES (Continued)

LIST OF FIGURES (Continued)

LIST OF FIGURES (Continued)

LIST OF FIGURES (Continued)

I. INTRODUCTION

Modern products impose many requirements and constraints on the materials from which they are fabricated. High performance materials often require a high strength to weight ratio at room as well as elevated temperature. One example is a turbine blade which is stressed and heated simultaneously. The need for these modern materials has stimulated a great deal of research in the areas of composite materials--materials composed of metals and ceramics, metals and polymers, and various other combinations. Since composite materials will often be stressed or under some type of load while in service, the bulk properties of each material in the composite, as well as the interface between the two materials will determine the mechanical properties of the composite. This thesis investigates the structure and chemistry of a metal/ceramic composite interface as a function of the process parameters of a modern materials processing technique. This technique, ion plating, is a plasma-assisted physical vapor deposition process which incorporates features of both sputtering and evaporation. Using this technique, thin Cu films are grown on a ceramic substrate and with the analytical tools available at the Materials Research Laboratory, the interface boundary structure and chemistry is characterized. Some of the questions which this thesis addresses are:

1) How does energetic ion bombardment affect the growth and mixing of the Cu film on the ceramic?

2) How do the mechanical properties of the composite relate to the observed interface microstructures and microchemistries?

3) What is a suitable processing window for manufacturing considerations in the application of microelectronic packaging?

II. BACKGROUND

The following section is a literature survey which should serve as an introduction to the field of metal/ceramic composites as well as the science in vacuum deposition technology. The particular examples chosen from the literature are relevant to many of the considerations which arise in a research project of this topic.

II.A. CERAMIC/METAL COMPOSITES AND INTERFACES

A particularly important topic in the areas of ceramic/metal composite materials and microelectronic packaging is the adhesion between two dissimilar solids and the relationship between adhesion and the structure and chemistry of the interphase boundary. The concept of adhesion is not well understood from an experimental point of view since it is difficult to say that adhesion strength is actually being measured by current testing techniques. From a theoretical point of view, quantities such as the work of adhesion and surface energies are well defined and relationships are readily derived. It is thus one objective of this thesis to present some scientific concepts of adhesion; to discuss some of the problems encountered with adhesion testing, including the pull test which was used for evaluating adhesion strength in this study of the Cu/cordierite system; and to describe as clearly as possible the adhesion strength of the Cu/cordierite interface as a function of the interphase boundary structure and chemistry.

II.A.1. EQUILIBRIUM INTERACTIONS

Quite often, a materials system is not in an equilibrium

state. Examples of non-equilibrium situations, as imposed by kinetic constraints, include the presence of martensite in steels as well as super-saturated solid solutions of Cu in Al. Surface energies, which are related to the topic of adhesion, are thermodynamic quantities that are determined experimentally at elevated temperature under near-equilibrium conditions. Surface and interface energies thus give an indication of the thermodynamic stability of an interface between two particular materials.

II.A.1.a. WETTING

Wetting is a very important concept in adhesion. Wetting, according to Huntsberger[1] is a process of achieving intimate molecular contact between two materials. Complete wetting corresponds to a situation in which atomic contact is realized at every point along an interface. In contrast, one might imagine a very rough surface on one of the phases, which experiences a low percentage of intimate contact at the interface (see Fig. 1). The change in free energy[2] due to wetting of a solid surface by a liquid in an ambient vapor is given by:

$$\Delta F = A^{sv}F_{sl} - [A^{sv}F_{sv} + A^{lv}F_{lv}] \qquad (1)$$

where A^{sv} and A^{lv} are the actual areas of the solid-vapor and liquid-vapor interfaces, respectively, in the non-wetted state. F^{sv} and F^{lv} are the surface free energies of the solid and liquid phases in equilibrium with the saturated vapor phase and F^{sl} is the free energy of the solid liquid interface. The sessile drop

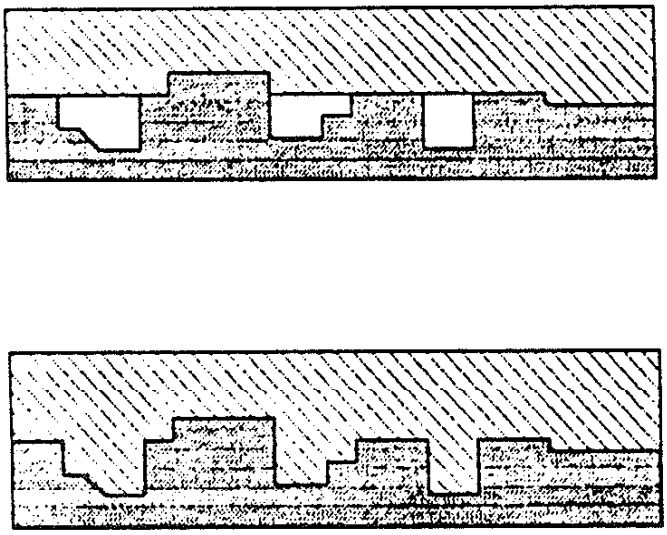

Fig. 1. Wetting of solid substrate by fluid adhesive.
Upper: Substrate incompletely wetted.
Lower: Substrate completely wetted.

model[3,4] describes a liquid drop at equilibrium with a solid surface, the two of the phases being at equilibrium with the saturated vapor (see Fig. 2). If $\theta > 90$, the system is in a non-wetted state; if $\theta < 90$, the system is in a wetted state; if $\theta = 0$, then spreading occurs. The Young-Dupree equation, which describes this system, may be written in terms of the interface free energies as (2):

$$\Delta F_{sv} = F_{sl} + F_{lv}\cos\theta \qquad (2)$$

where the subscripts sv, sl and lv represent the solid-vapor, solid-liquid, and liquid-vapor interfaces free energies, respectively. If spreading occurs, that is, the migration of the liquid over the solid surface, then the system is not at equilibrium and the Young-Dupree equation is no longer applicable.[2] Huntsberger[1] has pointed out that the equilibrium which may be present in the sessile drop model is actually an indication of the extent to which the liquid will spread over the substrate and not the extent to which the substrate is wet. This seems reasonable as the drop may drape over defects such as steps in the surface, while not intimately contacting it at each atomic site. The Dupree equation[2,5] gives the reversible work of adhesion as:

$$W_A = F_a + F_b - F_{ab} \qquad (3)$$

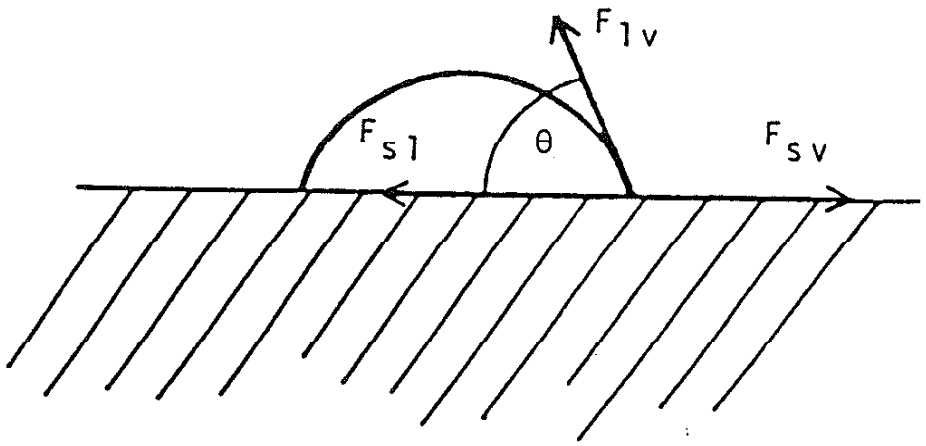

Fig. 2. The sessile drop model. This system describes 3 phase equilibrium between a liquid drop, a solid surface, and an ambient vapor.

for unit surface area, where F_a and F_b are the surface free energies of surface a and b, respectively, and F_{ab} is the free energy of the ab interface. This equation essentially states that the work in separating two materials at an interface, where no interdiffusion or chemisorption is present is given by the energy necessary to create the surfaces a, b of the two phases less the energy required to destroy the ab interface.

Concepts of wetting give some idea whether interaction between two phases is likely under equilibrium conditions, but the interaction is quite complicated and the exact nature of the interaction is not understood. Wetting experiments are usually conducted at elevated temperature to ensure that equilibrium conditions are present, and the parameter measured is the contact angle $\underline{\theta}$. The following section will review a metal/ceramic wetting experiment to illustrate some typical results.

II.A.1.b. WETTING EXPERIMENT

Wetting behavior of liquid metals on ceramics and other materials[6] is important in soldering and brazing where spreading of one material on the other is desired. A study of the wetting behavior of Cu-Ti alloys on Al_2O_3 was conducted by Nicholas, Valentine, and Waite,[7] using contact angle measurements. It was observed that the additions of 8% Ti (atomic %) to Cu would allow Cu to wet Al_2O_3 while only 3.5% Ti was needed if the Cu was already alloyed with 11.8% Sn. This experiment was conducted at 1423°K. Two possibilities were cited for this observed behavior. The first states that since the solubility of Ti in Sn is less than in Cu,

the Ti activity in the alloy would increase, thus providing greater driving force for the alloy to wet. In other words, a greater free energy decrease of Ti is realized as a result of wetting in the presence of Sn. The second possibility is that since Sn has a low surface energy, it segregates to the surface which then increases Ti activity locally at the surface, also resulting in enhanced interaction with the ceramic. By monitoring contact angles in experiments of this type, which are performed under high temperature equilibrium conditions, an indication of the thermodynamic stability of a particular alloy/ceramic interface may be determined. Interfaces produced by modern day materials processing techniques, however, are most often not at equilibrium. Thus, it becomes difficult to have a sense of parity between wetting phenomena and the properties of engineered interfaces.

II.A.2. ADHESION THEORIES

Since wetting does not refer specifically to the type of interface between two phases, some adhesion theories will now be presented which describe possibilities for interface atomic arrangement and interaction between phases.

In the presence of sufficiently intimate contact between two surfaces, the adhesion question then reduces to the nature of bonding forces present at an interface. There are several proposed mechanisms[8] for the adhesion of two bodies, a few of which are mechanical interface, diffusion interface, electronic interface, and the adsorption interface. In real systems, it may well be that more than one of these mechanisms is operative for a given inter-

face. These theories will now be briefly reviewed. For a more complete discussion of this topic, the reader is directed to references 2 and 8.

II.A.2.a. MECHANICALLY INTERLOCKING INTERFACE

This mechanism of adhesion may be understood by considering the joining of two materials; one of the materials being somewhat ductile and the other with a hard, rough, and porous surface. If sufficient pressure is applied to a sandwich of these materials, then flow of the ductile material into the pores and encircling of the protuberances of the harder material would be expected. Thus the materials would be bonded together in a mechanical keying fashion.

Perrins and Petit[9] performed an experiment which was designed to reveal the relative importance of chemical and mechanical contributions to adhesive failure strength, for Cu electroplated on polypropylene. To change surface roughness, which should in principle change the density of mechanical keys, they used a good etch and a bad etch on a particular sample. The good etch was used to roughen the surface as opposed to the bad etch which did not particularly roughen the surface. The chemical component of adhesion was changed by rinsing both well and badly etched surfaces in HCl to reduce the reactivity via the removal of reactive species. Some samples then had their reactivity restored by rinsing in a second acid. Table 1 shows the results of this study. Rough and reactive surfaces exhibited the highest peel strength, while surfaces which were both less rough and less reactive displayed the least strength.

Table 1

Chemical and Mechanical Components of Adhesion for a Cu/Polypropylene System (KN/m)

Surface Chemistry	Mechanical Component	
	Well Etched Good Acid	Poorly Etched Bad Acid
Treatment with hydrochloric acid to completely remove surface activity	0.66	0.17
Reactive etch (good acid) applied briefly after removal of surface activity	3.94	1.37

Peel strength refers to the adhesion test known as the peel test. This basically involves measuring the energy necessary to 'peel' a film off its substrate. This data in Table 1 clearly shows that there are components from each adhesion mechanism. Wake[8] suggests that chemical and mechanical components of adhesion may be represented in an equation of the form,

$$\text{Peel Strength} = (\text{Constant}) \times (\text{Mechanical Component}) \times (\text{Chemical Component}) \quad (4)$$

to yield peel strength.

Another study by Evans and Packham,[10] involved the adhesion mechanisms of polyethylene to Cu. These experiments were similar in objective to those of Perrins and Petit in that they were designed to distinguish between mechanical and chemical components of adhesion. It was observed that Cu surfaces oxidized to the Cu (II) state formed arrays of whiskers. In contrast, when Cu was oxidized to the Cu (I) state, a continuous array of nodular fibres formed and was less rough than the Cu (II) surface topography. They then proceeded to change surface topography without altering the chemical state as well as change the chemical state without modifying the topography. The former situation was accomplished by buffing the oxide with filter paper until shiny to damage the fibres; the latter scenario was accomplished by reducing the Cu (I) oxide to the metallic state. The results indicate that the polished oxides have poorer adhesion to the polyethylene than the original oxide and also that the reduced surface has poorer adhesion to the polyethylene than the original oxidized surface. The authors maintain

that the reduction in peel strength observed in the reduced oxide case is likely due to topography damage resulting from manipulation in the reduction sequence.

II.A.2.b. DIFFUSE INTERFACE

The diffusion theory of adhesion describes the mechanism of adhesion as an inter-penetration of two macroscopic bodies on a microscopic scale.[2] Voyutskii[8,11] has been a principal supporter of the diffusion theory of adhesion, especially in regard to polymer systems. As a result of his vast works, Voyutskii[8] believes that the diffusion mechanism of adhesion is observed for the systems of 1) polymer self-adhesion, 2) adhesion between different polymers, 3) heat sealing of thermal plastics, and 4) the importance in formation of films from lattices. The only situation of these four in which it is not generally accepted that diffusion adhesion is important is that of the adhesion between dissimilar polymers.[8]

Vasenin[8] added quantitative results in support of the diffusion mechanism of adhesion. Vasenin developed on theoretical grounds that the diffusion coefficient of a diffusing species is given by:

$$D_\phi = D_o\left[\frac{D_1}{D_o}\right]^{1-\exp[-\beta\phi(1-\phi)]} \qquad (5)$$

where D_ϕ is the diffusion constant at volume fraction ϕ and β is a constant. In order to connect the diffusion properties of a polymer with the force of separation, Vasenin considered a concept by

Einstein and arrived at an expression for the resistance to movement (f):

$$f = (\frac{mv}{2})\nu\eta \qquad (6)$$

where m is molecular mass, v is the rate of extraction of the molecule, ν is vibration frequency of a CH_2 group and η is the number of CH_2 groups diffused. Following further development it is derived that the force F required for separation at v cm/sec is given by:

$$F = 11\nu[\{\frac{(2+P)}{M}\rho\}^{2/3} K_d^{1/2}]vt^{1/4} \qquad (7)$$

where P is the number of chain branches in the molecule, ρ is the density, and M is the molecular weight, and K_d is a constant characteristic of the diffusing molecule and the mass into which it diffused. This equation is for the case of self-adhesion. Experimental data fits this equation rather well.[8] Some of the experimental data of Voyutskii[8] which takes into account contact time as well as polymer molecular weight also fits this equation. Thus, it appears that Vasenin, by considering fundamental properties of diffusing species, was able to predict macroscopic adhesive behavior.

II.A.2.c. ELECTRONIC INTERFACE

This theory states that the adhesive strength of a junction is based on charge transfer between the two materials.[2] When two

materials of differing band structures are brought together, there is likely to be some charge transfer from one to the other, which results in an electrical double layer of charge at the interface. Deryaguin[2,8] and other Russian scientists have considered this double layer to be analogous to a parallel plate capacitor and have calculated the energy for separating the plates of the capacitor. Good agreement was reached between measured work of adhesion and the condenser energy. This model of the electrostatic theory is quite interesting; however, the condenser energy was essentially arrived at by equating it to the adhesion energy. As a result of this, complete agreement is unavoidable between adhesion energy and the condenser energy.

It has been reported that sputtering a substrate prior to depositing a thin film will improve adhesion.[12] Stoddart, et. al,[13] have observed some type of electrical alteration of a glass surface in a sputtering experiment. It is observed that when one-half of a glass substrate is exposed to a glow discharge that the electron emission intensities of the two halves as observed in an SEM are different. When air or oxygen is used to sputter the surface, the emission is increased relative to the unsputtered half and when nitrogen, H_2, H_2O vapor or Ar is used, the emission decreases. The altered emission effect is observed on several insulators and persists after extended periods of exposure to atmosphere. A possible reason for this effect cited by the authors is the absorption of gases into the glass surface. If the atoms are acceptors, such as oxygen, the electrons near the surface would be more easily ejected resulting in enhanced emission. If adsorbed atoms displace oxygen, then a decrease in emission could result.

II.A.2.d. ADSORPTION INTERFACE

The adsorption theory of adhesion proposes that surface forces acting between two surfaces will cause the materials to adhere.[2] Two categories of interaction that are considered to be adsorption processes are that of physisorption and chemisorption. Conceptually, these bonds may be understood in terms of an atom approaching a surface in a vacuum. If a Van der Waals bond, which is a physisorption type of bond, is produced between the two bodies then the atom will reside in a potential well of depth q_p at a distance r_p from the surface. Van der Waals bonds may be formed as a result of induced dipole-dipole interactions or due to the attraction of permanent dipoles. An induced dipole-dipole interaction is one in which a momentary dipole present in the adsorbing species or in the surface triggers a dipole to form in the conjugate body. A system for which this type of bond is applicable is noble gas atoms on graphite.[14] A permanent dipole-dipole interaction is due to attraction from a polar molecule, for instance, with another permanent dipole present at the surface of a solid. Huntsberger[2] has calculated the attractive forces between two planar bulk phases due to Van der Waals type forces as 100 MPa at a distance of 1 nm. This sort of adhesion strength is often not realized in present day technology where adhesion is of great interest, such as the thin film industry. If, on the other hand, an atom reacts chemically with the surface, constituting a chemisorption bond, then the atom is more tightly bound to the surface in a potential well of the magnitude q_c and distance r_c from the surface. See Fig. 3, which schematically represents these two situations and indicates the

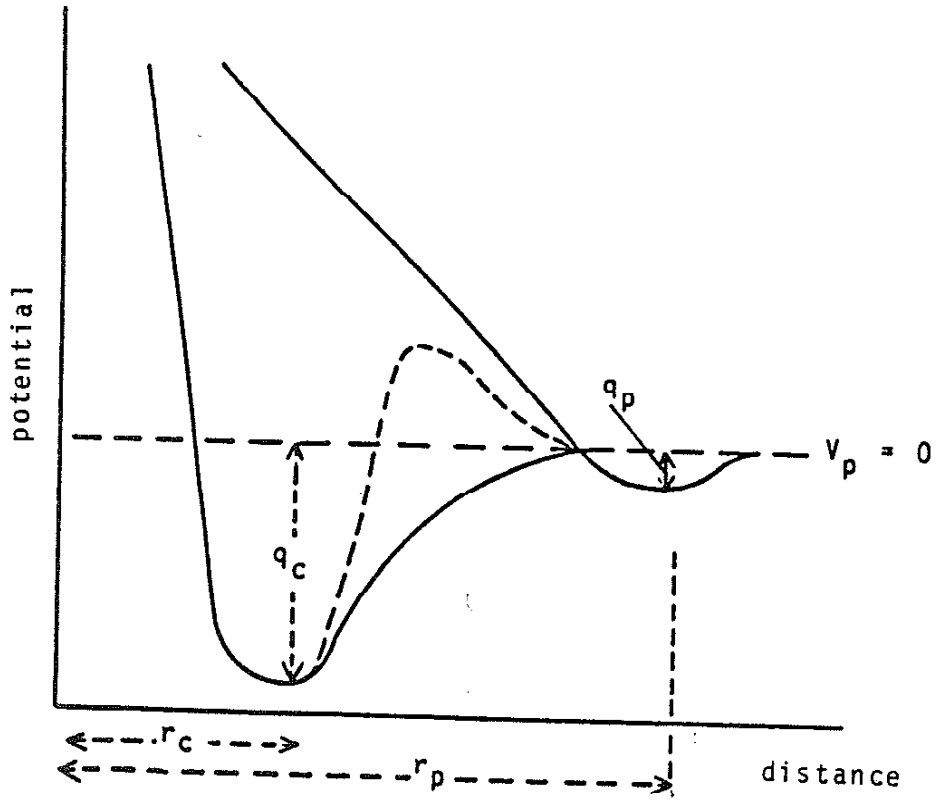

Fig. 3. Schematic of the potential energy as a function of distance from a solid surface. Two 'wells' are present representing a chemisorbed and physisorbed bond.

different potential energy depths for chemisorption and physisorption bonds. A system exhibiting chemisorption type of bonding is that of CO on Co.[15]

The following section will be concerned primarily with experimental studies of ceramic/metal interfaces: the types of interaction and, where possible, the mechanical properties of the interfaces. It is useful to separate this discussion from the theoretical considerations since at present it is often not possible to determine from first principles which physical mechanisms are responsible for observed physical properties.

II.A.3. PROCESSING TECHNIQUES AND CASE RESULTS

There are many materials processing techniques which may be used to produce an interface between two dissimilar materials. The interfaces discussed in this thesis will largely be from the category of solid state bonding and vapor deposition. Solid state or diffusion bonding[16] is usually performed under conditions of elevated temperature and pressure commonly resulting with interface structures that possess reaction phases and interdiffusion.[17,18] Vapor deposition techniques such as vacuum evaporation[19,20] and sputtering[19,21] are commonly used to produce material junctions on a very small scale for uses in the areas of electronic device fabrication as well as tribological applications.[22] Mechanical properties of interfaces used in tribological applications are critical and intimately related to the structure and chemistry of the interface. The next section will review some examples of metal/ceramic interfaces.

II.A.3.a. CERAMIC/METAL INTERFACES

Kingery[17] discusses several different types of interaction that occur in a variety of metal/ceramic systems at elevated temperatures. A cermet is a ceramic/metal composite. Practically speaking, the temperature at which cermets are used should be much lower than the bonding temperature. Hence, it is desirable to determine the lower temperature range of reactions which might occur.[17] The first type of interface formed upon firing involves the formation of a new phase observed as an interface layer, which is insoluble in either the metal or ceramic reactant phases. Systems which exhibit this behavior include Si-MgO, Si-Al_2O_3, and Ti-MgO. The type 2 interface is considered to be corrosion of the metal to an oxide. Products of the reaction in this case are soluble in one or both of the reactants. Systems which appear in this category include Ti-TiO_2, Ti-ZrO_2, and Zr-Al_2O_3. The type 3 interface usually involves metal penetration of the oxide along grain boundaries which may occur with or without corrosion or interfacial layers. This penetration along grain boundaries progresses to envelopment of the oxide grains. This type of reaction is observed in systems such as Nb-BeO, Be-ThO_2, and Ti-Al_2O_3. The final type of interface is characterized by the absence of a product phase, appearing to be an abrupt metal/ceramic interface. The bonding process could therefore be interdiffusional in nature. Systems exhibiting this behavior include Ni-Al_2O_3, Ni-ThO_2, and Mo-MgO. It is important to realize that this work by Kingery was published in 1953 and thus, with the more widespread use of TEM, some systems may actually prove to be of a different type than cited above.

Noble metals such as Au, which do not form stable oxides but bond to ceramics, are an interesting class of materials for studying metal/ceramic interactions. Bruin, Moudie, and Warble[23], have compared the behavior of noble and transition metals on oxides and have determined that two types of interactions occur. For noble metals, a small scale surface type reaction occurs while the transition metal/ceramic couples exhibit a more bulk or macroscopic type of reaction. For the case of $SiO_2/Pt/SiO_2$ and $Al_2O_3/Au/Al_2O_3$ couples the bonding phase observed via TEM is of the order of 10 nm in thickness. In some regions a reaction of this type was observed in-situ with a hot stage TEM experiment. A Pd support grid was used to suspend small MgO particles. Near 1373^oK, 723^oK below the melting temperature of Pd, a liquid like phase formed in areas where the metal and ceramic were in contact. This phase was observed to spread over the MgO surface, and the authors maintain that the presence of MgO thickness fringes disqualify this reaction to be of a bulk or diffusional nature. As the "liquid" spreads over the MgO, a wide fluctuation in contact angle is observed, with angles as low as 65^o measured, much lower than the 110^o found in a previous study. Quenching the sample with liquid nitrogen introduces little strain in the MgO lattice as evidenced by the thickness fringes; the bond between the amorphous phase and the MgO remain intact.

Baily and Black[24] studied the bond strength of $Al_2O_3/Au/Al_2O_3$ composites formed at various times, temperatures and pressures. A summary of the effects of the experimental variables on bond strength indicate that heat treating both ceramics and metals increased bond strength considerably over the case of no heat treat-

ment to the components. Heat treating the Au foils prior to making the composite resulted in a substantial increase in bond strength though not as great as when all components were heat treated. The authors consider the hypothesis that the heat treatment is a good cleaning procedure for the surfaces and that it could be this effect which is observed by the increased bond strength. Pre-evaporation of Au onto the Al_2O_3 which was subsequently bonded to Au foils increased bond strength over samples without pre-evaporation. Bonding pressure appears to be not so critical as a saturation in bond strength is observed at approximately 0.2 MPa.

The authors believe that pressure serves primarily to provide intimate contact between the materials. The authors also state that bonding in a hydrogen atmosphere greatly reduces the chemical components of bonds and exemplifies the fact that chemical bond contribution to joint strength is much larger than the mechanical keying component. It was observed that bonds formed in hydrogen tested in shear made with polished sapphire were 2 MPa while those formed in air were greater than 90 MPa. Mechanical keying contributions are expected to be minimal for this case.

II.A.3.b. GLASS CERAMICS

The class of materials commonly known as glass ceramics are becoming increasingly popular for use as catalyst supports,[25] heat exchangers, microelectronic substrates,[26] and biomaterial implants.[27] Systems with useful glass ceramics include:

Li_2O-Al_2O_3-SiO_2, Li_2O-MgO-SiO_2, Li_2O-ZnO-SiO_2,
Na_2O-BaO-Al_2O_3-SiO_2, MgO-Al_2O_3-SiO_2,

and others.[26] Glass ceramics are distinguished from more typical ceramics in that they are produced by crystallization from a solid glass phase. This is accomplished through control of nucleating agents and scheduled heat treatments which yield a primarily crystalline material with an amorphous phase usually present as a minority constituent. The typical heat treatment schedule (see Fig. 4) is comprised of initially heating the material to a so-called nucleation temperature[3] followed by heating to elevated temperature for growth of the crystalline phase.

II.A.3.c. BONDING GLASS CERAMICS TO METALS

Glass ceramics have been thermally bonded to metals by Partridge and Elyard[28] using three scenarios for interface formation. The first of these is active metal braze bonding which involves a reactive layer of alloy or braze material which bonds the bulk glass ceramic onto the bulk metal. The second technique employs an additional glass or glass ceramic which is capable of wetting and bonding both the metal and ceramic. The third technique involved applying the glass ceramic to the metal while the glass ceramic was still vitreous, in a liquid or viscous state, followed by a devitrification/bonding heating cycle. Optical micrographs as well as electron probe microanalysis line profiles were provided of the various interfaces. For the case of bonding Cu onto a Li_2O-ZnO-SiO_2 glass ceramic, a Ti-Cu/Ag sequential interlayer was used as a joining medium. The most interesting feature of the line profile results in a Zn-rich zone at the interface. The Ti and Cu layers are clearly indicated in the profile.

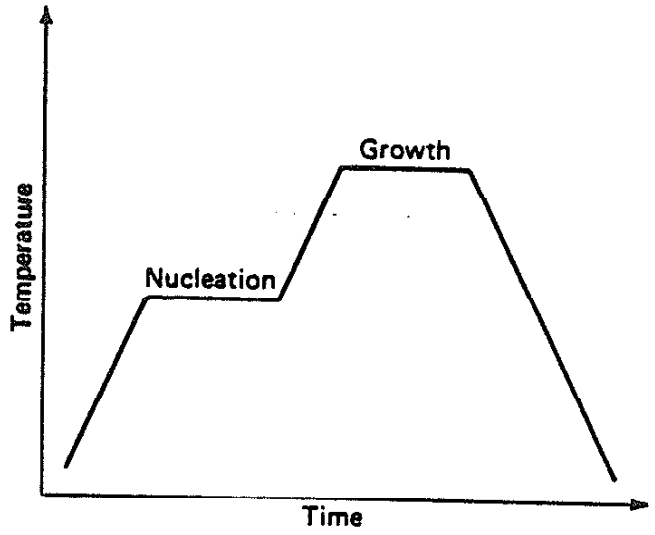

Fig. 4. Example of a glass ceramic heat treating schedule. The nucleation period correlates with glass-in-glass phase separation in some systems, while the growth portion of the treatment results in growth of a crystalline phase(s).

For the case of vitreous bonding, using a Li_2O-ZnO-SiO_2 type glass ceramic as the bonding media, steel was joined to another Li_2O-ZnO-SiO_2 glass ceramic. A zone enriched in Mn was detected following the thermal bonding process.

The directly bonded glass ceramic to metal seals exhibited various degrees of interaction. The case of an Li_2O-Al_2O_3-SiO_2 glass ceramic bonded to an Ni-Fe alloy exhibited segregation of Mn from the metal side to the interface and K from the glass ceramic side, also appearing at the interface. The Mn segregated to the surface during a pre-oxidation treatment of the metal and upon joining diffused into the glass ceramic. Another example of a Li_2O-ZnO-SiO_2 glass ceramic that was directly bonded to an 18/8 stainless steel exhibited less interfacial interaction with apparently no preferential segregation to the interface. The microstructure of the glass ceramic adjacent to the metal appears different however, compared to the bulk phase. The authors do not give exact details on the nature of the difference.

II.A.3.d. CORDIERITE

Cordierite glass ceramics are from the MgO-Al_2O_3-SiO_2 ternary system, the glass forming region of the system is shown in Fig. 5 and the liquidus surface may be seen in reference 29. Cordierite glass ceramics are well known for excellent thermal shock resistance.[30] Thermal expansion coefficients for cordierite are a function of composition.[31] Thus, cordierite is often used in service where thermal cycling is encountered. Cordierite has several polymorphs[32] including a low temperature stable form "β", a meta-

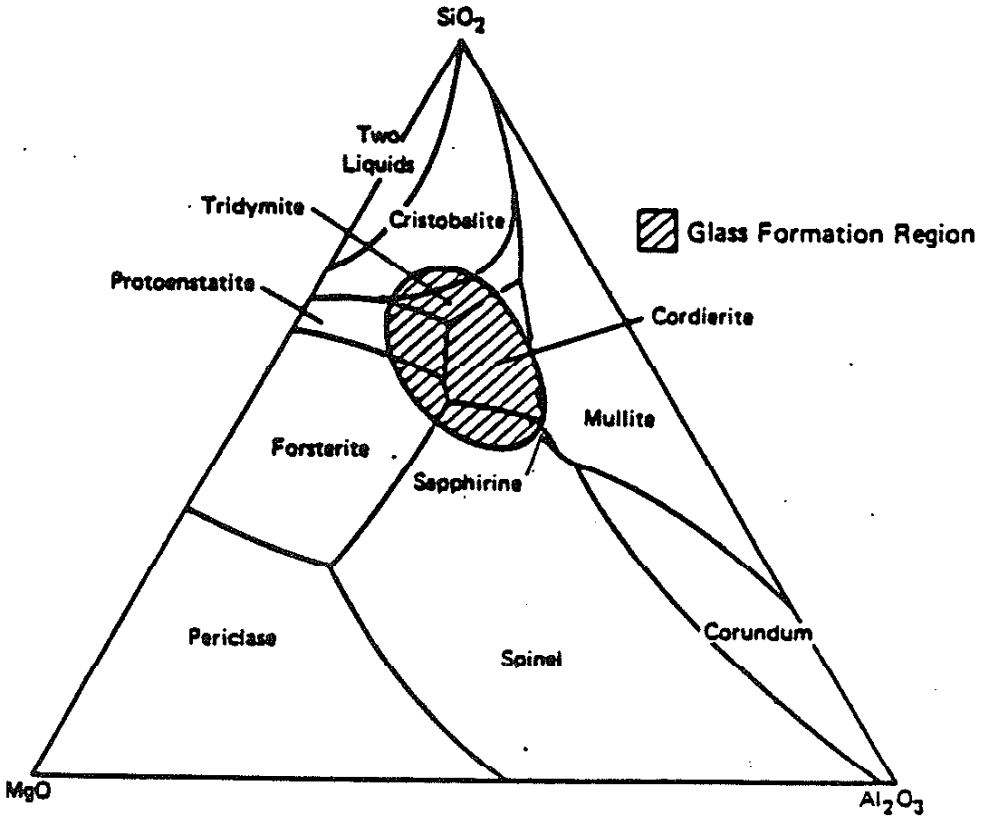

Fig. 5. Ternary phase diagram of the $MgO-Al_2O_3-SiO_2$ system. The glass forming region is clearly indicated.[2]

stable form "μ" and a higher temperature stable phase "α". The α and β phases show hexagonal symmetry.[32] Smart and Glasser[33] observed two high temperature polymorphs, one hexagonal and isostructural with indialite, which is a naturally occurring mineral polymorphous with cordierite, and the other orthorhombic or pseudohexagonal. A vertical section of the ternary phase diagram is presented in their work which traverses the cordierite phase field (see Fig. 6). As may be seen, the stoichiometric $2MgO\text{-}2Al_2O_3\text{-}5SiO_2$ composition extends through the mullite liquidus. The high temperature $\underline{\alpha}$ phase is retained easily on quenching to room temperature. The unit cell dimensions are given in Smart and Glasser[33] for the orthorhombic and hexagonal polymorphs. The space group of each structure with the lattice parameters is given in Table 2. Fig. 7 is a two-dimensional basal projection of Beryl which is isostructural with hexagonal cordierite.[34] Many intermediate structural states exist between the hexagonal and orthorhombic forms.[29,34] The transformation between hexagonal and orthorhombic forms is probably of an order-disorder type.[34] Miyashiro[35] originally introduced a 'distortion index' to account for deviations from hexagonal symmetry, towards orthorhombic-like symmetry. This polymorphism results in splitting x-ray diffraction peaks. The distortion index is defined as:

$$\Delta = 2\theta_{131} - \frac{2\theta_{511} + 2\theta_{421}}{2} \qquad (8)$$

where $\Delta = 0$ for the hexagonal form.

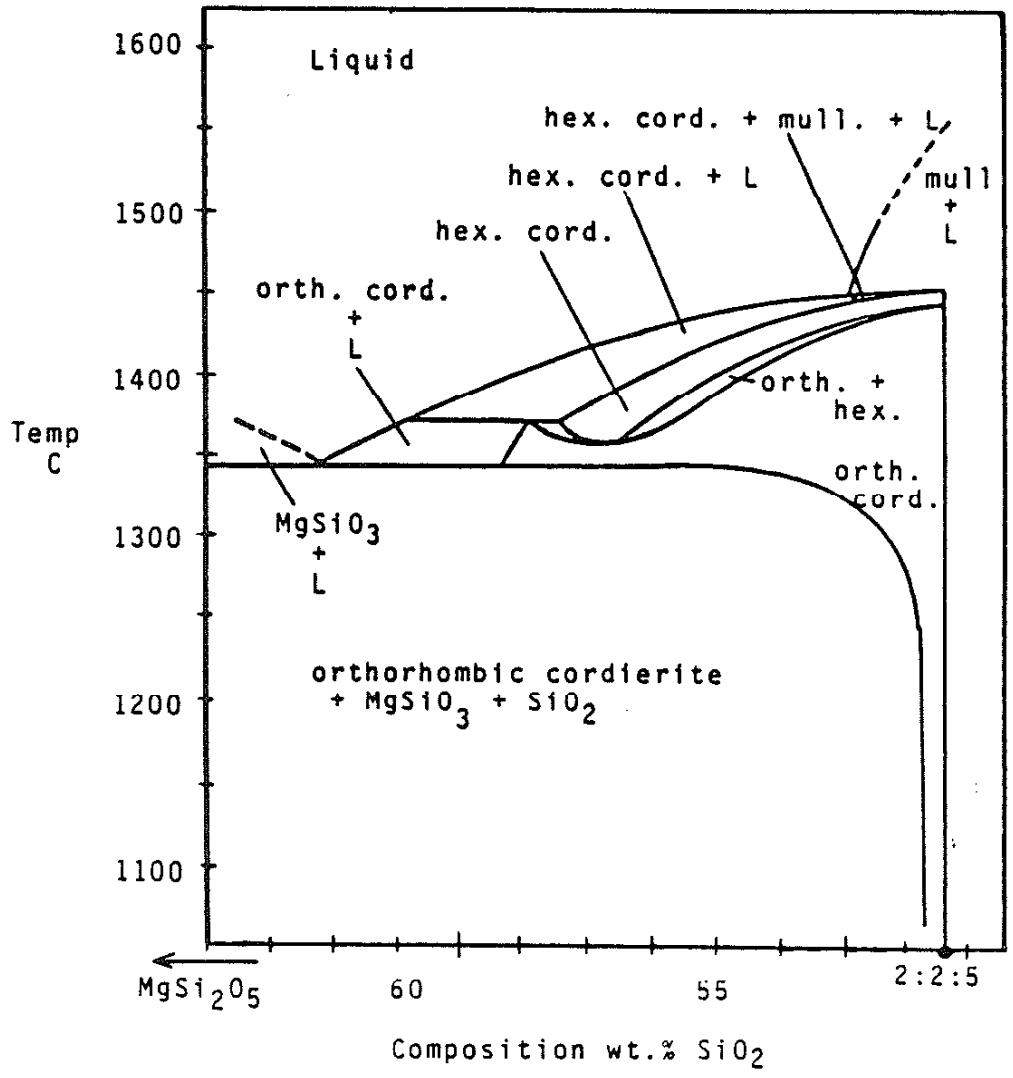

Fig. 6. Vertical section across the cordierite phase field.

Table 2

Cell Dimensions of Cordierite Solid Solutions (Å)

Composition	Hexagonal		Orthorhombic		
	a	b	a	b	c
$Mg_2Al_4Si_5O_{18}$ (51.36% SiO_2)	9.784	9.343	9.717	17.063	9.344
"$MgSi_2O_5$ rich"	9.781	9.339	9.720	17.059	9.344
Space Group	P6/mcc		Cccm		

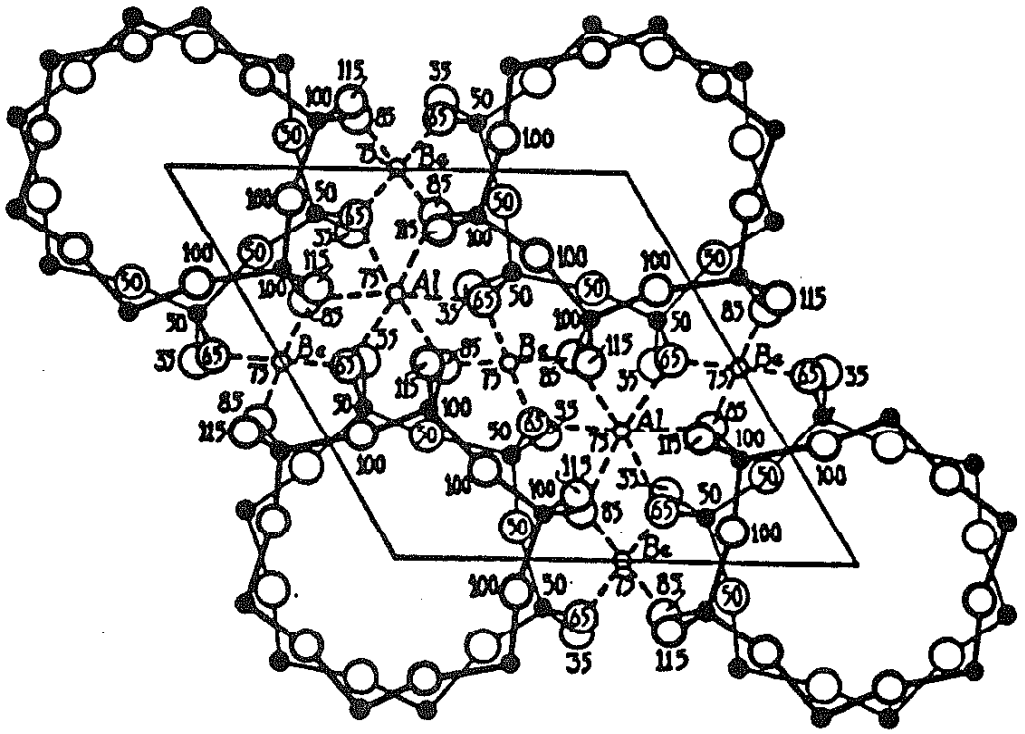

Fig. 7. Two dimensional basal projection of the mineral beryl. This is isostructural with hexagonal cordierite. The numbers in the figure represent the relative heights of atoms in the unit cell.

Cordierite: $Al_3Mg_2Si_5AlO_{18}$

Beryl: $Be_3Al_2Si_6O_{18}$

The crystallization sequence of cordierite glass ceramic follows the traditional process for glass ceramic formation. The microstructural evolution of a particular glass will be reviewed briefly. The composition of this glass is 48.9 SiO_2, 22.2 Al_2O_3, 13.3 MgO, 4.5 CaO, and 11.0 TiO_2 (wt %), compared to the stoichiometric composition of 51.36 SiO_2, 34.86 Al_2O_3, and 13.78 MgO (wt %). Several different heat treatment schedules were investigated in this study by deVekey,[36] including schedules without the 'nucleation' heat treatment. To investigate the effect of time and temperature of the final heat treatment while maintaining a constant nucleation heat treatment, a series of samples were heat treated in the temperature range of 1273°K to 1523°K with a constant nucleation treatment of 1013°K for 4 hours. Following this initial nucleation treatment, it was observed that crystalline cordierite did not form below 1273°K. The phases present following 1273°K heat treatments up to 12 hours were a magnesium aluminum titanate and a crystalline solid solution based on enstatite. Following final heat treatment in the range of 1323-1523°K, the final microstructure contains cordierite, aluminum titanite rutile and sometimes anorthite. Anorthite would only be expected as a result of metastable processes or due to elemental segregation. The limiting cordierite content for this temperature appears to be 55% by weight.

Some microstructures following heat treatment contained distinctly different "zones" or phases. Zoned microstructures were commonly observed. The different zones gave different electron contrast in the SEM. Zoned microstructures were inhibited in samples without nucleation heat treatment or when the crystallization tem-

perature was kept below 1323°K, where cordierite begins to appear. Cordierite formed without any prior nucleation heat treatment exhibited a granular microstructure composed of acicular crystallites. The zones tended to be chemically different. High electron contrast zones were richer in Ca and poorer in Mg than the low contrast areas. Cordierite is initially observed in the Mg Rich zones as microcrystals, forming larger crystals with time at temperature.

Nucleating agents such as TiO_2, ZrO_2, P_2O_5, CeO_2, $AlPO_4$, and CaF_2[37] are used to control subsequent bulk crystallization of a glassy matrix. The exact mechanism by which this is achieved is not resolved. Thakur[38] divides nucleating agents into four groups: 1) metals and compounds such as sulfides and flourides; 2) oxides which assume a defect structure at high temperature and possess a nigh nucleation rate; 3) oxides which can exist in two valence states in glassy melts; and 4) oxides with high coordination for the cations.

Tomozawa,[39] investigating the effects of different oxide nucleating agents such as TiO_2, P_2O_5, and ZrO_2 on phase separation in Na_2O-SiO_2 glasses, concluded that nucleating agents in small concentrations can affect the immiscibility boundary as well as alter the crystallization kinetics. Basically, the results indicated that P_2O_5 is the only nucleating agent of the aforementioned three which raises the immiscibility temperature, thus promoting glass in glass phase separation. TiO_2 and especially ZrO_2 suppressed the immiscibility gap. These conclusions are supported by small angle x-ray scattering data.[39] Another interesting point about P_2O_5 was mentioned in a study by Plumat[40] on a Ca-Mg alumino silicate glass.

His observations indicate that the P_2O_5 actually inhibited crystallization while efficiently inducing glass in glass phase separation. Thus, P_2O_5 prevents large grain growth yielding a fine grained matrix.[37]

Mechanical strength of cordierite glass ceramics are shown by deVekey and Majumder[41] to be a function of both heat treatment and composition. Flexural strength was observed to vary between 10 MN/M^2 and approximately 200 MN/M^2 for various compositions and heat treatments. The % cordierite phase observed in samples heat treated at 1423° C is a strong function of the proximity of the overall composition to that of the stoichiometric $2MgO-2Al_2O_3-5SiO_2$ (2:2:5) composition.

II.A.3.e. Cu/CORDIERITE

Poetzinger and Risbud[42] investigated the interface interaction between Cu and cordierite under various firing conditions. The cordierite base glass composition was similar to Corning 9606 with P_2O_5 added as a nucleating agent. Nucleation and binder burn off heat treatment was at 1058°K with varying oxygen partial pressures and times and the crystallization temperature was typically 1238°K. In summary, the following effects were observed during the processing. For temperatures in the range of 1058°K to 1163°K, diffusion of Cu^+ ions into the glass and sintering of the glass adjacent to the Cu was observed. In the temperature range of 1238°K, glass crystallization and precipitation of Cu-rich particles in the ceramic near the interface was observed. Precipitation occurred in the

cordierite matrix and in the amorphous droplet phase. They were noticed more often in the droplet phase.

Prior to crystallization, microprobe analysis indicates no more than 1 wt % Cu in the glass near the interface. Fluorescence data indicates Cu is present as the Cu^{+} ion. The diffusion coefficient of Cu in the glass was estimated as 10^{-11} cm^2/sec at $1058^{o}K$ using microprobe point analysis for data collection. The temperature was changed from $1058^{o}K$ to $1163^{o}K$ for the sample used in this measurement, however. The final cordierite microstructure contained: 1) structurally and chemically inhomogeneous matrix of a cordierite; 2) forsterite enriched in P_2O_5, as compared to the matrix; 3) alumina particles; 4) a light droplet phase that is amorphous and lower in Si relative to the matrix; and 5) dark crystalline microheterogeneities, which were crystalline but not identified. Following a nucleation heat treatment, the dark crystalline microheterogeneities are present, the light amorphous droplets form following 20 hours of heat treatment at $1058^{o}K$ and are indicative of phase separation. The phosphorous enriched forsterite phase is present following crystallization. Kriven and Risbud[43] identified Cu particles in a similar study of a Cu-cordierite system using the convergent beam electron diffraction technique.

II.B. PLASMAS

Before discussing the process of physical vapor deposition, a discussion of plasmas and ion surface interactions, topics which are intimately related to coating deposition processes, is in order. This section will present some of the important concepts involved with the plasmas used in coating deposition processes. These types

of plasmas are commonly known as abnormal glow discharges and may be maintained by either dc or rf power. A large portion of this section is from Chapman.[44] The reader may also find several references relevant to plasma diagnostics in the literature which are useful.[45-48] Initially in this section, some concepts related to collisions will be discussed, followed by the electron distribution function, floating potential, Debye shielding, dc glow discharge regions, and finally some experiments which investigate the character of plasmas.

II.B.1. COLLISIONS

The mean free path[44] of a gas species is the average distance the particles will travel between collisions with other particles of the same type. Most collisions in a gas at micron range pressures are binary, involving two species. An inverse relationship exists between pressure and mean free path. An approximate relationship for pressure (p) and mean free path (mfp) for atomic and molecular species is:

$$\text{mfp (cm)} = \frac{5}{\text{p(mTorr)}} \qquad (9)$$

The concept of mean free path may also be applied to the electrons, ions, and neutral atoms in a plasma.

A key idea in collisional processes is that of a cross section. The cross section basically reflects the likelihood that a particular event will occur.[43] The cross section for ionization of various gas species, as a function of electron energy is shown

in Fig. 8. It is thus observed that the electron energy which will most probably result in an ionization event, all else constant, is typically close to 100 eV.

II.B.2. ELECTRON DISTRIBUTION FUNCTION

The electron distribution function describes the system of electrons present in a plasma, defining the number of electrons with a particular velocity, at a specific position and at a particular time.[49] If the plasma electrons were at equilibrium, then the electron energy distribution function would be Maxwellian[50] and have the well known form shown in Fig. 9. The effects of an applied electric field, as from a cathode electrode in a sputtering system, and the inelastic collision depopulation, for instance due to energy loss from an excitation event, tend to shift the distribution from Maxwellian.[50] The field has the effect of pushing the distribution to higher energies while the inelastic processes tend to truncate the high energy tail (see Fig. 9). Deviations from Maxwellian behavior are particularly evident in the low pressure discharge regime,[51] possibly appearing bi-modal.

Qualitatively, one observes that the reaction that is producing ions is of the form:

$$e^- + Ar \rightarrow 2e^- + Ar^+ \qquad (10)$$

In low pressure gas discharges the reaction is essentially driven to the right, producing ions. The equation predicting the rate (R) of production[49] of ions is of the form:

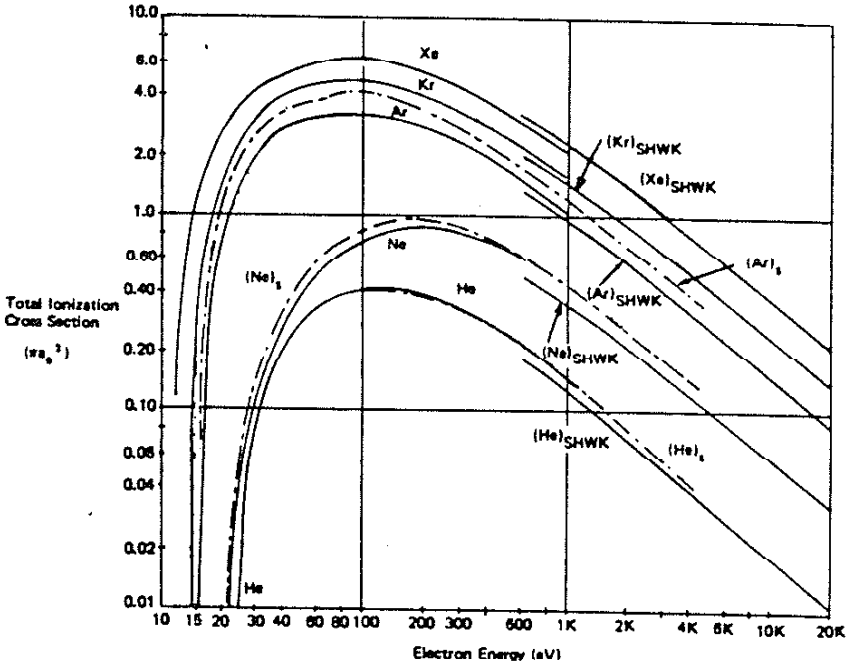

Fig. 8. Ionization cross section for inert gases as a function of electron energy. The results of three authors are presented here. See Chapman p. 29.

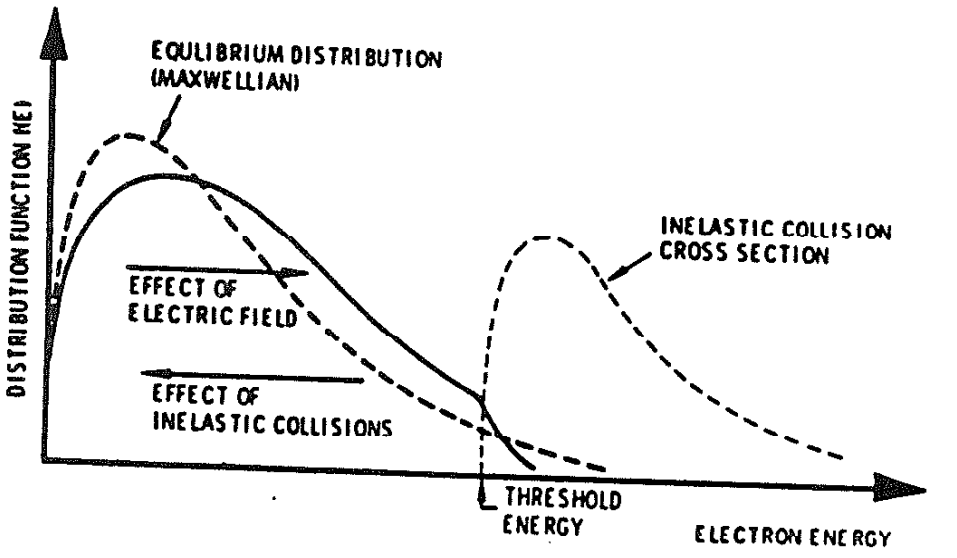

Fig. 9. The electron energy distribution function and factors which affect its form.

$$R = N_1 N_2 \langle \sigma v \rangle \tag{11}$$

where N_1 and N_2 are the densities of electrons and atoms and $\langle \sigma v \rangle$ is the average product of the electron velocity and ionization cross section. For the case of ionization, assuming a Maxwellian electron distribution function, the rate[51] is given by:

$$R_A = n_e N \sigma_o v_e \left(1 + \frac{E_o}{KTe}\right) \exp\left(\frac{-E_o}{KTe}\right) \tag{12}$$

Where n_e is the electron density, N is the target (atom) density, v_e is the thermal electron velocity[49] for a Maxwellian distribution which is,

$$\left(\frac{8KTe}{\pi m}\right)^{1/2}$$

and E_o is the threshold energy for ionization.

II.B.3. FLOATING POTENTIAL

If one imagines a plane suspended in a plasma, the number of neutral atoms, ions, and electrons passing through the plane is called the random flux[44] of each species and is determined by the equation:

$$F_i = \frac{N_i C_i}{4} \tag{13}$$

where C_i is the thermal velocity of the i^{th} species, and N_i is the density of the i^{th} particle, atom, ion, or electron.

Some of the most important characteristics of plasmas are determined by the fact that the ions have a much larger mass than electrons, thus they have lower mobilities and respond to fields much slower than electrons.[44] Electrons typically have a much higher thermal velocity than ions and therefore the random flux of electrons given by equation (13) is much higher than that of ions. Considering constraints of charge neutrality, $n_i = n_e$;[44] in the ideal case a plasma is considered to be electric field free.

One of the relevant considerations about discharges is the manner in which they interact with surfaces. If one imagines an insulating surface such as from a ceramic material which is brought into ambience with the plasma, the surface will initially begin to charge negatively since the random electron flux is greater than the random ion flux. As it becomes more and more negative, electrons of increasing energy will not be able to approach the surface due to the increasing electrostatic field. In the limit, the repulsion will be so great that the electron flux is reduced to the ion flux. In other words, electrons must wait for ions to enter the region of the electric field, more commonly known as a sheath, adjacent to the surface before they may approach the surface. This sheath is a region of net space charge, e.g., $n_i \neq n_e$, and has the action of accelerating positive ions toward the surface, while accelerating electrons away from it. The potential assumed by this insulator surface is known as the floating potential.[44] The plasma also has a potential known as the plasma or space potential.

The plasma potential tends to be the most positive potential in the system.[44]

II.B.4. DEBYE SHIELDING

Plasmas tend to stay electric field free through a mechanism known as Debye shielding.[44] If one imagines a sudden small potential perturbation in the plasma of <V>, which is negative, the plasma will respond to the voltage by forming a region of positive space charge (sheath) adjacent to it. This results in attenuating the field presented by the voltage fluctuation. Fig. 10 illustrates field attenuation as the region near the perturbation approaches the plasma potential. If Poissons equation is solved[45] to determine the variation in potential around the perturbation, then the solution is of the form:

$$\Delta V(x) = \Delta V_o \exp \frac{-|x|}{\lambda_D} \qquad (14)$$

where x is the distance from the perturbation, ΔV_o is the magnitude of the potential fluctuation, and λ_D is the Debye length. The Debye length gives an indication of how rapidly the field is attenuated, as it reflects the distance at which the voltage perturbation falls to 1/e of its maximum value. A value for λ_D = 105 μ is given in Chapman for <E> = 2eV and $n_e = 10^{10}$ cm^{-3}.

II.B.5. D.C. GLOW DISCHARGES

A plasma may be defined as a gas consisting at least partially

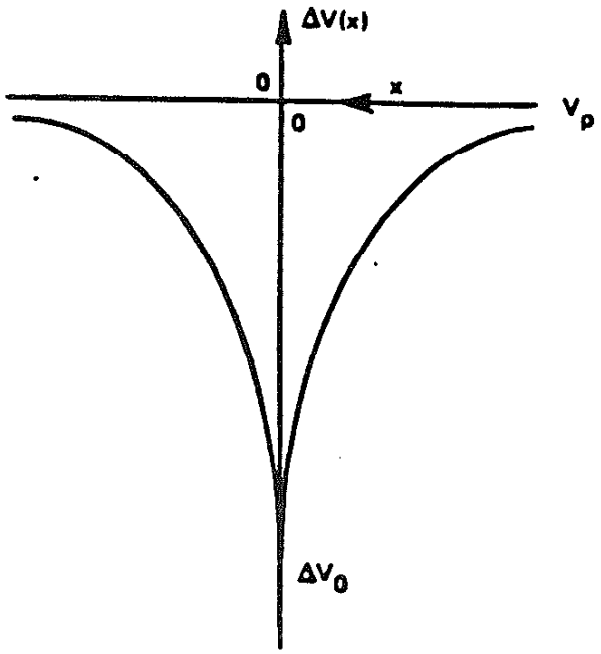

Fig. 10. Attenuation of electric field from a negative potential perturbation in a plasma. The potential rapidly approaches the plasma potential.

of ionized atoms and electrons in addition to neutral atoms, with charge neutrality.[44] The density of charged particles in the plasmas of interest in coating deposition processes is of the order of $10^9 - 10^{10}$ cm^{-3},[52] with a degree of ionization of less than 1%. In other words, the fraction of atoms which are ionized is less than 1 in 100. This section will refer to plasmas in this category, which are known as glow discharges.

There are several regions in a dc glow discharge which appear under experimental conditions which should be considered. The cathode region, the negative glow, and the positive column are of widely varying character and have been identified.[44] Fig. 11 is a schematic of the various regions in a dc glow discharge with graphs of intensity, potential, field, space charge density, and current density. The cathode region has a very strong electric field as the cathode may be negatively biased to several kV. Adjacent to the cathode region is the negative glow which is a region of moderately strong and varying field. The positive column follows on the side of the negative glow, opposite the cathode. This region has a weakly varying field and most nearly resembles a plasma in terms of being electric field free as well as space charge neutral compared to the others.

There is a variety of phenomena occurring in the cathode sheath. These include: positive ion acceleration to the electrode; secondary electron emission from the cathode due to various processes such as the ion bombardment and photon bombardment and subsequent acceleration of these secondary electrons across the

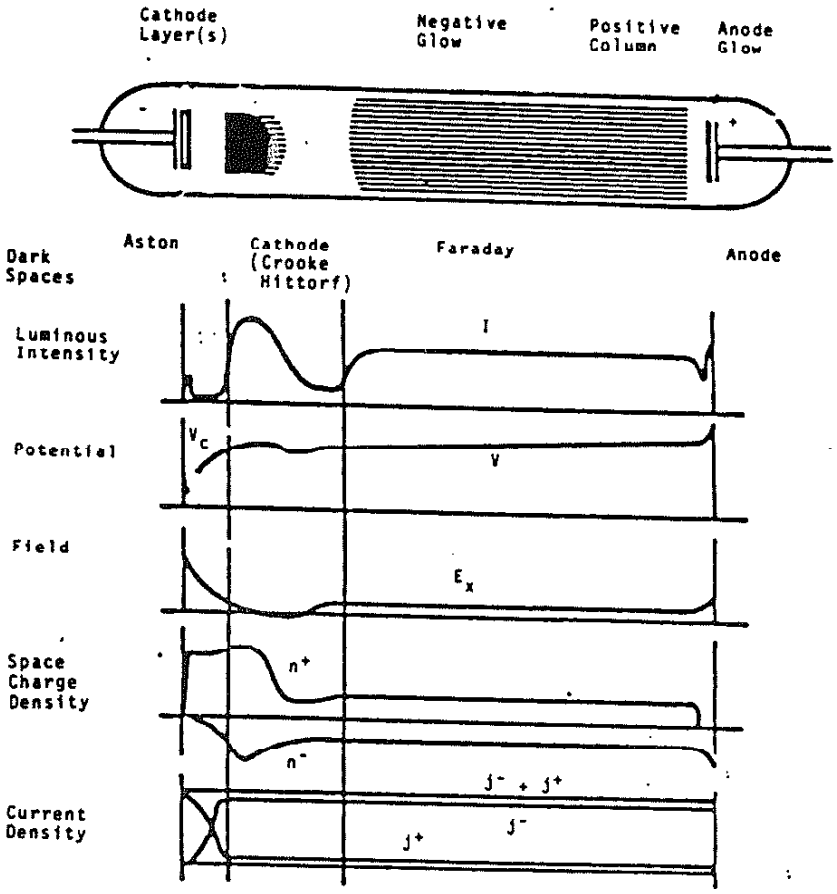

Fig. 11. The various regions in a glow discharge and the general character of each.

sheath and away from the cathode; some inelastic processes of excitation in the sheath as electron energies approach the highest cross section value near 100 ev; and charge exchange processes. Charge exchange processes occurring in the sheath are responsible for the production of energetic neutral particles as well as slow ions.[44] The situation is depicted in Fig. 12. When an ion enters the cathode sheath it will likely collide with a neutral particle prior to impacting the surface since the sheath thickness may be several times the mean free path and the degree of ionization is low. The process of charge exchange, whereby the neutral atom gives up an electron to the ion, during the collision, has a high cross section. The cathode sheath is typically much greater than a Debye length. The reason for this is that the cathode sheath consists of three regions: 1) a pre sheath satisfying the Bohm criterion, 2) a Debye region, and 3) a space charge limited current region.[44] The Bohm criterion essentially states that there exists a minimum energy that an ion must have upon entering the large potential drop adjacent to the cathode. This condition is imposed by conservation of energy, and thus a weak field is present to increase the ion energy beyond the critical value. The Debye region is present as the potential variation in that region is of appropriate magnitude where the Debye shielding phenomena is applicable. The space charge limited current region is present due to the fact that as ions initially enter the high field they may locally experience repulsion due to interaction with other ions; hence the space charge limitation. Cathode sheaths may be several cm in thickness. Further discussion may be found in Chapman.[44]

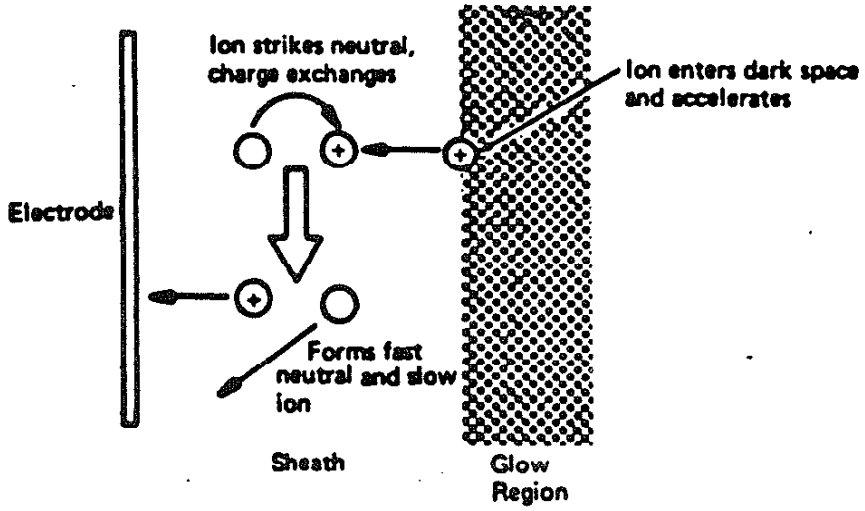

Fig. 12. A charge exchange event in the cathode sheath. An ion becomes an energetic neutral while a neutral becomes a slow ion.

The negative glow is a region of the plasma adjacent to the cathode sheath. As indicated in Fig. 11, the electric field is of a varying character. The negative glow may be the least understood of the regions in an abnormal glow discharge. The majority of ionization which sustains the plasma is believed to occur here, according to Chapman. One of the key considerations in rationalizing that statement is that although the secondary electrons which probably sustain ionization in the plasma upon exiting the sheath have a high energy, their energy is rapidly attenuated by plasma waves, which are regions of space charge that move through the discharge at various frequencies, much like waves in a lake. The electrons then have a mechanism for increasing the collision cross section for ionization, which is a function of their energy. Some of the ions produced in the negative glow will end up at the sheath edge where they will be accelerated and collected as current.

The anode has a sheath also which is very thin since the ion density does not vary as much as near the cathode sheath. The grounded walls of a vacuum chamber are commonly the anode in practical deposition experiments. According to Chapman, the anode sheath also tends to accelerate electrons into the plasma, since the anode is usually negative with respect to the plasma.

II.B.6. GLOW DISCHARGE EXPERIMENTS

Davis and Vanderslice[53] derived a theoretical expression to compare to the measured ion energies impinging on a cathode in an abnormal (ion plating type) glow discharge. The model they used consisted of four elements:

1) All ions originate in the negative glow or the low field region between the glow and the cathode fall.
2) For the charge transfer process previously mentioned, it is assumed that the ions produced begin acceleration from zero velocity.
3) The collision cross section for charge transfer is constant, independent of energy.
4) The electric field is linear between the cathode and negative glow.

The experimental portion of the study involved measuring the ion energies that would impinge upon the cathode in a discharge. Pressures in the range of 13.3 Pa to several hundred Pa were used. In some cases, significant ion intensities were obtained at energies equivalent to the cathode potential. This seems to occur when the charge exchange mean free path is large. Gas pressure did not greatly influence the ion energy distribution at constant voltage. The authors state this is possible since the product of pressure and dark space distance is constant at constant voltage. Therefore, the average number of collisions sustained by each ion traversing the dark space is approximately constant. With a small mean free path, ions tend not to impinge on the cathode with the energy of the entire cathode electric field.

Carter, et. al.,[54] pursued a similar experiment and directly measured ion and neutral particle energies incident on the cathode of a glow discharge. Pressures used in this study are in the range

of 4 Pa to approximately 60 Pa. Increasing pressures were observed to decrease the maximum ion energy measured, as well as generally shift the distribution to lower energies. The effect of discharge voltage on the Ar ion energy distributions is shown in Fig. 13. The effect that the applied voltage has on neutral support gas particles and Cu^+ ions in an Ar supported discharge is shown in Figs. 14a and 14b. Generally, it is observed that increasing voltages shift the distribution to higher energies. This experiment exemplifies the importance of charge exchange collisions as essentially no particles were collected with greater than 1/3 to 1/2 of the applied discharge voltage. It also illustrates the fact that neutral species impinge on the cathode with substantial energy, much greater than thermal. Neutral particles deposit more total energy on the cathode than the ion species. Although the pressure ranges investigated by Davis and Vanderslice and the Carter group are quite different, the conclusion that pressure does not greatly affect the distribuiton of ions as well as the statement that the maximum ion energies typically arriving at the cathode have less than the maximum possible energy seem to be in concurrence. Teer[55] modeled the region of the cathode fall and found that most of the deposited energy from particles came from neutrals under specified conditions.

II.C. ION AND ENERGETIC NEUTRAL ATOM/SURFACE INTERACTIONS

While the previous subheading was related to the sheath and some of the various processes occurring in the ionized gas, the following section is related to observations, and phenomena that

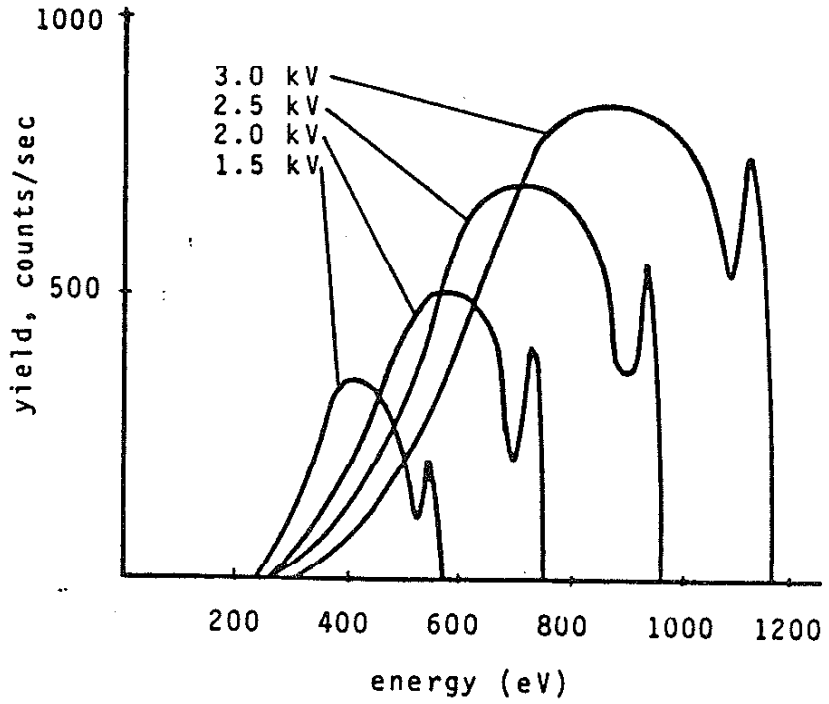

Fig. 13. The effect of cathode voltage on the Ar support gas ion energy distribution impinging the cathode. The pressure is approximately 4 Pa.

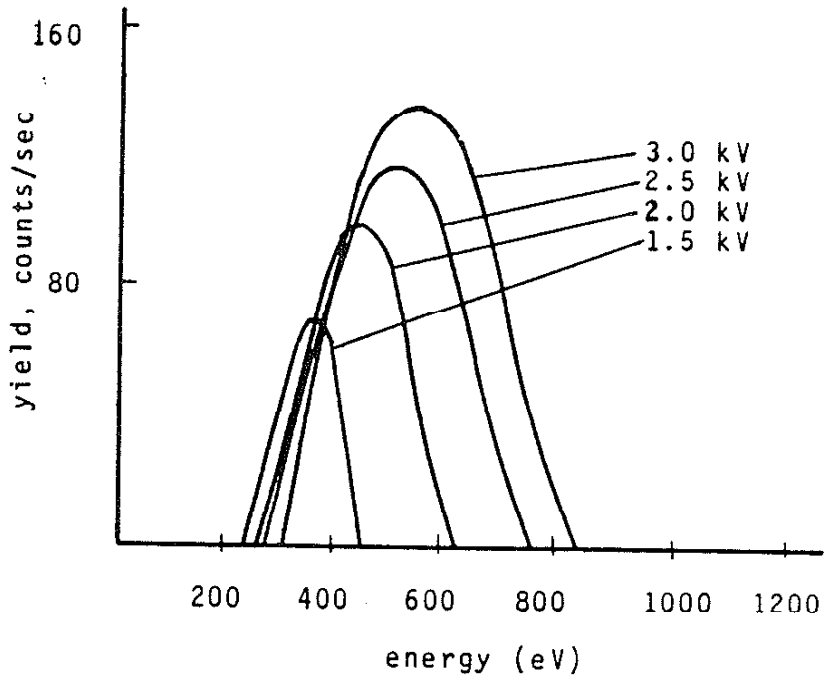

Fig. 14a. The effect of cathode voltage on Ar support gas neutral energy distribution impinging the cathode. The pressure is approximately 4Pa.

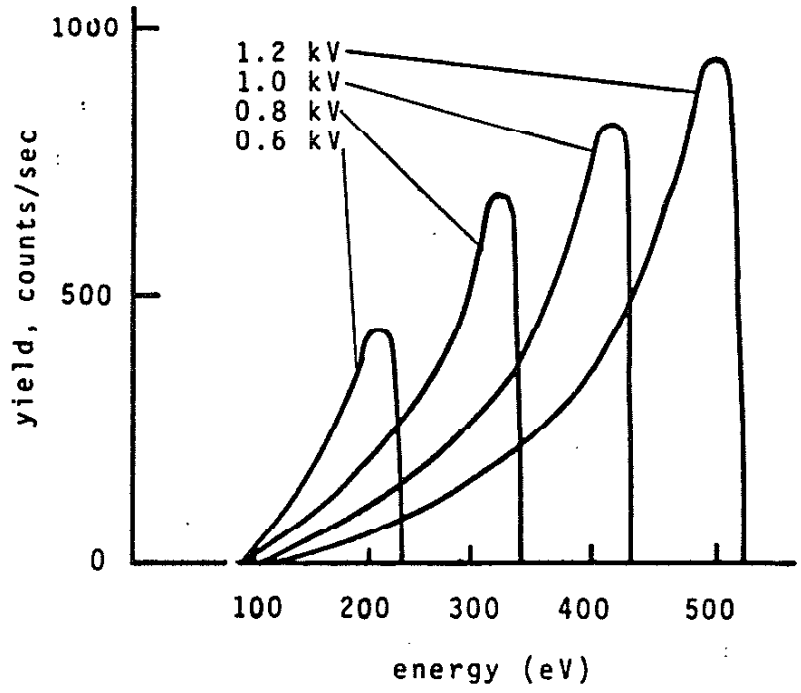

Fig. 14b. The effect of cathode voltage on Cu ion energy distribution impinging the cathode. The pressure is significantly greater than 4 Pa.

occur as a result of energetic particle bombardment of the solid (cathode) surface.

II.C.1. ION NEUTRALIZATION

As described in detail by Hagstrum[56] one process which occurs as an ion approaches a surface is that of ion neutralization. Prior to impacting a solid surface, an ion may be neutralized due to electron emission from the surface.[56] The two processes which may result in neutralization are that of 1) Auger neutralization and 2) resonance neutralization followed by Auger deexcitation. Figs. 15a and 15b are schematics of these two processes. Qualitatively, the Auger neutralization process involves 2 electrons; 1 electron tunnels from the solid at E less than the Fermi energy to the ground state of the approaching ion, while a second electron is emitted from the solid. Tunneling refers to the wavelike properties of an electron.[57] An electron has a certain probability of traversing a potential barrier, in this case the work function, of less than infinite height. The first electron loses energy, while the second escaping electron gains the same amount of energy. The second neutralization scenario begins by an electron in the solid tunneling from $E < E_f$ (Fermi energy) to an excited state of the same energy in the approaching species. This neutralization is followed by Auger deexcitation of the species. This may occur in one of two ways. Either the excited atom decays to its ground state with the emission of an electron from the solid or an electron in the solid may transfer an electron to the ground state of the atom followed by emission of the electron from the excited state energy level of the atom.

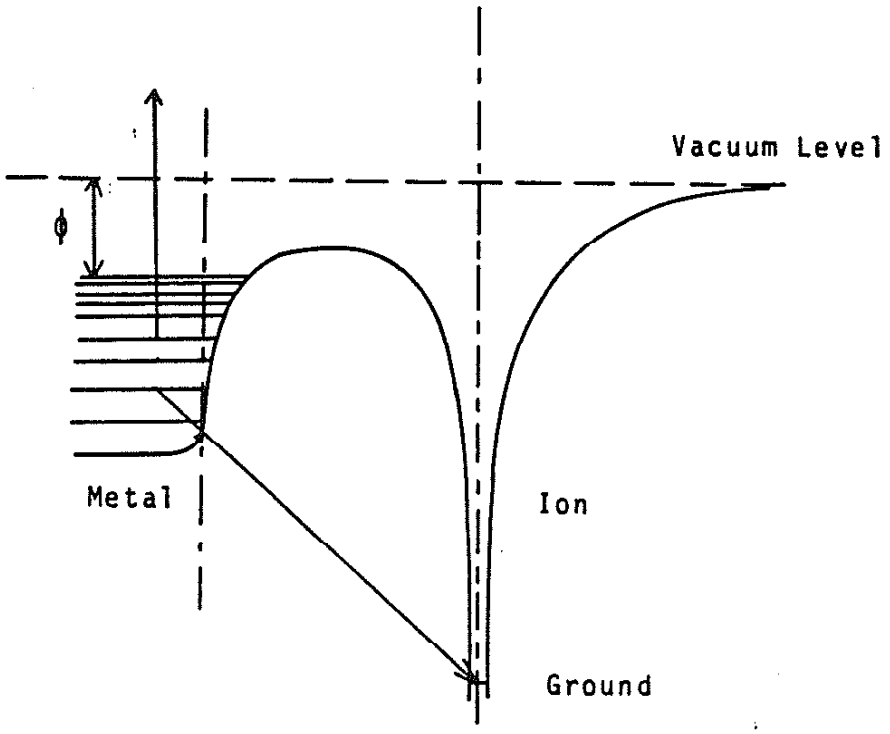

Fig. 15a. The Auger neutralization process. An ion approaching a metal surface receives an electron in its ground state while the solid emits an electron of the same energy as the first transition.

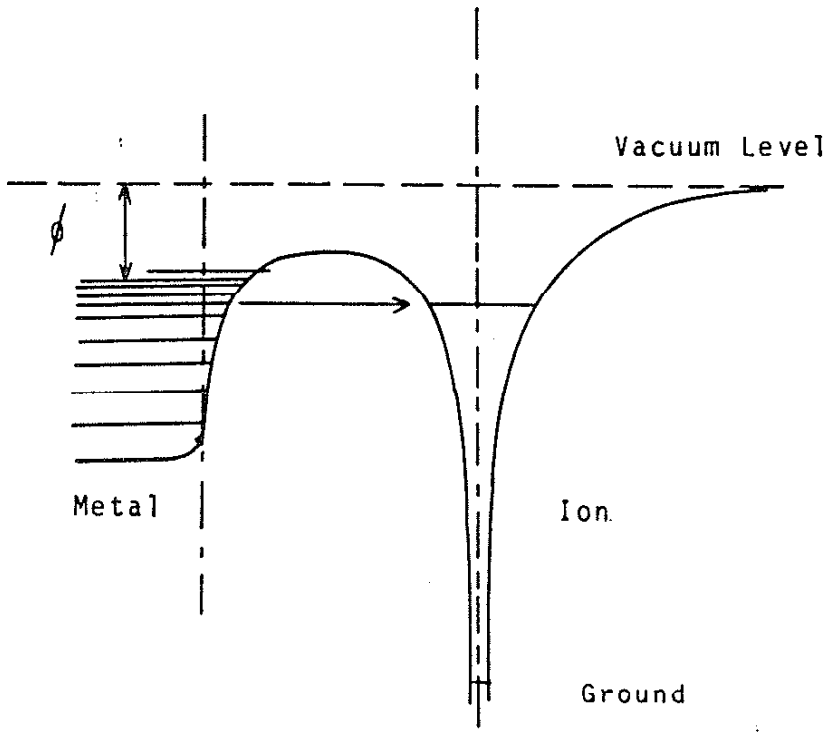

Fig. 15b. The resonance neutralization process. An ion approaching a metal surface receives an electron in an excited state. This may then be followed by a relaxation event.

II.C.2. SURFACE DIFFUSION

Surface diffusion, the migration of atoms on surfaces, is influenced by ion impact as indicated in several studies.[58,59] The study of Rossnagel, Robinson, and Kaufman,[58] involved sputtering Cu and Al substrates with impurity additions to the surface of either Ta, Mo, or C. This experiment is based on the premise that impurity atoms migrate and form clusters which lead to cone formation. Impurity shadowing is a mechanism by which cones are believed to form.[60] Cones commonly form on sputtered surfaces and will be discussed in the section on surface topography. The average cone spacing was calculated, following SEM observation, as a function of substrate temperature and ion current density. Generally, cone spacing is observed to increase with increasing current density. By using the random walk path length equation, which is:

$$r = r_o \exp\left(\frac{-E_d}{2KT}\right) \qquad (15)$$

where r is the path length, r_o is a frequency factor, and E_d is the activation energy for surface diffusion, the authors determined an 'effective' E_d, which increased with increasing substrate current density. This equation is from another study examining thermal and bombardment modified diffusion.[58] Also, the pre-factor r_o in the random walk equation was being affected as a function of ion current density. Since an increased binding energy would probably be considered to limit diffusion and thus decrease cone spacing, the authors deduced that the increase in the pre-factor r_o in the random walk equation must be dominating over the effects of increased binding energy.

A study by Marinov[61] supports the hypothesis that surface migration of adspecies is enhanced by ion bombardment. The apparatus used in this experiment sputtered a region of a surface onto which material was being deposited. The presence of deposited material was clearly observed on regions of the substrate which were neither bombarded, nor deposited onto. This sample was compared to another sample which was subjected only to depositing material, without bombardment.

II.C.3. SPUTTERING

Sputtering is the process of ejection of atoms or molecules from a solid surface which is experiencing bombardment by an energetic particle.[62-66] The energetic particle may be a neutral, ion, or a fast atom (electron). The sputtering process itself occurs very near the surface and involves the movement of several or many atoms in the solid. When an energetic particle enters a solid, atoms are displaced from their lattice sites. These primary knock-on atoms may also be very energetic and cause further atomic displacements within the solid. This process is continued until the energy is dissipated. The collection of atoms which is caused to move and interact within the solid in this fashion is called a collision cascade.[67] If the lattice structure is preserved within the cascade volume, and a small fraction of the atoms is in motion, then the process is said to be in the linear cascade regime.[67] Linear in this sense means that the cascade may be considered as a series of independent binary collisions between atoms.[67] The linear regime refers to 10^3 to 10^5 eV medium mass in-

cident particles. A typical cascade has a radius of 100 Å.[68] The spike regime is achieved when the atomic order is destroyed local to the cascade and all atoms within the cascade volume are in motion. Figs. 16a and 16b compares the linear and spike regimes. Intuitively, it should be clear that the spike regime refers to incident particle energies significantly greater than the linear regime. A sputtering event occurs when a cascade delivers energy to a surface atom which is greater than its binding energy, U_o. The third regime of sputtering is called the low energy or light ion region. The modeling of this regime is extremely complex due to the fact that crystallographic considerations of the solid come into play.[68] For the linear and spike regimes, the solid is considered as an isotropic media, hence the complexity of considering crystallographic directions is not necessary.

The sputtering yield is defined as the number of atoms ejected per incident ion. According to Sigmund's model[44] of the linear region, the sputter yield S is given by:

$$S = \frac{3\alpha}{4\pi^2} \frac{4m_i m_t}{(m_i + m_t)^2} \frac{E}{U_o} \qquad (16)$$

where E is the incident ion energy, U_o is the surface binding energy, m_i and m_t are the masses of the incident ion and target atom, respectively, and α is a monotonic increasing function of m_t/m_i. There are a few key features about this equation which should be noted. The effect that E and U_o have on the sputter yield are clear; as the incident energy increases, the yield increases and as

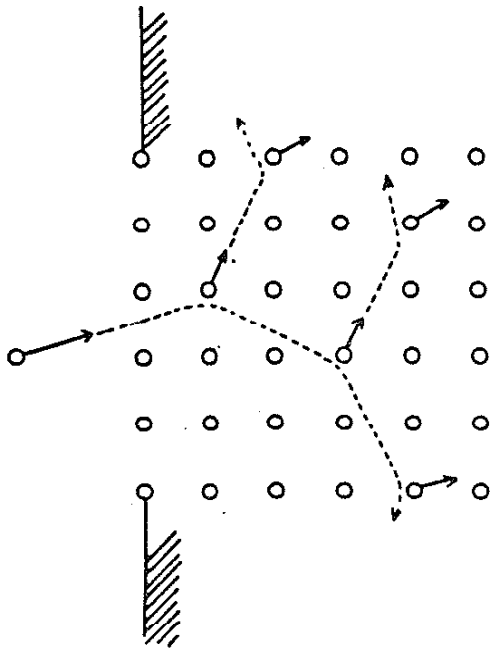

Fig. 16a. The linear cascade regime. The structure of the cascade volume is preserved and a small fraction of the atoms is in motion.

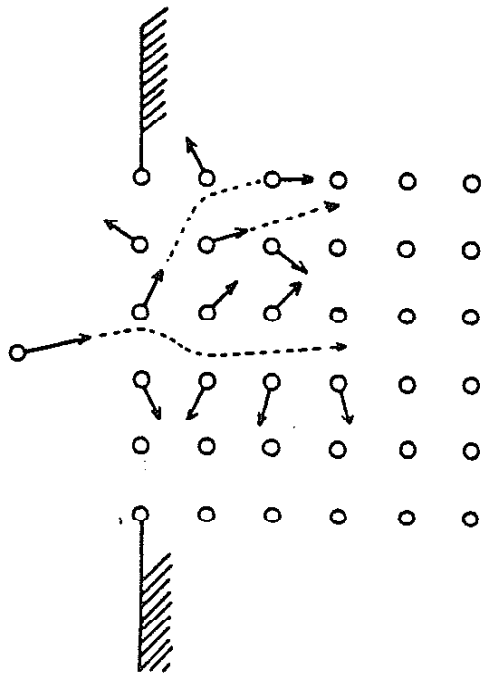

Fig. 16b. The spike cascade regime. The structure of the cascade volume is destroyed and all atoms in the cascade volume are in motion.

the binding energy increases, the yield decreases. The quantity

$$\frac{4m_i m_t}{(m_i + m_t)^2} \tag{17}$$

is popularly referred to as the energy or momentum transfer function for two particles in a binary collision.[44] This quantity has a maximum value when m_i and m_t are equal, which corresponds physically to the greatest amount of energy being transferred from the incident to the target particle.

Sputtering is a very inefficient process. It is estimated that 1% of the incident particle energy results in particle ejection while 75% goes into target heating and the balance drives the secondary electron emission process.[69] A typical experimentally determined curve for the sputter yield as a function of ion energy is shown in Fig. 17. At lower energies, S increases with energy, goes through a peak and drops off at higher energies as implantation events become significant.

II.C.4. ALTERED SURFACE LAYERS

There are several events which may occur during particle bombardment of a solid surface which will effectively alter the stoichiometry and possibly the structure of a non-elemental solid.[70] Some of these events are cascade mixing, recoil implantation, radiation enhanced diffusion and preferential sputtering. Discussion of each of these phenomena will be presented in succeeding sections. They are relevant to ion plating processes and thus form a

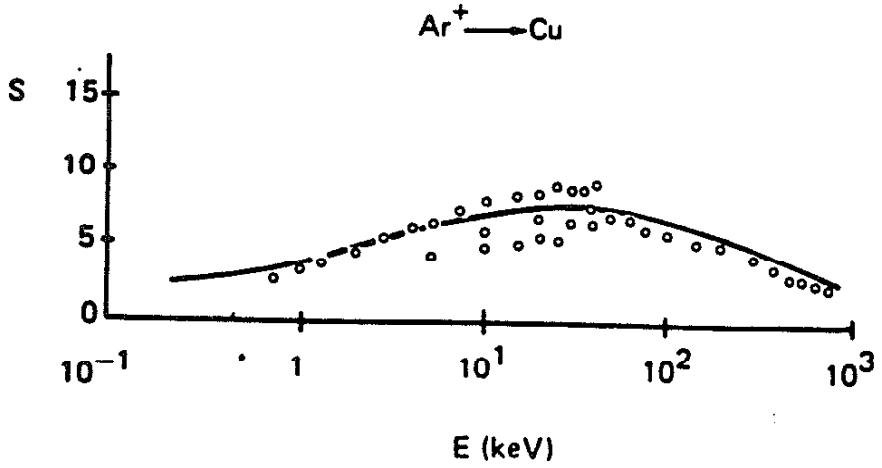

Fig. 17. Sputtering yield of Cu as a function of incident Ar ion energy. The experimental values are close to those predicted by theory.

foundation on which to understand the film substrate mixing and defect structures observed in ion plated samples.

II.C.4.a. CASCADE MIXING

Cascade mixing[71,72] is a process by which atoms in the near surface region of a solid are rearranged or mixed as a result of bombardment. In cascade mixing, collisions occur not only between the incident ions and target atoms but also between target atoms, which receive sufficient energy from the incident species to displace other atoms from lattice sites. Recoil implantation, which is the implanting of a target species due to a collision with an energetic particle is thus a subset of this mixing process and will be discussed in the next section.

Carter and others[73] have applied a diffusion approximation to cascade mixing. Carter's approach is to modify the Einstein relation,

$$D = \frac{1}{6} \nu l^2 \qquad (18)$$

where D is the diffusion coefficient, ν is associated with the atomic migration attempt frequency and l is related to the atomic hop distance. The modification is incurred by using the atomic recoil frequency of an atom in a solid under bombardment in place of the migration attempt frequency. From this study it was deduced that the broadening width of a plane of atoms at a distance R below the surface is given by,

$$(\Delta x)^2 \approx \frac{4}{6} \frac{n(E)}{Y} l^2 \qquad (19)$$

where Y is the sputter yield and n(E) is the number of atomic displacements within a volume v(E). It should be clear that one effect of bombarding a solid is the production of damage in the near surface region. Miranda and Rojo[73] discuss some effects of this damage.

II.C.4.b. RECOIL IMPLANTATION

Qualitatively, recoil implantation is the displacement of an atom from a lattice site where the impacted atom has energy imparted to it by the incident particle.[74-76] The recoiled atom then continues through the solid, displacing atoms if it has sufficient energy and finally coming to rest. One area of practical relevance for this process is ion beam mixing,[77-79] which usually involves radiating the surface of a solid with high energy ions thereby driving atoms near the crystal surface deep into the bulk. Nelson[75] has presented an equation for the recoil flux of species from a thin layer of deposited material on a bulk solid subjected to ion bombardment. The flux of recoils across any plane in the solid with energy within an interval dE at E is:

$$\phi(E,E_1) \approx \frac{D}{E^2} \int_E^{\hat{E}_r} S(E_r) E_r dE_r \qquad (20)$$

where $S(E_r)$ is the primary recoil flux which initiates further recoil events, E_1 is the energy of the incident particles which is sufficiently large that energy loss in the evaporated layer may be ignored, $S(\hat{E}_r)$ is the energy transfer function for a binary collision,[44] and D is the mean interatomic spacing. An interesting point to consider is the difference in the distribution shape for recoiled species and those directly implanted. Fig. 18 compares the distribution of directly implanted B into Si with B which has been recoil implanted by bombardment with Ne^+ ions. The figure indicates that the recoil spectrum of B is quite concentrated near the Si surface. The directly implanted B takes on a well known gaussian form, which is quite typical for directly implanted species.[80] The fact that the recoiled distribution is so concentrated probably reflects the fact that species are seldom recoiled more than once by an incident ion, along with the fact that the recoiled species obtain a small fraction of the incident energy during the collision.[75]

II.C.4.c. RADIATION ENHANCED DIFFUSION

Ion enhanced diffusion at a surface is generally some sort of accelerated mass transport process which results in a compositional profile (for binary or non-elemental materials) at the surface which quite often may not be explained by bulk thermal effects alone. An experiment by Shimizu and Ono is a good illustration of the phenomena.[81] They were monitoring the near-surface chemistry of two binary alloys (Cu-Ni) which were being bombarded with 3 keV Ar ions. The experimental variables were the current density to

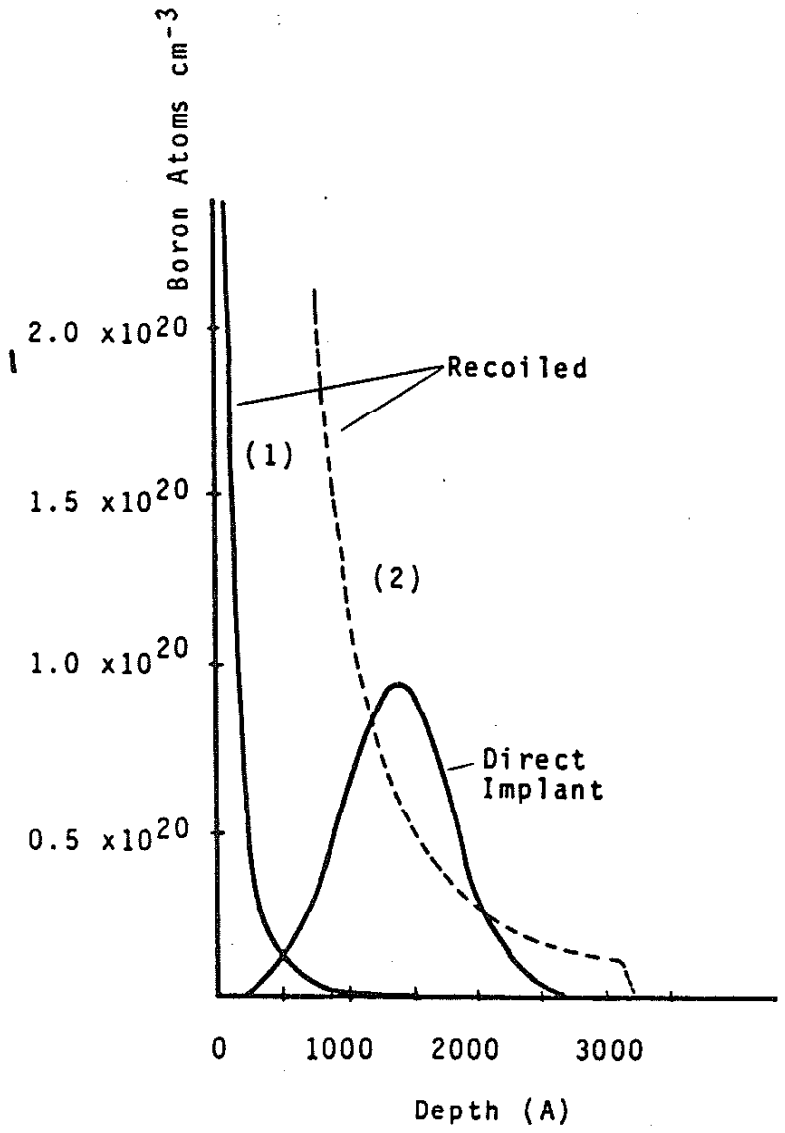

Fig. 18. Recoil and calculated direct implant spectra for B into Si. Curve 1 is a recoil distribution for 10^{15} B atoms with a recoil energy greater than 1 keV from a thin surface layer radiated with $5x10^{16}/cm^2$ 100 keV Ne ions. The gaussian curve represents 10^{15} B atoms directly implanted at 40 keV. Curve 2 is a recoil spectrum of B radiated with a very large dose of $5x10^{18}$ Ne^+.

the target and the temperature of the target. It is instructive to note at this point that these two variables compete with each other. Cu sputters preferentially from the alloy, while temperature will drive Cu to the surface from the bulk. Thus, the rates at which Cu is being removed and supplied to the surface are the experimental variables. Typically, the results of these experiments are the production of a Cu depleted region (see Fig. 19) adjacent to the surface which is more or less at a steady state condition with the surface and the bulk matrix after some amount of time. The authors fit their data to a diffusion equation which was developed by Eltouky and Greene[82] to determine the ion enhanced diffusion coefficients as well as the effective activation energies for this enhanced diffusion. The equation is relevant to diffusion of elements in a solid under bombardment. The equation is:

$$\theta(x) = C + [\theta_{(o)} - C] \exp(-xV/D^*) \qquad (21)$$

where $\theta(x)$ is the concentration of a species at a depth x, C is the matrix composition, V is the surface recession velocity, and D* is the ion enehanced diffusion coefficient. This equation is for a steady state condition, thus time independent, being a function only of depth. The steady state profile is a function of temperature also, i.e., at constant V, as T increases then the surface concentration increases. At temperatures > 573K they observed repeated recrystallization of the sputtered sample near the surface region. The activation energy for the enhanced diffusion was 5.4 kcal/mole,

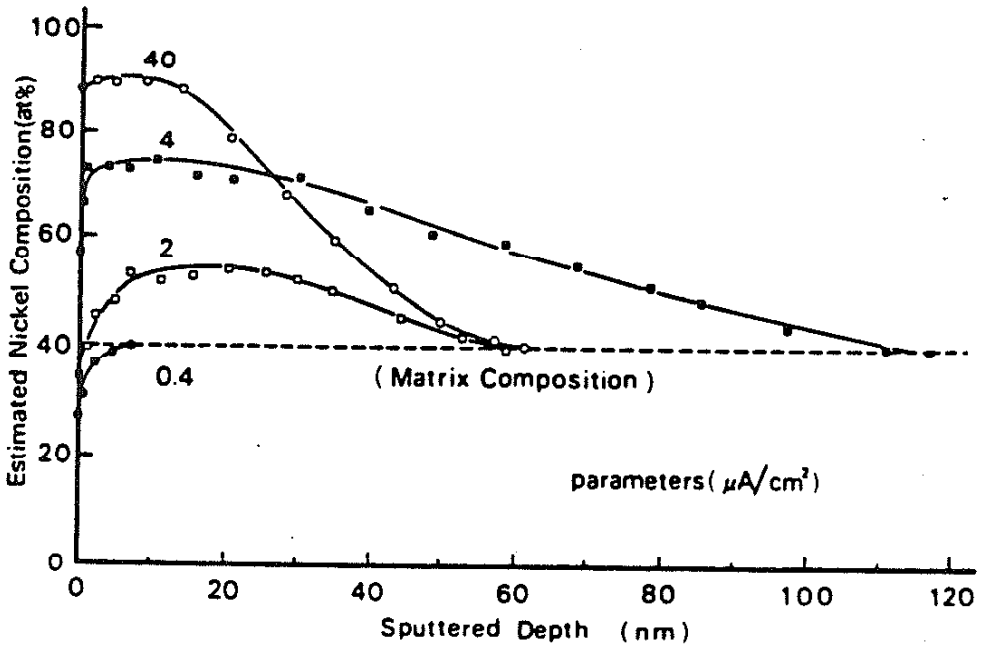

Fig. 19. Steady state Ni concentrations as a function of depth and current density. These samples were sputtered at 873 K for 1 hour.

which is in good agreement with an interstitial type mechanism. Knock-on and implanted atom depths are too shallow by an order of magnitude to account for the measured profile.

Rivaud, et. al.,[83] studied the effect of low energy ion bombardment on the near surface region of a Cu-10% In alloy, which was in a super saturated state (single phase) prior to irradiation. Precipitation of delta phase particles was observed for ion energies of 1 and 3 keV (Ar^+) at doses of approximately $10^{16}/cm^2$ in the STEM. The proposed mechanism of this observation is that vacancies produced in the near surface region allow mass transport of solute to matrix nucleation sites, e.g., dislocation tangles present in the near surface region. Vacancy currents flow to the surface as well as to these dislocation tangles. This ion induced precipitation is observed to occur at $T < 373^oK$. Thermal precipitation is observed at the grain boundaries but not the matrix as for the ion-induced case and did not occur for $T < 523^oK$.

II.C.4.d. PREFERENTIAL SPUTTERING

Preferential sputtering of a multi-element target can result in an altered surface layer composition relative to the composition prior to sputtering. This is due to the preferential removal of one or more elements in the near surface region, thus resulting in stoichiometric shifts relative to the bulk chemistry. A survey for oxide sputtering is given by Kelly.[84] Kelley[85] has investigated the dependence of bombardment induced compositional change relative to target masses as well as binding energies in the solid. By modelling recoil sputtering which is the sputtering of atoms im-

pacted directly by the incident particle, and recoil implantation, the theory predicts that binary target surfaces tend to become enriched in the heavier component.[85] Several oxides show loss of oxygen in the surface region while a substantial number do not have a loss of oxygen. Binary alloys have also been investigated for evidence of preferential sputtering of a component. Binary alloys exhibit preferential loss of heavier components, lighter components, as well as a preferential loss when components have nearly the same mass. Thus, the authors conclude that mass differences do not appear to be relevant to preferential sputtering experimentally, although theoretical grounds for such relevance are clear.

Near surface compositional changes as a result of particle bombardment related to chemical binding effects could be produced by cascade sputtering, thermal sputtering and surface segregation.[85] Cascade sputtering is related to the surface binding energy. If sufficient energy in a collision cascade is delivered to a surface atom then it will be sputtered. Good correlation is observed between the atoms preferentially lost from binary alloys and the atom with the lower heat of atomization. Thermal sputtering [85,86] may be divided into two groups, prompt and slow. Prompt thermal sputtering is understood in terms of vaporization as a result of a temperature excursion. Slow thermal sputtering is vaporization without the thermal excursion. Thermal sputtering is shown to have good correlation between sputtering yield ratios and observed composition changes of sputtered binary alloy targets. Surface segregation,[85,87] is the preferential transport of an element to the surface. The driving force for this is a reduction in surface energy.

Surface segregation can sometimes result in 100% coverage by one component.

II.C.4.e. RADIATION INDUCED SEGREGATION

The phenomenon of radiation induced segregation is the preferential transport of elements to defect sinks.[88] A defect sink is a region in the solid where the vacancies are annihilated, such as a surface, interface, or dislocation loop. There are two processes which must occur to establish radiation induced segregation.[88] The first criterion is that defect fluxes must be present, into or out of spatial regions, persisting in time. The second necessary condition is a preferential coupling of certain alloying elements to these fluxes. It is important to note that unless the exact atomic fractions of the bulk alloy participate in these defect fluxes, segregation must occur. The most straightforward reason for a defect flux into a particular region is that the vacancies are being annihilated in that region. Direct evidence for the presence of persistent defect fluxes may be found in the growth of dislocation loops and voids.

Rehn, Lam, and Wiedersich,[89] studied the surface vs. depth compositional profile of an ion bombarded Cu-Ni alloy using Auger spectroscopy. They identified two distinct exponential-like compositional variations at different depths in the alloy. Radiation enhanced diffusion is believed to be the cause of the profile in the shallower region, on the order of 100 nm, while radiation induced segregation is responsible for the profile at larger depths, on the order of 100's of nm. This data was for the case of 5 keV

Ar^+ ions at a temperature of 773°K. Previous work by this group[90] presented a model describing various atomic processes which influence compositional profiles. Processes in this model include: Gibbsian adsorption, preferential sputtering, displacement mixing, radiation-enhanced diffusion and radiation induced segregation.[90]

Cauvin and Martin[91] observed precipitation of Zn $\underline{\beta}$ phase particles in undersaturated solid solutions exposed to electron irradiation. The precipitation was observed in-situ in a 1 MeV HVEM at temperatures above the Zn solvus boundary. The authors attribute this phenomena to radiation induced precipitation.

II.C.4.f. CHEMICAL MIXING

Baglin, Clark, and d'Heurle,[92] point out that chemical effects in ion mixing related experiments are often neglected. To illustrate chemical effects in mixing, they formed metal bilayers via evaporation techniques, followed by Kr^+ ion irradiation and subsequent Rutherford Backscattering Spectrometry (RBS) analysis to determine the amount of mixing between layers. The initial deposit layer was either Zr or Pd onto oxidized Si followed by a deposit of a thin layer of one of the following elements: Hf, Ta, W, Ir, or Pt. By observing the periodic chart, Hf is most like Zr chemically while Pt is least similar; conversely, Pt is most similar to Pd chemically, while Hf is the least. The remaining 3 overlayers lie in between the two extremes with respect to Pd and Zr. it should also be noted that while these 5 different overlayers differ greatly in chemical behavior, the physical attributes such as atomic

scattering cross section are quite similar. It is observed in this experiment that bilayers which have the greatest value of the square of the electronegativity difference, exhibit the most mixing, while mass effects do not positively correlate with the observed mixing nearly as well. Baglin and co-workers also note that the mixing does not correlate with the melting points of the components in the different systems, which is interpreted as a measure of atomic mobility. No mention of mobility enhancement due to damage in the materials is stated, however.

Tan, et. al.,[93] monitored the binding energy shifts of Si atoms deposited onto Ni and Mo at room temperature for different coverages, using X-ray Photoelectron Spectroscopy (XPS). For the case of Si on Ni, a wide variation in binding energy shift is observed prior to attainment of a value which would be expected for amorphous Si. Si binding energy shifts on Mo approached the amorphous Si value much more directly than the aforementioned system. The authors attribute these observations to a broader interfacial region for the case of Si on Ni, which is induced via greater chemical interaction between this pair of elements.

II.C.5. NUCLEATION EFFECTS

It is generally considered in the literature that ion bombardment of a growing film modifies the nucleation and growth kinetics over those of conventional evaporation. Several studies have investigated the effects of energetic bombardment on the initial stages of nucleation and coalescence of deposited films. The experimental apparatus of Marinov[61] allowed the formation of thin

evaporated films with marked ion bombardment, weak bombardment and absence of bombardment, all in one deposition run. Some of the general characteristics to be noted which distinguish radiated and non-radiated regions are the fact that the coalescence stage in interface formation is accelerated[61] by ion bombardment. Larger and fewer clusters of atoms are observed with increasing bombardment. This is attributed to enhanced mobility of atoms. Also, a more non-uniform size distribution of islands results from ion bombardment. In another experiment by Marinov,[61] films in a later stage of growth, just prior to complete coverage of the substrate, were bombarded and atom depleted zones developed around the growing clusters.

Another study conducted by Shawki, El-Sherbiny, and Salem,[94] involved ion plating Ag films 10-400Å thick onto carbon films approximately 50 Å thick. Some of the relevant features of these ion plated thin island structures are that the nuclei size is smaller than that produced during evaporation with equal pressures and only gas scattering, and the nuclei density appears greater than that observed in conventional evaporation or gas scattering evaporation. Also, significant coalescence was not observed. From this observation it is concluded that the dominant deposition mechanism in ion plating is the production of new nuclei or addition onto pre-existing nuclei, resulting in a columnar growth mode. The uniform nucleation that was observed is believed to be due to a uniform ion implantation of the substrate or preferential nucleation of defect sites which were generated from the bombardment.

Babeaven, Bykov, and Guseva,[95] considered the condensation properties of Zn and Sb on Cu_2O and NaCl, respectively, under the

influence of Ne and Ar ion irradiation. Some of the general effects of the bombardment observed during the course of the experiments were that the critical condensation pressure for film formation was decreased as ion beam power density increased to the substrate, in the temperature range of 473-573°K. The ion beam effect was found to change with the stage of film formation in which it was introduced. If introduced early on in the deposition process, a finer structure and improved film continuity are observed. A coarse structure and impaired coverage coefficient is observed if ion bombardment is introduced during the final stages of monolayer formation. An effect was also observed in regard to epitaxy. Ion bombardment lowered the epitaxial temperature of Sb onto NaCl from 503 to 423°K while inducing nuclei to assume a preferred orientation. Nuclei observed without bombardment had mixed orientation while one particular orientation was observed following a run with bombardment.

Stroud,[96] indicated that preferential deposition of Ag occurred on regions of an SiO film which were previously exposed to Au irradiation using ion energies in the range of approximately 80 eV to 350 eV and maximum doses of the order of 5×10^{14} ions/cm^2. The key point is that for an Ag flux of 2×10^{14} atoms/cm^2 sec for 2 min at a substrate temperature of 713°K, an Ag deposit was only observed in regions previously exposed to Au irradiation, thus the surface was "sensitized" by the Au bombardment. The critical Au dose which would sensitize the SiO surface at a particular ion energy was defined as that which would allow a visible deposit following an Ag vapor fluence of 2.4×10^{16} atoms/cm^2. It was also

determined that the critical Au dose increased with ion energy as shown in Fig. 20. Basically, this effect is explained in terms of ion penetration in the solid which is a function of energy. Since the mean depth at which an ion travels into a solid is a strong function of the ion energy; it appears that only atoms trapped in the first few atomic layers have an effect on the process of preferential nucleation. Thus, qualitatively the concentration of implanted atoms in the near surface region will decrease with increasing ion energy and so a larger dose is needed at higher energies for a comparable dose in the surface region.

Pilyankevich, Kulykovski, and Shaginyan,[97] studied the formation of In islands deposited onto conductive and insulating substrates. Some of the general results of this study indicate that increasing bias voltage from 0 to 600 V on conductive substrates increases island density while decreasing the average island size. Films deposited on C coated Cu became continuous earlier when the applied bias was -100 V or 0 V in the presence of a plasma, than films deposited at -600 V bias with the plasma or without the discharge at 0 V bias. Films deposited onto the C coated NaCl at -600 V bias had island size and density characteristics similar to films deposited on C coated Cu with 0 bias in the presence of a plasma. The authors consider the observation of similar film continuity time scales between the biased insulator substrates and the low or 0 V bias conductive substrates to be related to the formation of additional nucleation sites as well as activating impurity atoms on the surface. Impurity atom activation is supported by an In_2O_3 electron diffraction line observed for films deposited at low bias

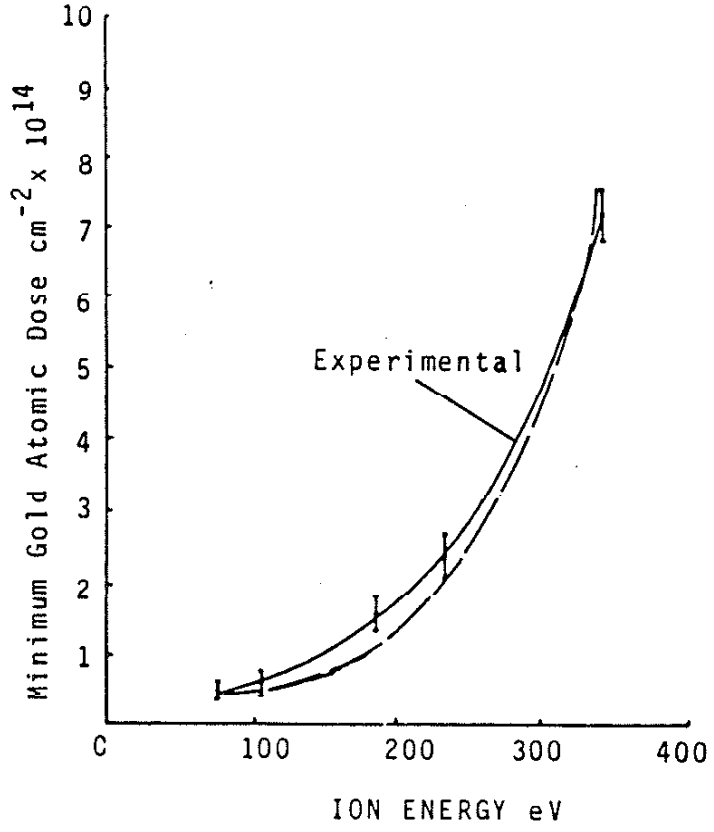

Fig. 20. Critical Au ion dose on an SiO surface as a function of ion energy to induce preferential Ag deposition.

voltages. Diffraction rings are not observed for the case of -600 V on C coated Cu, presumably due to impurity removal from the surface.

II.C.6. SURFACE TOPOGRAPHY

Particle bombardment of a surface is often associated with the formation of cones, pyramids or pits in the surface.[60, 98-100] Some of the theories used to explain this phenomena include variables such as the sputter yield dependence on the incident angle of bombarding species, crystal orientation, surface contamination, and surface energy variations on different crystal planes.

Carter, Nobes, and Lewis,[98] considered the driving force for the formation of facetted cone-like structures and attempted to determine the relative importance of surface energy considerations vs. differential erosion processes. Ultimately it is argued in the paper that since there is an alignment behavior of various protuberances on Cu single crystals with the incident ion flux, then the driving force to achieve these particular shapes is given by differential erosion processes. This is deduced since the cone alignment would be independent of ion incidence angle if the driving force indeed were minimization of surface energy.[98]

Kelley,[99] has investigated the influence of defects, surface impurities, atom migration, redeposition, grain boundaries, and pre-existing asperities on the formation of pyramids. Their results indicated that pyramids evolved on rough surfaces only once. That is to say that the pyramids developed on rough surfaces, but, after the initial set of pyramids developed, no new pyramids nucleated and

the initial pyramids eroded away. Grain boundaries did not present a particularly active region for the nucleation of pyramids, unless the surface is initially rough. Subsequent bombardment eventually erodes the pyramids away.

Surface impurities reportedly can influence cone formation by locally slowing down the sputtering process, thus producing asperities which develop into cones[60] as the surrounding surface recedes. This may be understood by considering a low sputter yield impurity particle which shadows the higher sputter yield substrate material beneath it. This will progress to form a plateau on top of which the particle is sitting. Following etching away of the impurity particle, the pillar of material is eroded away due predominantly to erosion rate variation with beam incidence angle.

II.D. PHYSICAL VAPOR DEPOSITION

Physical vapor deposition is generally considered to be a particular class of processes involving the atom-by-atom deposition of thin solid films onto a substrate. This thin film technology has wide areas of application such as surface protective coatings for wear and corrosion resistance, and films for electronic devices for high technology components.

II.D.1. ZONE MODELS

During the course of many experiments in evaporation and sputtering it has been observed that film structures tend to show particular trends in terms of morphology. These trends have been presented as structural zone diagrams, a few of which will be briefly reviewed.

II.D.1.a. MOVCHAN AND DEMCHISHIN

Movchan and Demchishin[101] produced one of the earliest zone models for the process of evaporation. The diagram is divided into three zones which are separated by transition temperatures T_1 and T_2. The lowest temperature zone, $T < T_1$, has a structure of tapered columns with domed tops and with spaces between the columns. As T increases, the dome diameter increases. Upon surpassing the first transition temperature, T_1, there is a gradual change in structure to a well defined columnar morphology that has a smoother, matt surface and much reduced inter-column porosity. With increasing substrate temperature, this intermediate columnar zone gradually changes to the equiaxed structure of the high temperature zone, $T > T_2$. The atomistic process considered important in the structural evolution is that of surface diffusion on the growing surface. Another conclusion drawn by the group is that relative size of tapered crystallites is a strong function of substrate purity.

II.D.1.b. THORNTON

Thornton[102] extended the ideas of Movchan and Demchishin with a revised thin film zone model which is strikingly similar to that of the Russion group (see Fig. 21). Instead of only a temperature axis, an Ar pressure axis was also added to show the effect of an ambient sputtering gas. Thornton has explained the various zone morphologies in terms of the atomistic processes occurring during film growth. Zone 1 is a columnar zone with open inter-column boundaries. This structure is explained to be present

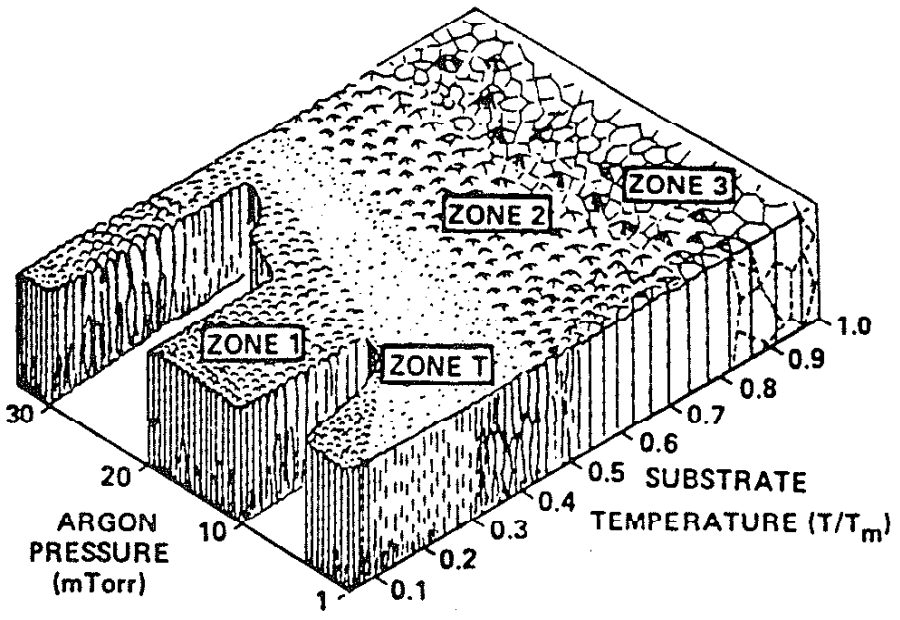

Fig. 21. The Thornton Zone model for sputtering which illustrates film microstructure as a function of temperature and Ar pressure.

as a result of dominating shadowing effects which influence the incident flux of depositing atoms. Shadowing may be understood by considering a rough surface, some points higher than others, with an incident coating flux that has an oblique component. As atoms impinge upon this surface, the high points will tend to block flux from depositing in the low points, or valleys. If surface diffusion is not extensive, then the atoms may not migrate into the valleys, thus not filling in the open boundaries. Factors which tend to enhance the formation of open boundary zone 1 structure include substrate roughness, oblique coating flux and low T/Tm which tends to limit surface duffusion. Thornton also added a transition zone, zone T which is composed of poorly defined fibrous columnar grains. This structure is considered to be within the zone 1 structure, with denser boundaries, terminating at approximately T/Tm = 0.3.

Zone 2 is observed at higher T/Tm in the range of $0.3 < T/Tm < 0.5$. It is composed of dense columnar grains, just as Movchan and Demchishins' zone 2. In this zone surface diffusion processes appear to become significant as evidenced by the suppression of the open inter-columnar boundaries, presumably filled in by migrating species.

In the regime of $T/Tm > 0.5$, bulk diffusion processes become significant resulting in film microstructures that have an equiaxed character. This equiaxed structure is probably the result of recrystallization and grain growth. The general effect of pressure in Thornton's zone is to permit formation of open boundaries at higher T/Tm with increasing pressure.

II.D.1.c. MESSIER, GIRI, AND ROY

Messier, Giri, and Roy[103] followed up Thornton's work and considered a zone diagram with axes of film thickness and specimen voltage in the presence of a plasma in addition to the temperature axis, for the range of T/Tm < 0.5. The thickness variable indicates an evolution of structure from thickness near 100 Å to 10 μm. At very low thicknesses (<100 Å) a structure of very small 'nano' columns, 10-30 Å in diameter, is observed, which are surrounded by low density void-like regions. Increasing film thickness indicates a repetitive cycle whereby larger voids form which surround larger columns. The five characteristic column diameters are approximately 10-30 Å, 50-200 Å, 200-400 Å, 500-2,000 Å, and 2,000-4,000Å, with the formation of these columns taking place in the sequential manner outlined briefly above. See Fig. 1 in reference 69 for an indication of the relative morphology of each column generation. Ion bombardment-induced atom mobility has the effect of suppressing zone 1 formation at lower temperatures. They show that Thornton's diagram could possibly be interpreted in terms of bombardment induced mobility instead of pressure since the two effects are similar. That is, higher pressures would decrease incident particle energy. The effect that enhanced mobility, thermal and bombardment induced, have on the thickness axis of the diagram is to allow smaller diameter columns at greater film thicknesses.

II.D.2. EVAPORATION

This vacuum deposition process is generally considered to be

heating of a solid source material to sufficient temperature that the material is transferred efficiently into the vapor phase.[70] This may be accomplished in a number of ways, a few of which are resistance heated wires and boats as well as electron bombardment of the source. The particular method of heating is chosen on the basis of such factors as the desired rate of deposition, the type of source material, and the vacuum environment. Some good reviews of this technique are available in the literature.[19,104]

Some of the earliest work on evaporation theory was performed by Hertz, who studied mercury vaporization.[105] One of the conclusions of his study was that the evaporation rate was proportional to the difference in vapor pressure of the source and the ambient hydrostatic pressure of the vacuum. This led to the development of the following equation:

$$\frac{dNe}{A_e dt} = (2\pi KT)^{-1/2}(p^*-p) \qquad (22)$$

where Ne is the number of evaporating molecules, A_e is the evaporant surface area, dt is the time interval of evaporation, p* is the equilibrium vapor pressure, and p is the hydrostatic system pressure. The maximum rates of evaporation are then obtained by setting p = 0. Hertz, in practice, was able to obtain only 10% of the predicted theoretical value.

Knudson[106] considered the phenomena of gas phase particles reflecting from the liquid instead of solely incorporating into it. The role these species would play is that they would contribute to

the evaporant pressure, but not the actual net flux of material from the source. Thus, Knudson introduced an evaporation coefficient, α_v, which is the ratio of the observed evaporation rate in vacuum to the theoretically preducted value. This coefficient appears in the Hertz-Knudson equation, given by,

$$\frac{dNe}{A_e dt} = \alpha_v (2\pi mKT)^{-1/2}(p^*-p) \qquad (23)$$

Knudson further determined that evaporation rate was a strong function of the source surface purity, and was able to achieve the maximum evaporation rate by using a very pure source material.

Along some more practical considerations in evaporation scenarios, one must consider the thickness distribution of a deposited film. Films are often non-uniform in thickness due to an uneven flux of material to the substrate. This is intimately related to the angular flux distribution of source material being emitted by the melt pool. The flux is not constant in all directions from the source but follows the cosine law of emission, one form of which is:

$$dM_e(\phi) = M_e \cos\phi \frac{dw}{\pi} \qquad (24)$$

where M_e is the total mass of evaporated material, ϕ is the chosen direction with respect to a reference direction normal to the source surface plane, dw is the solid angle at the angle phi through which the considered flux is passing (see Fig. 24 of reference 19). As

may be seen from the equation, the mass flux is greatest at phi = 0, which is normal to the source surface plane. From the emission equation, an equation describing deposited film thickness on a flat substrate may be arrived at by considering a plane of material located directly over the source (see Fig. 24 of reference 19). This equation is:

$$D = \frac{1}{\rho} \frac{dM_r}{dA_r} \qquad (25)$$

where D is film thickness, ρ is density, M_r is the mass and A_r is the surface area. Non-uniform film thicknesses may be largely alleviated by moving the substrates in the vacuum during deposition.(19) The effect of this is to even out the net fluence of material at each point on the substrate.

Electron beam evaporation, which is appropriate to the context of this thesis, is accomplished by placing a W filament in the role of a hot cathode.(107) The filament is biased to a negative potential in the range of 5 to 20 kV. Upon thermionic electron emission a beam is formed by neighboring plates also at the cathode filament potential. The electromagnetic coils are used to direct the beam through a 270° arc where it impinges at high energies on the source material. Most of the electron beam energy is converted to heat with temperatures greater than $3200^{\circ}K$ achievable.(19) Energy loss processes to this scenario include heat loss by conduction, convection, radiation, and vaporization. The incident electron/solid interactions also produce secondary electrons and x-rays and cause

gas phase processes such as ionization and molecular dissociation. The surface temperature of the melt is critical since to a large extent it dictates the energy flow. At low electron beam energies and correspondingly low surface melt temperatures, the processes of conduction and convection (in the liquid) predominate. As the surface temperature and electron beam power density increase, losses due to radiation and vaporization become equal, and at higher temperatures, vaporization is most important. Evaporated particle energies are thermal, thus on the order of 1 eV or less.

Beale, Weiler, and Bunshah,[108] investigated some of the general effects of process parameters for the evaporation characteristics such as cosine law deviations vs. support gas type and pressure, non-line-of-sight deposition, and condensation rate vs. evaporation rate. Pure evaporation was compared to the reactive evaporation (RE) and activated ractive evaporation (ARE) processes in this study. For the case of evaporating free Ti without a support gas ambient, deviations from the cosine law were observed as curvature reversals near the deposit edge (see Fig. 22). Fig. 22 also shows the effect of source to substrate distance. This deviation is also exhibited by the RE process in the micron pressure range. It is not, however, exhibited by the ARE process employing a reactive or non-reactive gas. Fig. 23 shows the effect of different gas species on the deposited thickness profile for the ARE process. The general effect of pressure on deposition efficiency is that as pressure increases, the efficiency decreases for gas-scattering-evaporation (GSE) and ARE. Overall, the ARE process is comparable to or slightly less than the RE and GSE processes for

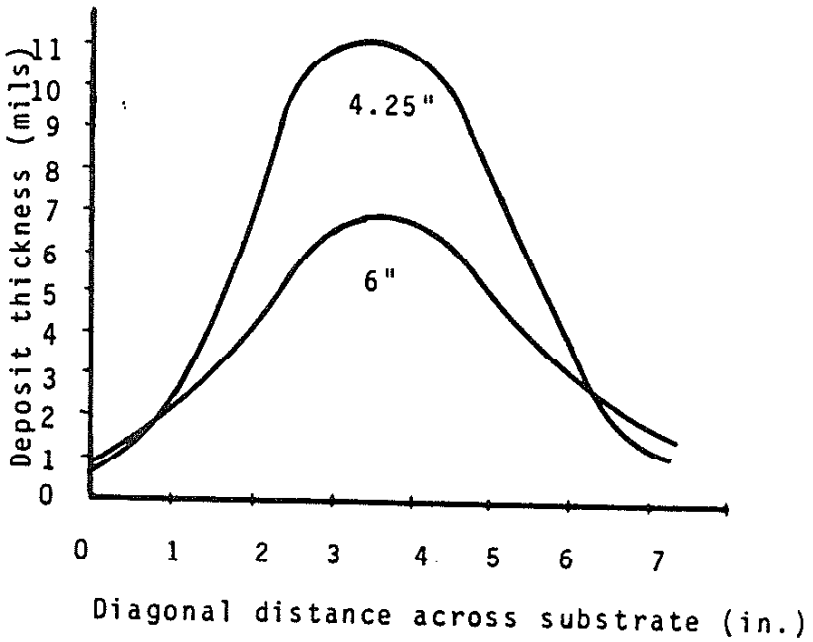

Fig. 22. Deposit thickness diagonally across the substrate for evaporating Ti at two different source to substrate distances. Deviations from the cosine law are shown as curvature reversals toward the extremities.

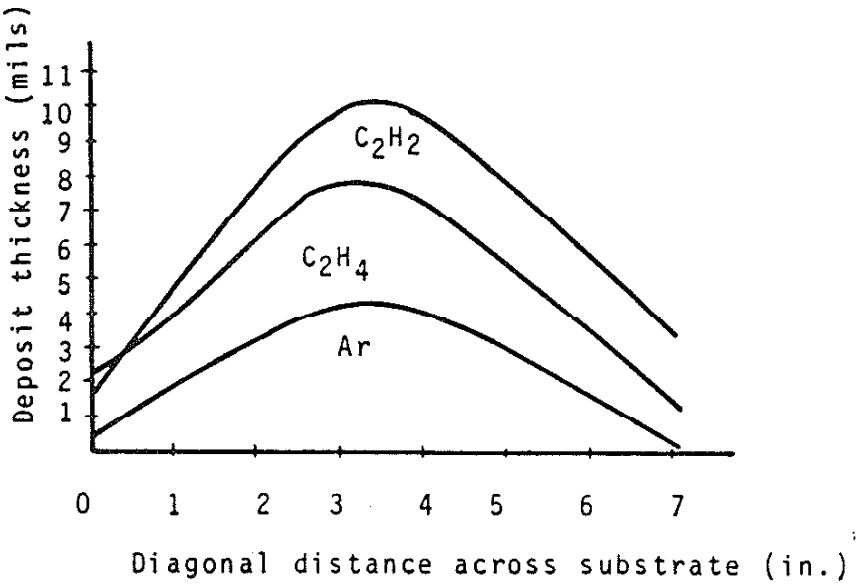

Fig. 23. The effect of different gas species on deposit thickness along the substrate diagonal for the ARE process.

efficiency. Non-line-of-sight deposition capability was determined by examining the deposit thickness behind a tab which was 45° from the general substrate surface.[108] The most important parameter in achieving material deposition behind the tab was support gas mass, with ambient pressure playing a secondary role.

Bauer, Schwartzman, and D'antonio,[109] investigated the dependence of recrystallization during deposition on thickness for vapor deposited Cu films. Thicker films tend to exhibit recrystallized structures while no recrystallization is observed for thicknesses less than 1000 Å. The substrate temperature as measured by a thermocouple is not greater than 306°K during the film formation. Two reasons are cited for this recrystallization behavior. One of the authors found in an earlier study that very thin films are composed of "hill and valley" topography. The possibility is then that a "hill" is smaller than the critical size for a recrystallization nucleus; thus, inhibition of recrystallization would be noted for very thin films. The second possibility is related to a temperature increase effect which is discussed in work by Belous and Wayman.[110] The temperature of a depositing film increases due to the exothermic heat of condensation; therefore, the thickness of a film determines to some extent its temperature and thus the extent of diffusional processes.

II.D.3. SPUTTERING

Sputter deposition is a method of depositing thin films which involves using the particular material to be deposited as the sputtering target. Atoms sputtered off the target then traverse

through an ambient support gas and impinge upon the substrate. Several varieties of sputter deposition equipment are available, such as the hollow cathode, planar diode, and magnetron sputtering systems. Fig. 24 is a schematic of a planar diode system. One of the advantages of sputtering over evaporation is that virtually any material may be sputtered.[111] Insulators are typically sputtered using an R.F. system while conductors may be sputtered using a dc potential. Sputtered particle energies are typically in the range of 10-40 eV,[101] while evaporated particle energies are typically less than 1 eV. Magnetron sputtering employs a magnetic field which serves to increase the percent ionization in the discharge, confine the electrons locally to the cathode, and sustain ionization at low pressures.[112] Thornton[112] has provided a good discussion on magnetrons. Some reviews of coatings deposited by sputtering will be presented in the next section.

Thornton[113] studied the dependence, as a function of process parameters, of open boundary formation for thick Cu coatings deposited using a hollow cathode sputtering system. The variables during these experiments were substrate roughness, sputtering pressure, bias voltage, deposition rate and backsputter fraction. The backsputter fraction is given as,

$$R = \frac{A\langle J_c\rangle S(V_c)}{(1+\gamma)\rho N}\left\{1 - \frac{\langle J_b\rangle S(V_b)}{\langle J_c\rangle S(V_c)}\right\} \qquad (26)$$

where $\langle J_c\rangle$ is the cathode current density, $\langle J_b\rangle$ is the average sub-

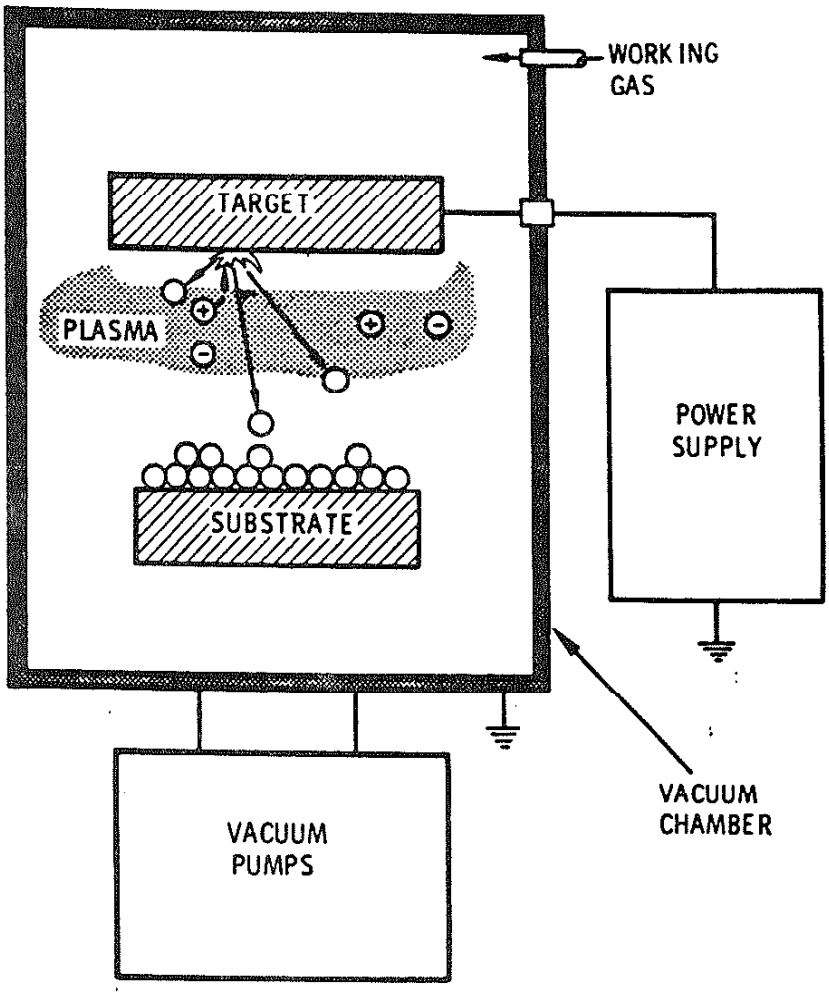

Fig. 24. Schematic of a diode sputtering system. Material is sputtered from the target into the gas and ultimately forms a film on the substrate.

strate current density, $S(V_b)$ and $S(V_c)$ are the sputter yields at the particular voltages V_b and V_c, γ is the secondary electron coefficient for ion bombardment, N is Avogadro's number, $\underline{\rho}$ is the coating density (assumed to be bulk) and A is the coating atomic weight. The denominator of the final term gives an indication of the amount deposited, assuming negligible gas scattering, and the numerator is an indication of the amount of deposit sputtered off the substrate. Briefly, his optical microscopy results show that the columnar microstructure is present without substrate bias at pressures of 0.13 Pa and with smooth substrates. Bias voltages of -100 V and backsputter fractions of 10% modified the surface topography without altering the coating microstructure significantly on polished substrates at low pressures. Open boundary formation was suppressed for higher pressure deposits under these conditions. Bias voltages of -250 V at low pressures tended to smooth coating surfaces as long as the backsputter fraction was significant (> 30%). The coating microstructure under these conditions was fibrous in nature. Other notable results of this study included the observation that at high substrate temperatures, thermal effects tended to dominate in establishing the coating microstructure. The example cited here was that a coating deposited at 973°K with a 40% backsputter fraction had a very similar structure to a deposit at 343°K without bias. Zone 3, equiaxed microstructures, were not reported in this study even under high temperature and significant backsputter conditions.

Craig and Harding[114] also studied the morphologies of Cu coatings deposited onto glass substrates by magnetron sputtering.

As pressure increases from 6.5 to 97.5 Pa at T/T_m = 0.23, coating structures shift from fine grained columnar character to columnar with voided boundaries. Surface topography for 3.0 and 10.0 μm films consists of arrays of cones. For T/T_m = 0.31, a fibrous morphology of tightly packed grains and dense boundaries is observed. Surface roughness is also observed to increase with increasing deposition pressure. For T/T_m = 0.41 and 0.51, a dense columnar structure is observed with open boundaries forming at higher pressures, while equiaxed grains form at low Ar pressure. For films of thickness 3.0 μm and 10.0μm, surface topography consists of large flat grains with grooved boundaries which and shifts to a highly faceted surface as pressures exceed 6.5 Pa.

II.D.4. ION PLATING

Ion plating is a vacuum deposition technique which has characteristics of both evaporation and sputtering[115] (see Fig. 25). Metal, ceramic, or other material is vaporized in crucibles into an ambient low temperature plasma which is sustained by the cathode electrode. A support gas such as Ar is usually present at pressures near 0.13 Pa, which facilitates gas scattering prior to evaporant atoms entering the cathode sheath. The sheath then has source vapor with support and/or reactive gases present, a small fraction of which is ionized and thus accelerated to the substrate. Characteristics of the various particle fluxes are described in Section II.B.6.

The ion plating process is generally considered to produce dense adherent coatings which often have applications in the areas

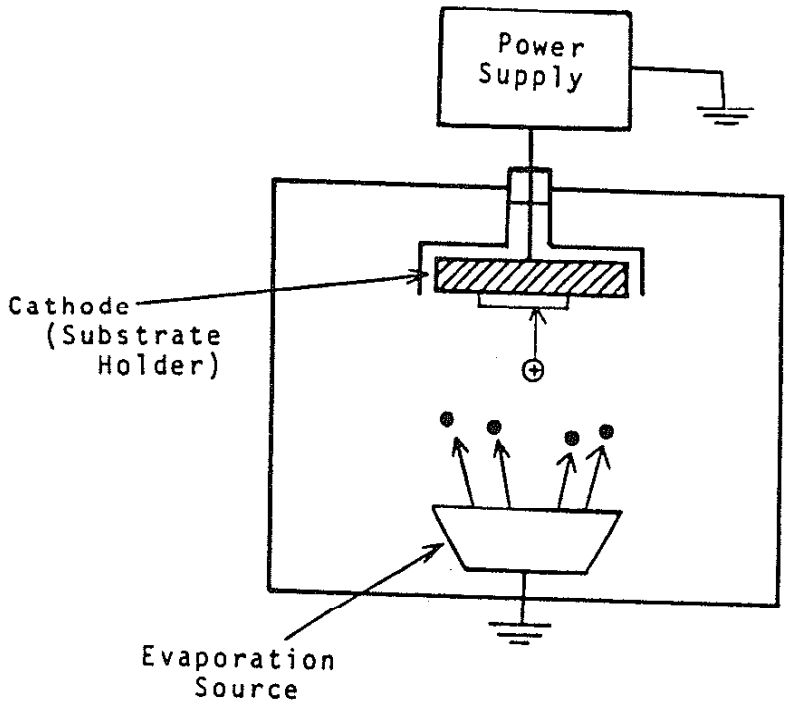

Fig. 25. Schematic of an ion plating system. Material is evaporated and impinges the substrate which is being sputtered simultaneously.

of corrosion and wear resistance. The reasons which are believed to explain the adhesive properties are:

1) sputter cleaning of the substrate to remove adsorbed impurity particles;
2) continued bombardment of the growing film when the deposition has begun; and
3) the development of a chemically graded interface via enhanced diffusion and atomic mixing events.[115]

It is one of the goals of this research to relate the process parameters to observed coating and interface structures and chemistries.

Several attempts have been made in the literature to model the ion plating process, taking into account the various physical events occurring which have been mentioned or discussed previously. These include recoil mixing events at the coating/substrate interface, radiation enhanced diffusion, and the associated defect production such as atom displacement and dislocation loops. Some of the important considerations in some of these models will now be presented.

Nelson,[116] discusses radiation damage, recoil implantation, and enhanced diffusion. Radiation damage effects may result in agglomerations of migrating interstititals and vacancies in metals.[117] Covalent materials may be rendered amorphous. Recoil implantation events will be significant with regard to film/substrate mixing as long as the damage profile of displaced

atoms spans the interface. Using the previous equation for the recoil flux (equation 20), and the assumption that 5 kV ions impinge upon the substrate, Nelson concludes that 10 to 100 monolayers will be recoil mixed at the interface.[116] Radiation enhanced diffusion is a result of defect super-saturation. It is important for the formation of a chemically graded interface that the substrate is at a temperature where the defects are mobile. Ion energies, as well as relative impingement rates of ions and coating atoms, are important considerations for the development of a chemically graded interface.[116]

Carter and Armour[70] have also considered some of the kinetic processes occurring during ion plating. Some of the processes considered in this study include impurity gas adsorption, the criteria for coating formation, energetic atom entrapment, and the sputtering and atomic mixing processes. A few of the key remarks or observations that arise in considering each of these processes are that for low ion energies, i.e., less than 1 keV, the sputtering yield of adsorbed impurities is typically larger than for the matrix material. As ion energies approach 1 keV, adsorbate sputter yields may become less than the matrix yield. In general terms, the criteria for net film growth is that the deposition rate must exceed the sputter rate. Mathematically, the criterion for coating growth was derived to be:

$$J_{cn} + J_{ce}\eta_{ce} > \bar{Y}_{cc}(J_{ce} + J_{se}) \qquad (27)$$

where J_{cn} is the neutral coating flux, J_{ce} is the energetic coating

particles, Y is a mean sputter yield for energetic coating and support gas particles, J_{se} is the energetic support gas flux, and η_{ce} is the entrapment probability. Energetic atom entrapment is another physical process occurring during ion plating, and this should be taken seriously, expecially in regard to inert and impurity gas bubble formation. Generally, the entrapment probability will be defined by an equation of the form,

$$\eta(E) = \int_0^\infty d_x f(x,E) \qquad (28)$$

where $\eta(E)$ is the entrapment probability, and $f(x,E)$ is a depth distribution of trapping positions. For $E > 5$ keV, $\eta(E)$ tends to unity. For the ion plating regime where $E < 5$ keV, there is not much computational or experimental evidence available. However, Carter maintains that $\eta(E) = 0.9$. 0.1 is reasonable for projectiles and target atoms of near equal mass in the regime of 1 eV to 1000 eV. For inert gas atoms, the $\eta(E)$ function varies much more. The discharge system should be as efficient as possible, sustaining ionization at the lowest possible pressure to minimize inert gas incorporation and the attendant formation of bubbles.

Carter and Armour consider the cascade mixing process most generally significant for producing a graded junction at the film/substrate interface. Radiation enhanced diffusion is quite capable of producing a chemically graded interface, but is probably dependent upon the particular film/substrate combination. Cascade mixing has also been shown to be more effective at intermixing than

recoil or direct implantation events as stated in Carter and Armour. Other work by Armour, et. al.,[118] has shown that the cascade mixing process could account for some observed graded interfaces, resulting in widths of the order of 30 Å for a generic metallic system.

Ion plated Cu coatings were investigated by Teer and Delcea.[119] Process variables investigated in this study include the substrate power density and the Ar gas pressure. Low power densities produced a nodular-like zone 1 type structure with weak boundaries. Increasing the bias voltage, and thus the power density at constant pressure, resulted in parallel columns reminiscent of a zone 2 structure with denser boundaries. Increasing pressure at constant bias voltage also increases columnar boundary density with a shift from zone 1 type to zone 2 type structures. The authors indicate that suppression of the open boundaries at higher voltages and pressures is probably a result of sputter redistribution of material as a result of increased power densities. Also, the deposit temperature is increased as a result of the sputtering. A coating made with a triode configuration to increase substrate current density at constant voltage produces a very fine grained, dense structure which is nearly featureless in cross section. A coating deposited at lower power density at constant pressure and voltage exhibits an open zone 1 structure.

Miyoshi, Spalvins, and Buckley[120] studied the chemically graded interface between Au deposited onto Ni and Fe substrates using XPS in a sequential depth profiling mode. The effects of coating/substrate solubility are essentially the variables as Au is

much more soluble in Ni than Fe. The profile results indicate that nearly 3.25 hours were necessary to profile through the Au/Ni interface while only 72 minutes were required for the Au/Fe interface. The authors attribute this marked difference in interface width, 6 μm for Au/Ni vs. 1.5 μm for Au/Fe, as due to thermal and chemical diffusion effects. Au films deposited without substrate bias onto Cu; Ni and 440C stainless steel were also depth profiled in a similar fashion. These vapor deposited interface widths were much thinner than the ion plated cases. Also, the Au/Ni and Au/Cu interface widths appeared broader than the Au/440C interface. The authors site greater chemical affinity, or enthalpy of interaction, for Au/Cu and Au/Ni couples than Au/440C as a possible reason for this observation.

III. EXPERIMENTAL PROCEDURE

This section describes the ion plating system used to produce thin film metal/ceramic composites as well as the analytical techniques which facilitated subsequent characterization. As a result of this combination, in depth microanalytical studies may be performed on samples which are characteristic of an industrial manufacturing process.

III.A. CERL ION PLATING EXPERIMENTS

The U.S. Army Construction Engineering Research Laboratory (CERL) is a government facility located in northeast Champaign, IL. As a principal investigator in the Corrosion and Coatings team, Mr. Vince Hock does extensive work in the study of metallic corrosion and methods, such as vacuum deposition, of inhibiting it. Vince Hock and Professor James M. Rigsbee are the principal investigators for the ion plating work performed at CERL.

III.A.1. EQUIPMENT

The U.S. Army CERL/University of Illinois ion plating facility was manufactured during the fall of 1983 by Torr Vacuum. The system is differentially pumped with two diffusion pumps, maintaining a system base pressure of approximately 1×10^{-4} Pa. Fig. 26 is a schematic of the system. Two electron beam guns capable of evaporating refractory material are positioned at approximately mid-section, a stainless steel water cooled cathode is positioned approximately 15 cm above them. Other features of the system include a residual gas analyzer (RGA) for analyzing gas composition within

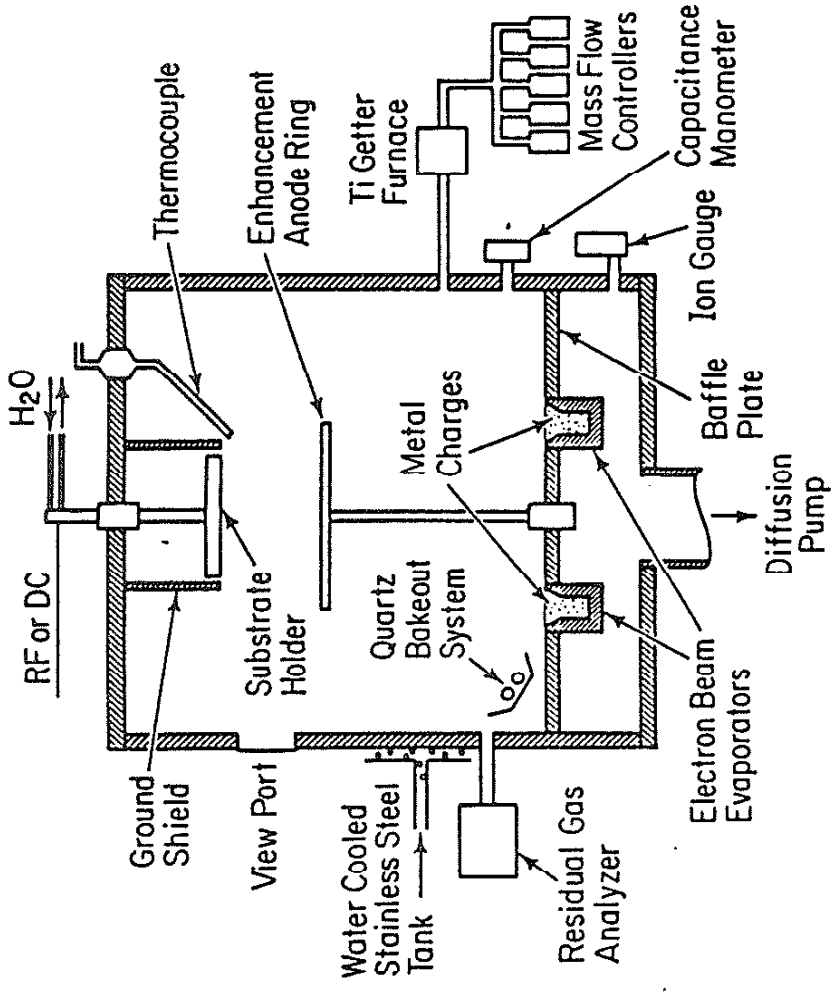

Fig. 26. Schematic of the CERL ion plating system.

the chamber, an enhancement anode for raising the space potential of the discharge resulting in electron confinement and higher cathode current densities, and pressure gauges for monitoring pressure both above and below the baffle plate. Mass flow controllers allow accurate partial pressures of vapors to be maintained. A bakeout system using quartz lamps has been used to raise the ambient temperature in the deposition chamber to 473^{o}K for desorbing wall species, thus resulting in lower ultimate pressures. See reference 121 for a detailed description of the system.

III.A.2. SUBSTRATE PREPARATION

Substrate surface preparation for vacuum deposition is very important since the chemistry present on the substrate surface will undoubtedly influence the state of the resultant interface. The particular method used in this study was to rinse the cordierite in acetone followed by a rinse in ethanol and hot air blow dry. Samples were then introduced into the vacuum chamber directly for evacuation. Smooth substrates were sequentially polished using standard metallographic techniques and 9, 3, 1 and 0.25 micron diamond paste prior to the solvent rinsing process just described. Due to the presence of pores in the ceramic surface in addition to the possibility that cordierite may be able to store H_2O molecules within the structure, rinsing times were kept as minimal as possible to prevent any type of surface alteration due to the solvent dissolving in the ceramic.

III.A.3. DEPOSITION PROCEDURE

The experimental procedure following initial substrate preparation generally involved evacuation of the chamber to a pressure in the high (1.3×10^{-3} Pa) vacuum region. D.C. sputter cleaning of the cathode then ensued, which involved achieving an upper chamber Ar pressure of approximately 1.3 Pa, followed by driving the cathode electrode to a negative potential of several thousand volts. Following sputtering of the cathode, ion plating or evaporation took place for coating growth. Evaporation times were typically 20 minutes following 10 minutes of sputter cleaning.

III.B. TEM SAMPLE PREPARATION

The technique used for producing cross-section TEM samples involves the following elaborate series of steps. The procedure used for the Cu/cordierite samples was:

1) encapsulation of diamond sectioned substrate/coating strips into epoxy filled stainless steel tubes;

2) sectioning of approximately 550 micron thick slices from the tube using a diamond saw;

3) mechanically polishing the slices with 600 grit SiC paper to a thickness of 200 micron;

4) flattening one side down to 1 micron diamond finish with the flattening tool on the VCR Model 400 mechanical dimpler;

5) flipping the sample and dimpling to a final thickness between 50 and 80 microns;

6) ion milling the sample to perforation at an angle of 12^{o} with 4 kV Ar^{+} ions for 10-15 hours using the LN_2 cold stage; and

7) carbon evaporation onto the perforated sample to prevent charge buildup in the TEM.

As with any TEM sample preparation technique, only a certain "yield" is achieved during the fabrication process. Other groups[122] have used similar techniques for interface characterization.

III.C. ANALYTICAL TECHNIQUES

All microanalysis was performed at the University of Illinois Center for Microanalysis in the Materials Research Laboratory and the Department of Materials Science. The multitude of analytical equipment and personnel expertise was crucial to the results section of this thesis. The following section is a brief description of the analytical equipment used in this study.

III.C.1. AUGER ELECTRON SPECTROSCOPY

Two Physical Electronics Auger systems, 545 and 595, were used in this study. The 545 has quite poor spatial resolution with an electron beam probe size of 10 microns. The 545 is quite suitable for many applications, however. The 595 has better spatial resolution with an electron beam probe size of 1 micron in diameter. The ion beam size is approximately 300 microns x 300 microns. the size of the sputtered area may be adjusted; a larger area yields a "crater" with a flatter bottom, though the net penetration rate is low. A smaller rastered area will yield a crater that is not so flat on the bottom, but the penetration rate is greater. The depth resolution of this instrument is 5-10 nm.

III.C.2. SECONDARY ION MASS SPECTROSCOPY

The Cameca ion mass spectrometer may be operated in either positive or negative ion spectrum modes and typically uses either O or Cs as an incident sputtering beam. The sensitivity of this instrument extends into the PPM range for some elements. The primary limitation of this technique is the difficulty of quantifying data without standards. The secondary ion yield for the elements varies over several orders of magnitude. It is a very useful technique when examining sample purity and the abruptness of a buried interface between two materials.

III.C.3. TRANSMISSION ELECTRON MICROSCOPY

The Philips EM 400 and EM 430 model transmission electron microscopes and attendant energy dispersive x-ray (EDAX) analysis equipment were used in this study. The EM 430 has a specified point to point resolution of 0.2 nm and is often used on thick samples due to the 300 kV accelerating potential. The EM 400 has an accelerating potential capacity of 120 kV and a specified point to point resolution of 0.4 nm.

III.C.4. ADHESION TESTING

The adhesion tester used was a Quad Group Sebastion normal stub pull tester. Stubs are bonded via thermal curing of epoxy and subsequently removed by a force directed along the axis of the pull test. The stress at failure may then be observed via digital readout. The maximum stress that may be applied is 73 MPa.

IV. RESULTS AND DISCUSSION

The following section describes the results and characterization of the metal/ceramic interfaces produced according to the experimental procedure. The microstructures and microchemistries observed are explained largely in terms of the sections in the background.

IV.A. EXPERIMENTAL VARIABLES

The experimental variables chosen for this study were applied substrate bias and the substrate smoothness. Substrate bias was chosen to optimize atomic mixing and substrate etching. Damage to the substrate could assist in promoting adhesion since Cu, being a relatively noble metal, typically bonds weakly to ceramic surfaces. Surface damage could promote chemical bonding of Cu. Substrate smoothness was chosen as the other major variable since polishing the substrate drastically altered its microscopic roughness.

IV.B. ADHESION RESULTS

The overall adhesion results obtained via the pull test for the 0, 1, 3, and 5 kV runs for polished and as-received substrates in the as-deposited and the heat treated condition are shown in Table 3. Heat treating samples in a reducing atmosphere was used as a measure of the stability of the metal/ceramic interface. The generally observed lower failure stress levels for the as-received cases could well be due to the presence of near-surface flaws at the coating/substrate interface which lower the threshold stress for failure. Polishing substrates prior to depositing a coating could

Table 3

Adhesion Failure Stress Values
of Ion Plated Cu/Cordierite (MPa)

Applied Substrate Bias (kV)	Polished	As-Received	H_2-Heat Treated
0	0.69 ± 0.34	2.10 ± 0.69	-----
1	41.9 ± 17.8	28.6 ± 19.2	-----
3	No Failure	34.1 ± 10.0	-----
5	-----	34.4 ± 11.9	1.4 ± 1.3

then be construed as a method of removing such flaws, at least partially. Films deposited with 0 kV applied bias on polished and as-received substrates failed completely by metal/ceramic interface failure as observed optically. Films deposited with 1 kV applied bias on both substrate surfaces show slightly better adhesion characteristics with failures still occurring at the metal/ceramic interface. Films deposited on polished substrates with a 3 kV applied bias exhibited the best adhesion characteristics. These films had an 83% occurrence of no failure at the maximum pull test stress of 73 mPa. Films deposited on as-received substrates at 5 kV had nominal failure stress levels of 3.45 MPa. The failure mode of this sample was most often related to ceramic fracture with macroscopic chunks of ceramic tearing out upon failure.

IV.C. FILM AND INTERFACE MICROSTRUCTURES

The bulk film microstructures of the various deposits is a strong function of the applied substrate bias. Films deposited with the substrate holder at ground potential under low pressure (1.3 MPa) conditions were predominantly microcrystalline with a distinct absence of columnar morphology. Fig. 27 is a bright field micrograph of a 0 kV film clearly illustrating the equiaxed nature. The average grain size for this case is approximately 50 nm. Since the low ambient pressure implies minimal oblique scattering near the deposit surface, the lack of columns is not surprising. Unique characteristics of this film include irregularly shaped grains over 1 micron in size. Fig. 28 is a TEM dark field micrograph of such a grain in contrast which is in direct contact with the ceramic. The

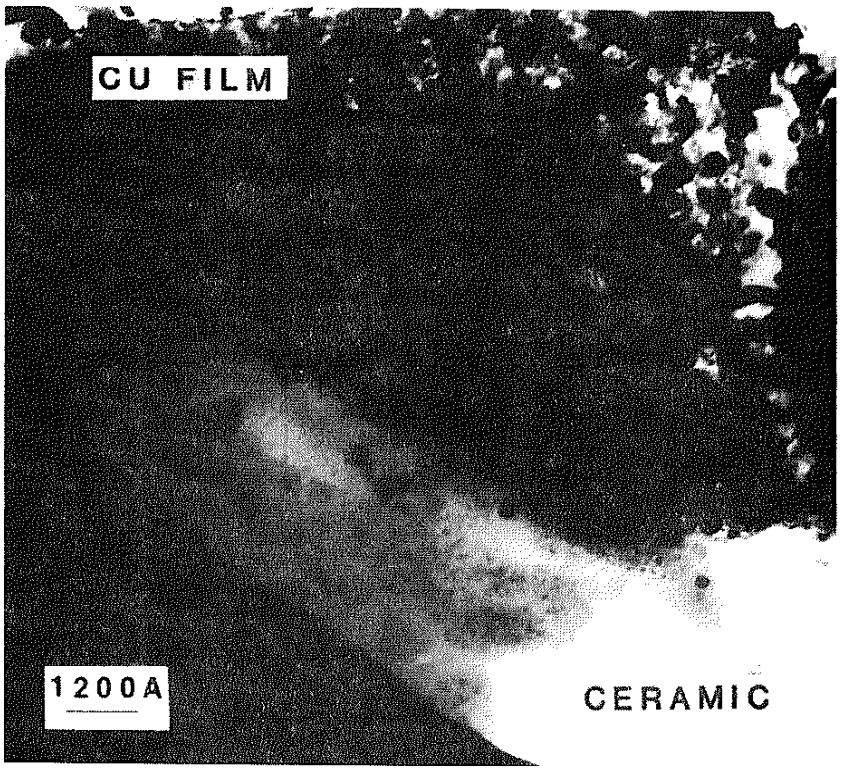

Fig. 27. Cross section bright field TEM micrograph of a Cu film deposited with sputter cleaning and no substrate bias during evaporation at a pressure of 1×10^{-5} torr.

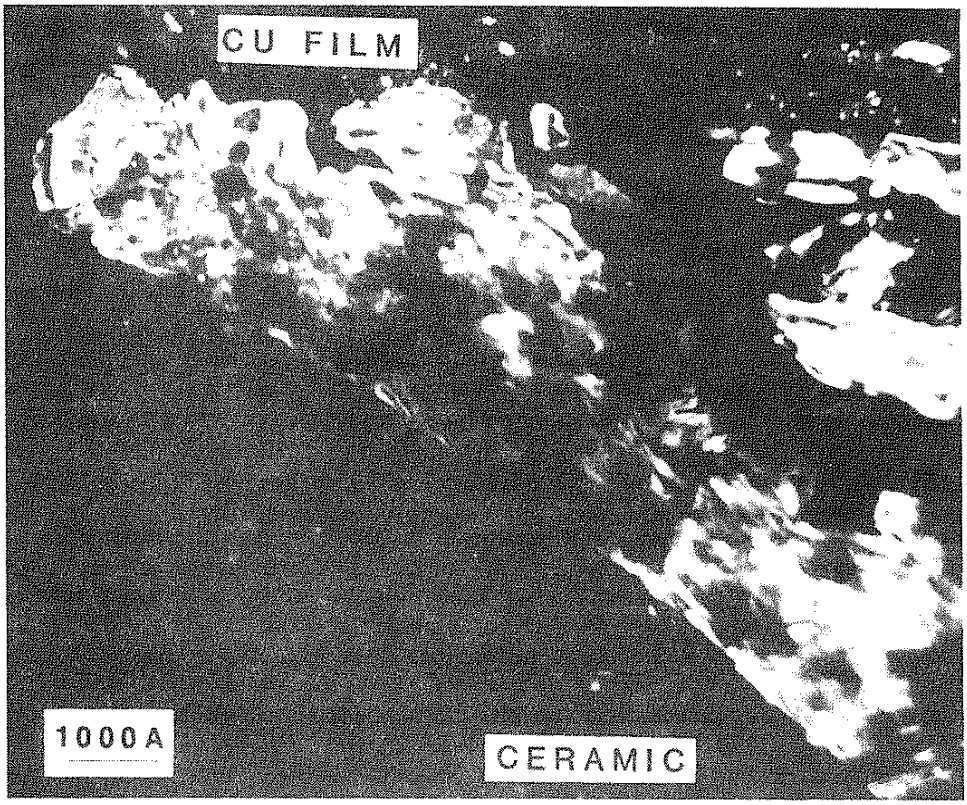

Fig. 28. Cross section dark field TEM micrograph of a Cu grain at the interface of the 0 kV film.

fact that it is not equiaxed coupled with the highly curved surface gives it a strange appearance. Growth twins are observed frequently in this coating. The film/substrate interface appears quite abrupt with Cu grains nucleating directly from the ceramic. Fig. 29 is a bright field TEM micrograph of a single twinned Cu grain in contact with the ceramic. No mixing is apparent between the metal and ceramic and no reaction phase appears to be present. The fact that both parent and twinned portions of the crystal are in contact with the ceramic may imply some specific characteristic about the nucleation and growth processes occurring very early in the film formation though drawing inferences is difficult. The fact that the interface is so abrupt complements the fact that the adhesion is quite poor.

The application of a 1 kV bias with pressures of several microns resulted in open boundary zone 1 type microstructures. Fig. 30 is a 1 kV Cu film cross section showing a very regular columnar structure with the open boundaries clearly present. The film is highly defective as indicated by the numerous contrasting features with extensive twinning and a column width of approximately 50 nm. The thickness of the film is 550 nm. The metal/ceramic interface was not clearly revealed in the sample that was analyzed.

Films deposited with 3 kV applied substrate bias with pressures of several microns also exhibited columnar growth. The higher bias appears to have suppressed open boundary formation, possibly due to increased adatom mobility. Fig. 31 is a bright field micrograph of this film clearly showing the densified boundaries which could be induced by mobile atoms on the surface, filling the

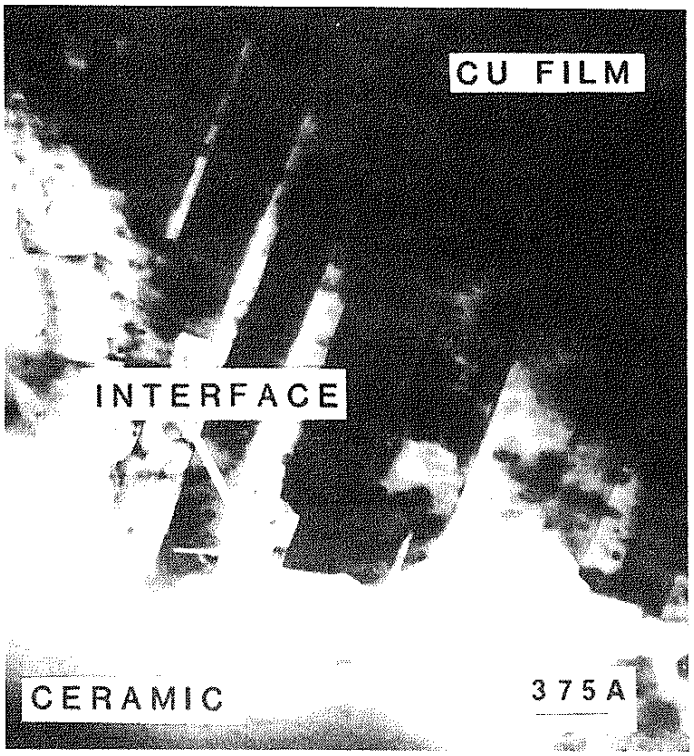

Fig. 29. Cross section bright field TEM micrograph of a twinned Cu grain at the metal/ceramic interface. No evident interface phase is present.

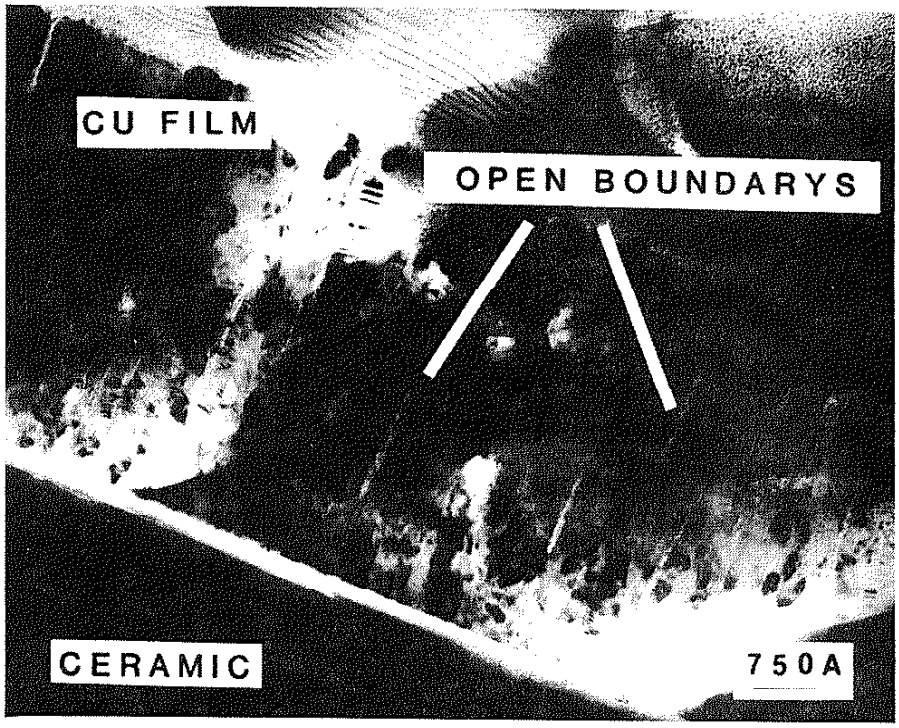

Fig. 30. Cross section bright field TEM micrograph of a 1 kV film deposited at 1.3 Pa. Note the columnar structure with open boundaries.

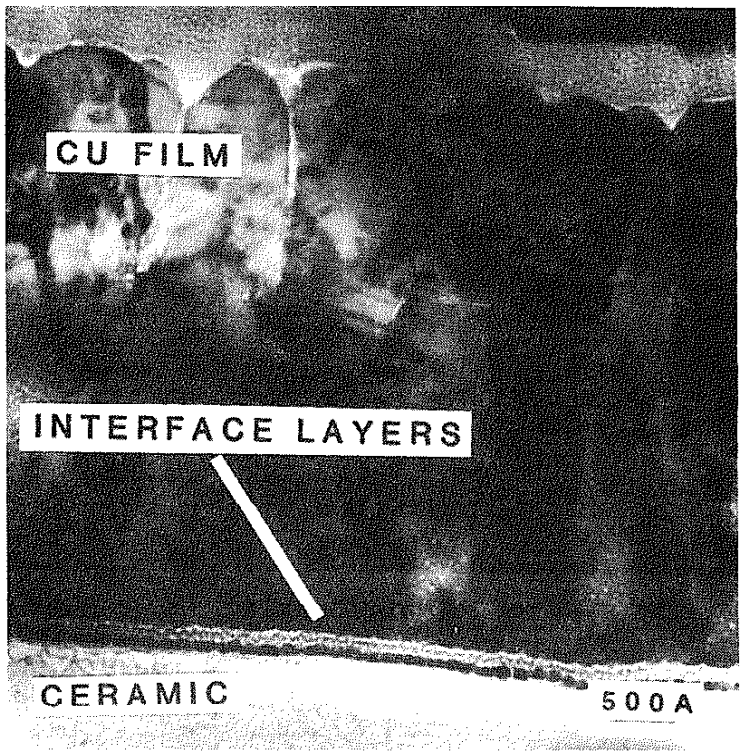

Fig. 31. Cross section bright field TEM micrograph of a 3 kV film deposited at 1.3 Pa. Note the dense columnar boundaries, the fine grained zone in the film near the interface, and the layered interface region.

boundaries or possibly due to "sputter redistribution" of material as suggested by Teer.[119] Boundaries appear open only near the film surface. The columns are extensively twinned, and it is not clear whether they have faceted tops from the cross section, which could imply a zone 2 structure. The coating growth appears to have been somewhat evolutionary since there is a very fine grained, non-columnar structure in the film near the interface, and the dense columns then grow from this region. The interface is characterized by a microcrystalline layered zone which is shown clearly in bright and dark field (see Figs. 31 and 32). Clearly shown in Fig. 32 is a distinct row of diffracting grains along the metal/ceramic junction. Fig. 33 is a typical EDAX spectrum of the cordierite substrate. EDAX analysis with the probe slightly overlapping both film and substrate clearly shows the presence of Ar, Ti, Fe, Mg, Al, Si, and Cu (see Fig. 34). An interesting characteristic of Fig. 34 is the irregular Mg, Al, and Si peak height ratios. They are drastically different from the typical cordierite spectrum, in Fig. 33, indicating significant Al depletion. This possibly is due to formation of a forsterite structure. Forsterite ($2MgO-SiO_2$) was not determined crystallographically here, but the chemistry observed in Fig. 34 suggests its presence. Forsterite could be formed possibly due to Ti rejection of the Al from the cordierite, in cooperation with damage, heating and enhanced mobility due to energetic particle bombardment. The presence of Mg, Al, Si, and Cu spectrum peaks in Fig. 34 are expected. The presence of Ti and Fe is likely due to sputtering of contaminated bolts on the cathode or another region near or on the cathode. The electron beam evapora-

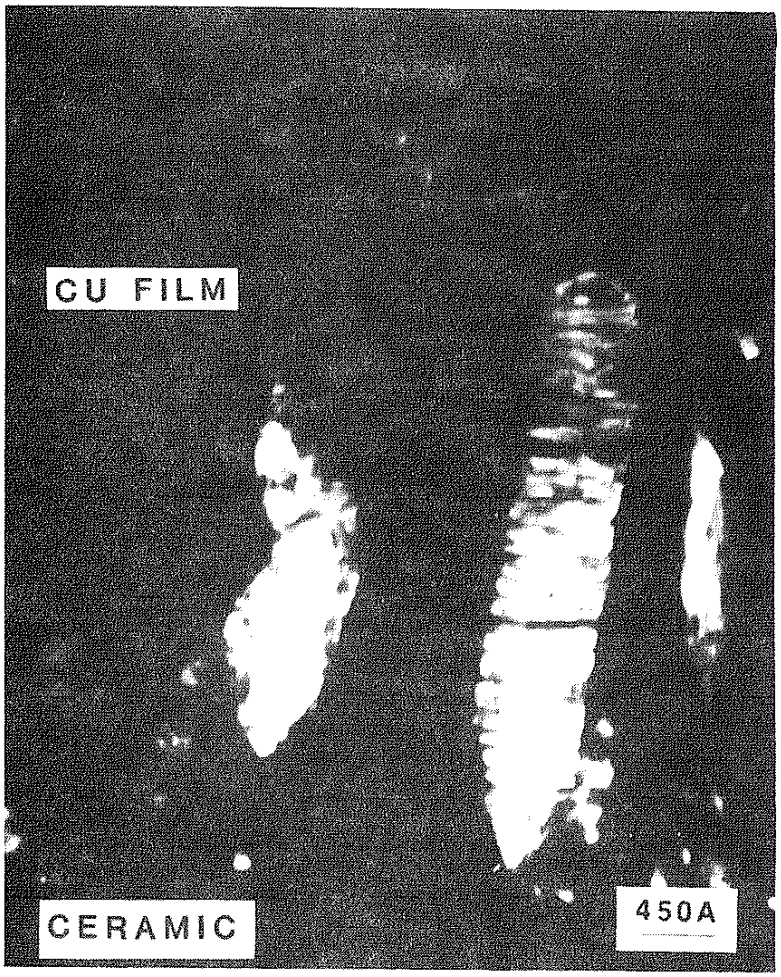

Fig. 32. Cross section dark field TEM micrograph of the 3 kV film. The interface zone is in contrast and clearly crystalline.

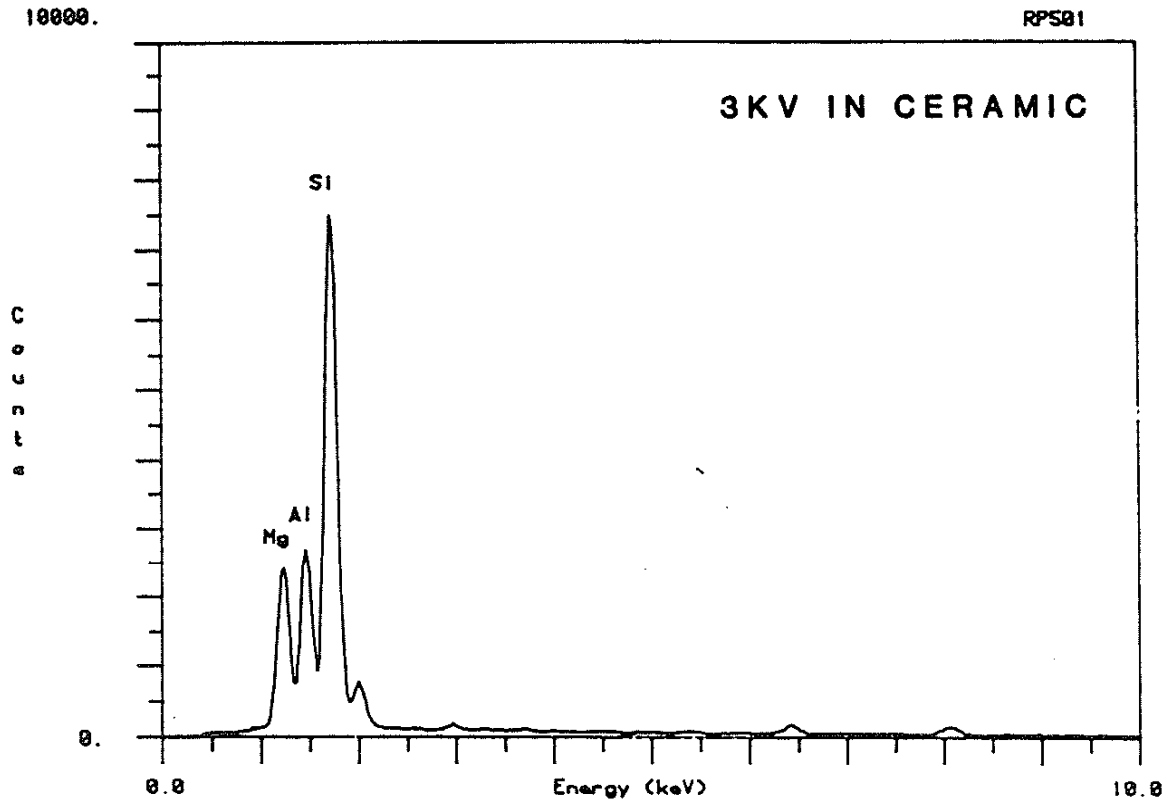

Fig. 33. EDAX spectrum of the cordierite substrate in the 3 kV sample. The Mg, Al, and Si peak height ratios are quite typical for cordierite. P is present in this material as a nucleating agent.

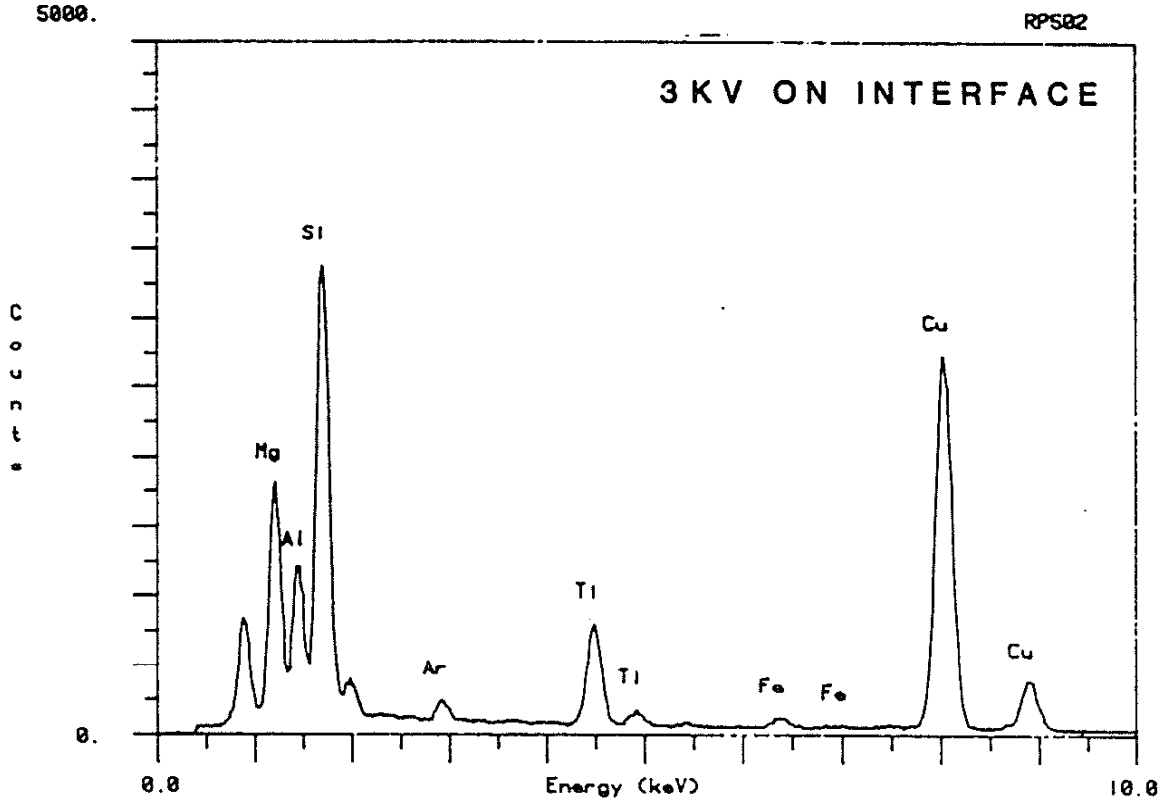

Fig. 34. EDAX spectrum of the interface region in the 3 kV sample. The Mg, Al, and Si peak height ratios are irregular and not characteristic of the matrix composition. Ti and Fe are also present.

tion source is an obvious suspect for contamination, but this film was deposited third following the 0 and 1 kV samples in which no Ti was detected. Contamination may also arise from ion milling due to the transfer of sputtered material, although under this condition it would not be concentrated at the interface. The presence of Ti is further documented in this 3 kV sample by Auger spectroscopy. A broadface portion of the Cu film was etched off using a phosphoric acid etch. A distinctly green layer was present on the surface at this point. Auger point analysis of this layer, following 5 minutes of Ar ion beam sputtering, revealed the presence of Ti, P and other elements (see Fig. 35). P is present likely from the acid etch. The presence of P could also be segregation to a forsterite type phase, if any is present. Similar solution behavior was observed during processing in another cordierite study.[42] The fact that the Ti is observed in both EDAX and AES analysis indicates that it was introduced during the ion plating process. It is possible that the layered zone contains one or more phases formed by reaction with the Ti. Energetic particle bombardment of the ceramic surface during sputter cleaning or the early stage of film growth and/or chemical driving forces appear to have facilitated Al transport from this region of the sample. The Al from the Cordierite could be mixed into the Cu coating but insufficient probe resolution and sensitivity precludes the evaluation of this hypothesis. Examples of the significance of chemical influences in mixing were presented in Section II.C.4.f., which described a relationship between mixing and chemical affinity in metal bi-layers. These results appear to support the conclusion that formation of this stable reaction zone

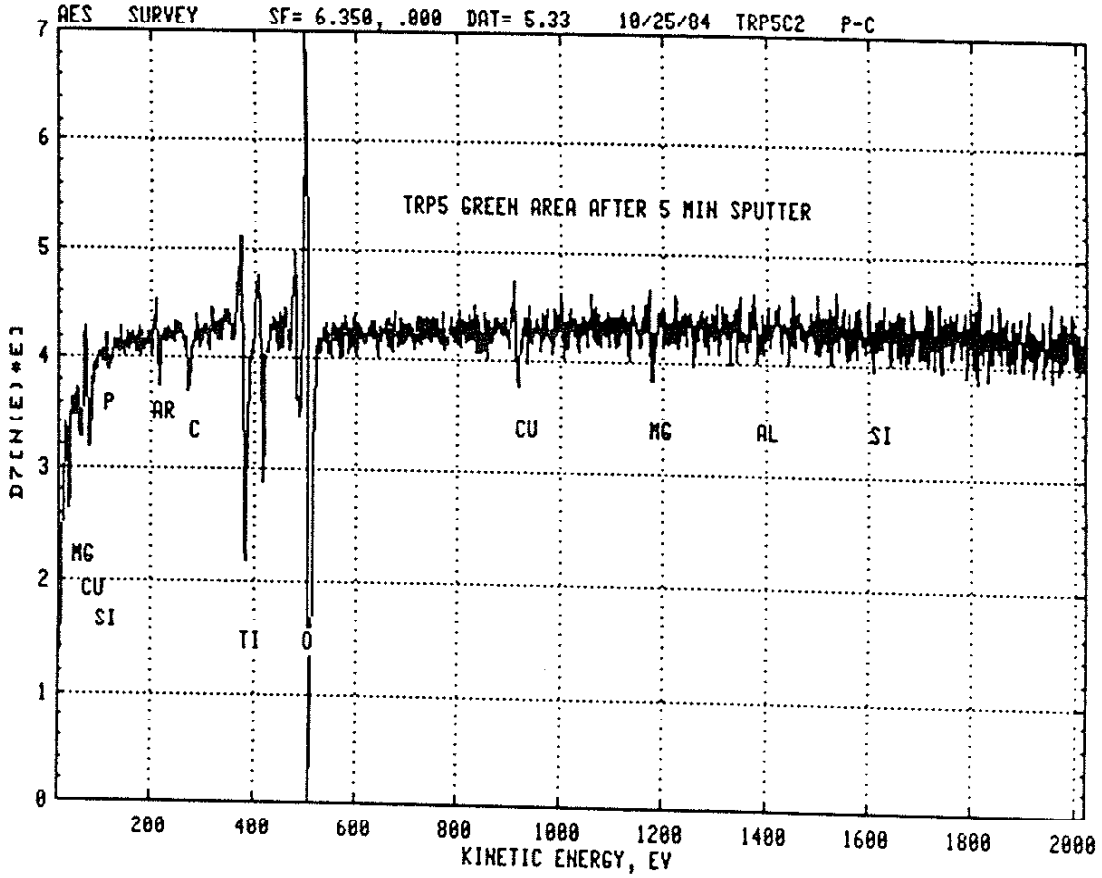

Fig. 35. AES point analysis spectrum of the 3 kV sample surface after the film was etched away. Ti is once again clearly present following 5 minutes of ion beam sputtering in the spectrometer.

plays a critical role in the observed macroscopic mechanical behavior of the interface.

This 3 kV sample brings into question the significance of "sputter cleaning" an insulator with a dc potential. Contamination or adsorbed impurities were evidently either deposited or not removed during the sputter cleaning stage of the ion plating process. It was independently observed that sputter cleaning cordierite using a dc bias often resulted in discoloration of the surface. When a sputter cleaned-only surface was Auger analyzed using the PHI 545, the chemistry revealed was essentially that of stainless steel (see Fig. 36) with Fe, Cr, and Ni evident. Approximately 15 minutes of Xe ion beam sputtering was necessary to profile through the contaminated layer. The bolts holding the sample in position in the plater were 304 stainless steel while the cathode itself was covered with Al foil. It seems likely that the bolts contributed the Fe, Cr, and Ni, while the small Al peak evident in Fig. 36 could be from the cordierite or from contamination by the Al foil backing. The fact that these contaminants were either deposited or not removed from the cordierite surface follows a similar argument given in Section II.B.3. The insulator surface will charge to the floating potential and hence very low energy bombardment will ensue, on the order of 10 eV, representing the difference between space and floating potentials. Even though the energetic particle flux impinging on the cathode is comprised almost entirely of neutrals, the net neutral energy is largely along the electric field lines since the energetic neutrals were ions in the sheath during some interval while traversing the sheath. If sufficient metal is deposited on

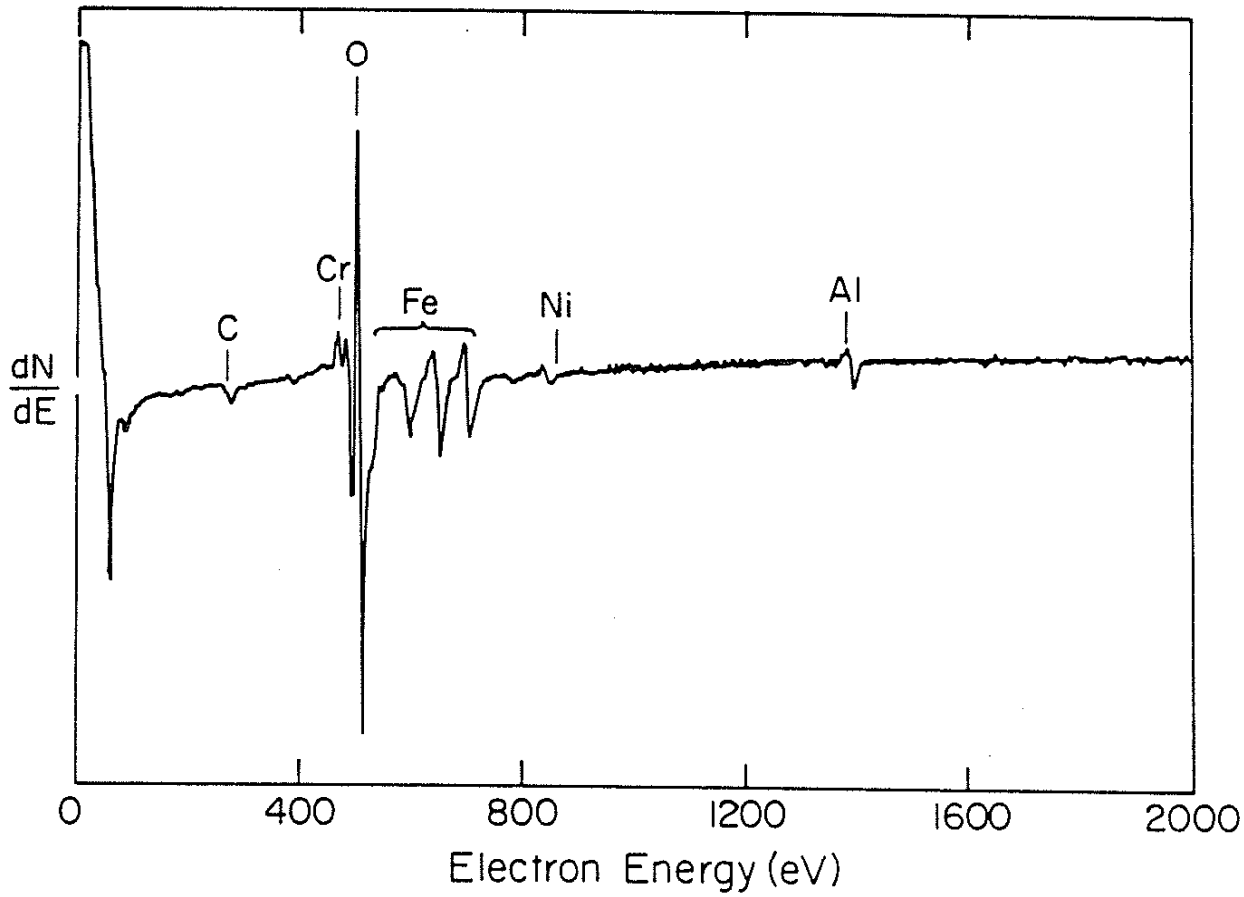

Fig. 36. AES spectrum of a sputtered cleaned cordierite sample. Fe, Cr, Ni, and Al are clearly present.

the ceramic from the nearby cathode fixtures, then a conductive path is formed between the ceramic surface and the cathode and high energy ion bombardment will begin. This would then result in mixing events and sputtering which could once again result in a poor or non-existent conductive path from the ceramic surface to the cathode electrode. The conclusion is then that dc sputtering an insulator is extremely inefficient at best, the net effect of which is to deposit a layer of contamination.

Films deposited onto as-received substrates with a 5 kV applied bias exhibited mixed morphology. A distorted columnar growth with equiaxed grains is clear in these fully dense, 3 micron thick samples (see Fig. 37). The columnar character is clearly shown by the "wavy" column shown in Fig. 37. Equiaxed grains are also observed. Once again the coating is twinned with evidence of a very fine grained structure in the film near the interface, similar to that observed in the 3 kV case. The interface region (see Fig. 38) in this sample is quite prominent. Fig. 38 clearly presents the interface layer which is amorphous and approximately 25 nm thick. The fact that it is amorphous is borne out in dark field mode, while tilting several degrees positive and negative. No diffracting crystals were observed (see Fig. 39). Presumably the layer contains both film and substrate elements (see Fig. 40). EDAX analysis, with the probe overlapping both film and substrate shows both Cu and substrate elements. This layer is a manifestation of the atomic mixing events occurring during the ion plating process. The fact that it is amorphous, and therefore probably quite brittle, supports the adhesion failure mode that was observed. Flaws present near the in-

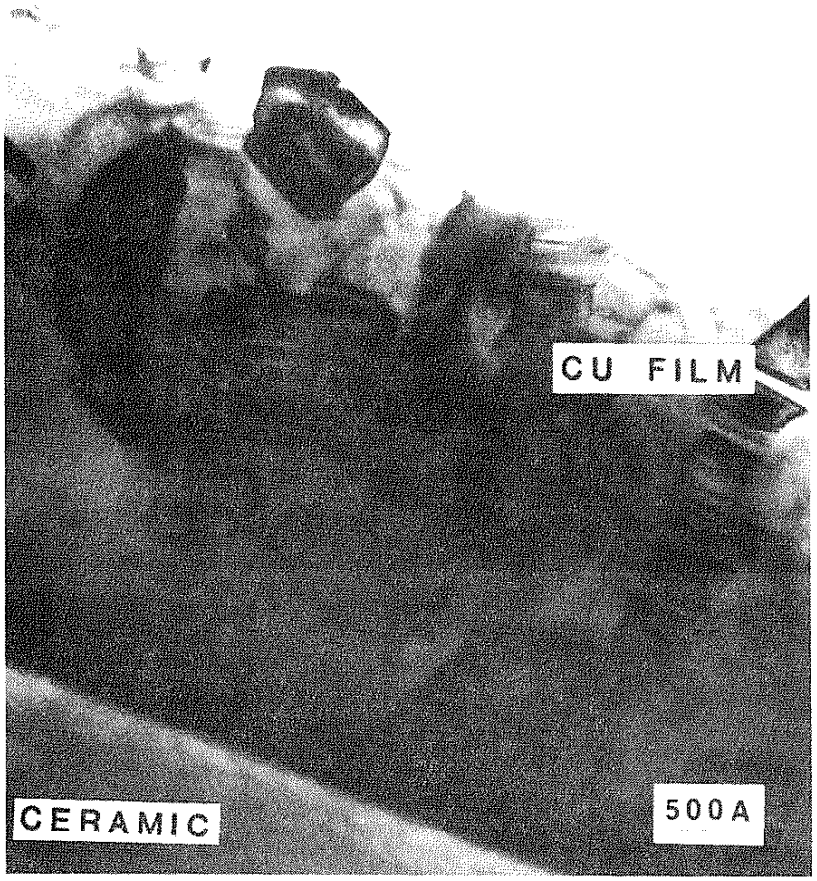

Fig. 37. Cross section bright field TEM micrograph of a Cu film deposited with 5 kV substrate bias. Columnar and equiaxed features are present in this film.

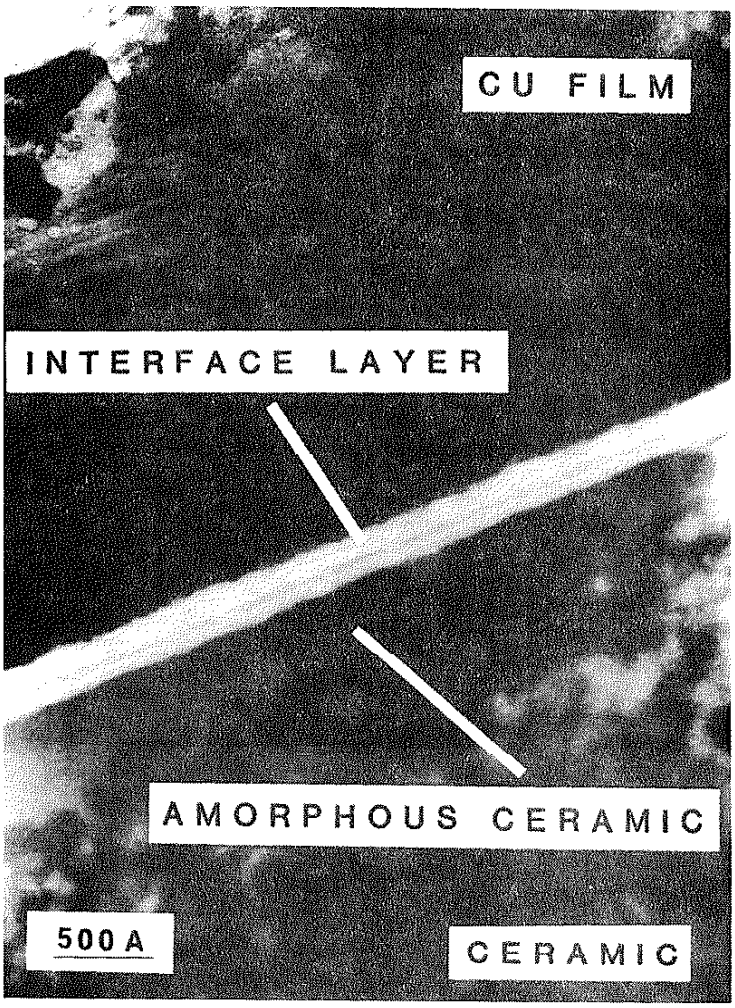

Fig. 38. Cross section bright field TEM micrograph of the 5 kV cu film. The interface layer is prominent and a microcrystalline zone is present in the film near the interface, similar to that observed in the 3 kV film.

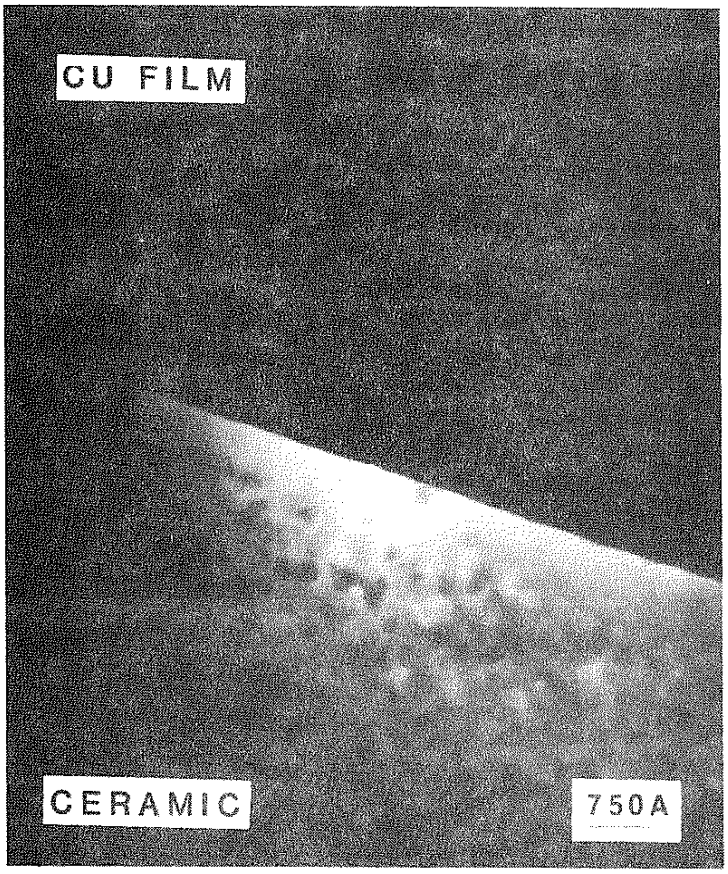

Fig. 39. Cross section dark field TEM micrograph of the 5 kV film. The interface layer is essentially featureless which manifests the amorphous structure.

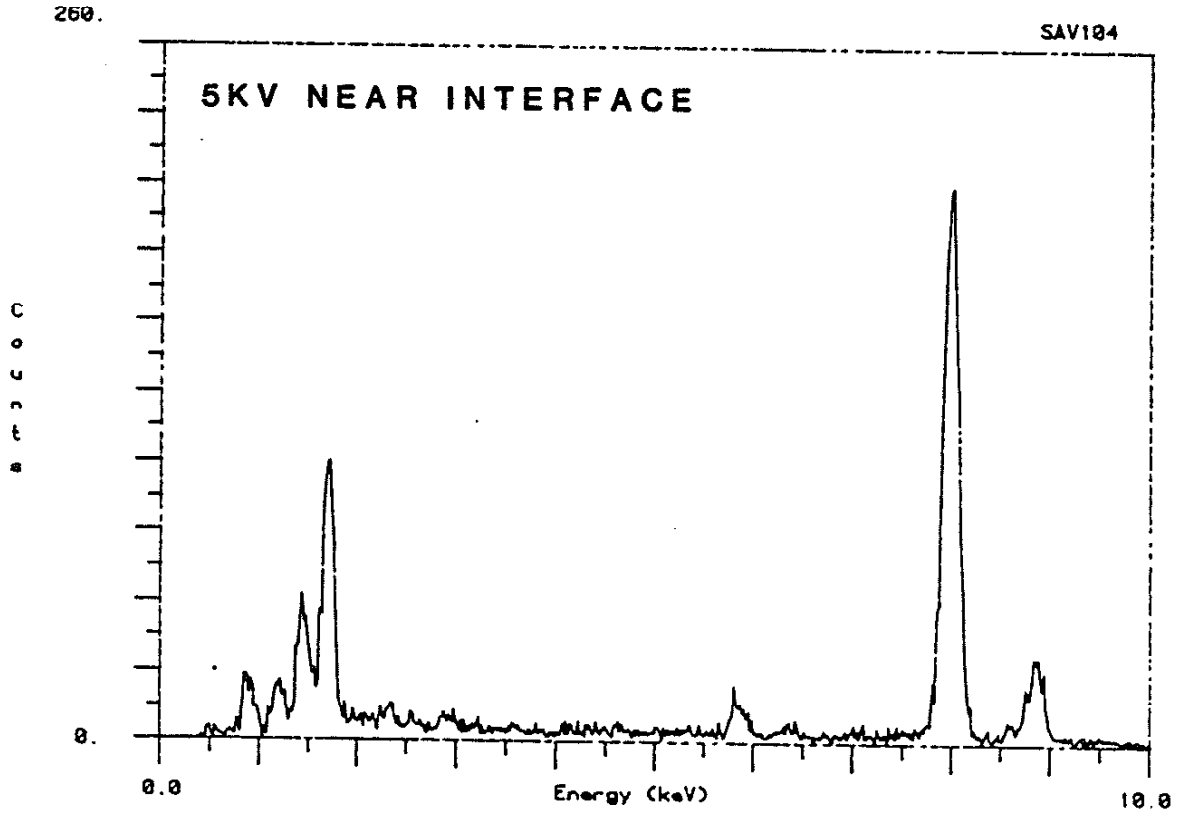

Fig. 40. EDAX spectrum of the interface region in the 5kV sample. Both film and substrate elements are present.

terface could quickly grow into the ceramic upon application of a stress resulting in ceramic fractures like those observed experimentally.

Another effect of the ion plating process is the formation of an amorphous layer in the ceramic near the interface (see Fig. 38). Fig. 38 shows this second amorphous layer at the ceramic surface which is essentially featureless. The thickness of this zone tends to be on the order of 10's of nanometers. It is not clear what causes the zone formation. Two possibilities are suspicious; the first is damage due to collision cascades and the second is radiant heating from the plasma and the incandescent electron beam evaporation source. Collision cascades could be responsible for an amorphous zone on the order of nanometers. This statement is inferred from some of Armour's work[118] which considered a diffusion approximation to cascade mixing (see Section II.D.4.). The heating from the source could account for a larger zone especially in view of the rather poor thermal conduction characteristics of oxide ceramics in general. However, if radiant energy alone were responsible, it would have to be sufficient to heat the cordierite over 1273^{o}K, at least at the surface. A cooperative mechanism may be in effect such that an amorphous layer is nucleated at the surface by cascades followed by "growth" of the zone due to the radiant heating. Such a situation may decrease radiant energy requirements for amorphous zone formation.

IV.D. MICROCHEMICAL INTERFACE ANALYSIS

Auger spectroscopy was employed on a series of very thin Cu

samples deposited with 0, 1, 3, and 5 kV onto cordierite polished down to 0.25 micron diamond paste. The objective of this experiment was to observe a variation in width of the interface by chemical analysis. Intuitively, a 5 kV deposit should have a wider interface than the 0 kV deposit, and this is observed in the TEM micrographs. Using identical sputter profiling conditions with an Xe beam in the PHI 595, these four samples were sequentially sputtered and analyzed. The results are shown in Figs. 41-44. The interface "widths" were compared by placing one profile over a second profile such that the point where the Cu and O peak to peak signals are coincident. A relative estimate is then made by comparing the sputtering time to reach the bulk substrate and bulk film from this reference point. By this method, it is concluded that no significant difference in interface width is observed between various pairs of samples. It is clear, however, from the various TEM micrographs that significant variations in interface width are present. The probable cause for the similarity in interface width is substrate surface topography. If the electron beam probe size is on the order of 1 micron across, and there are several "hills and valleys" of the order of 100's of angstroms in height within a 1 micron region on the surface, then this topography would effectively defeat the proper resolution of the chemically graded interface. Other considerations of depth profiling materials are discussed in the literature.(123)

Another attempt at resolving the metal/ceramic interface involved line profile analysis across the interface in a sample which was mechanically polished at a known angle of 13^{o} (see Fig. 45).

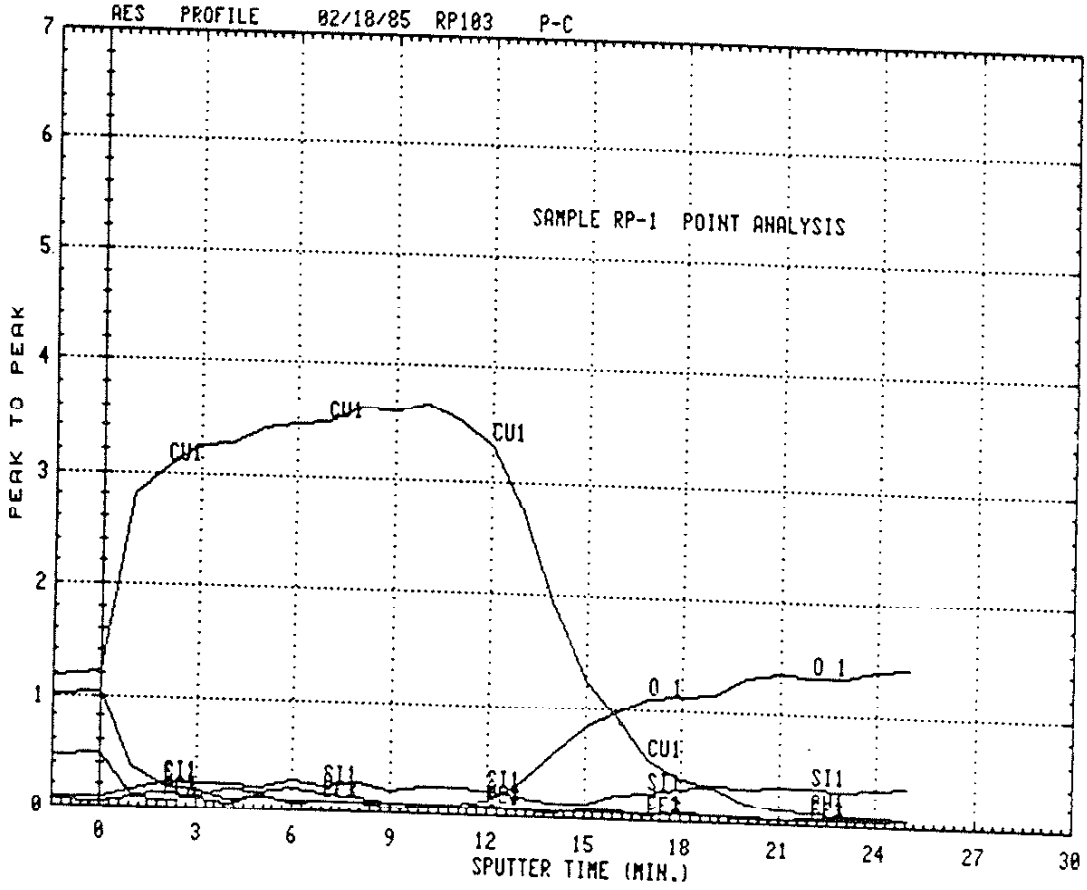

Fig. 41. AES depth profile of a film deposited with sputter cleaning and no bias during evaporation.

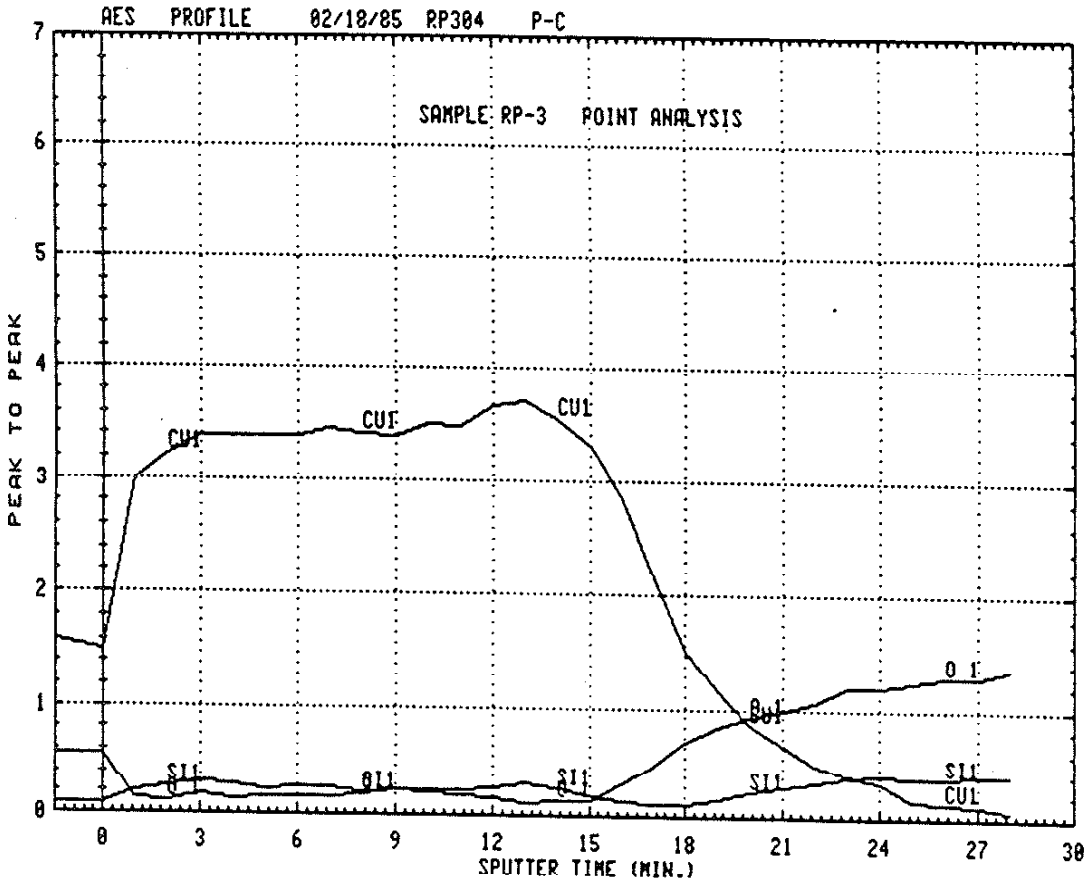

Fig. 42. AES depth profile of a film deposited with sputter cleaning and 1 kV bias during evaporation.

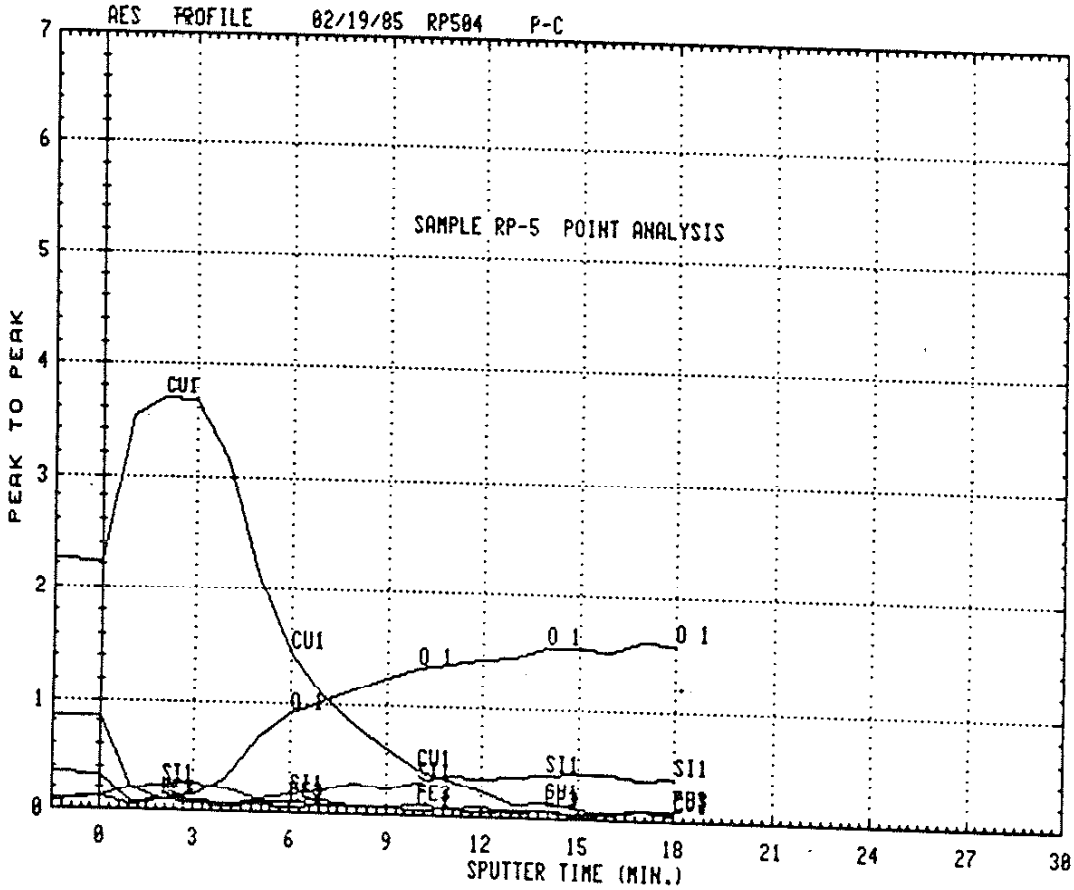

Fig. 43. AES depth profile of a film deposited with sputter cleaning and 3 kV bias during evaporation.

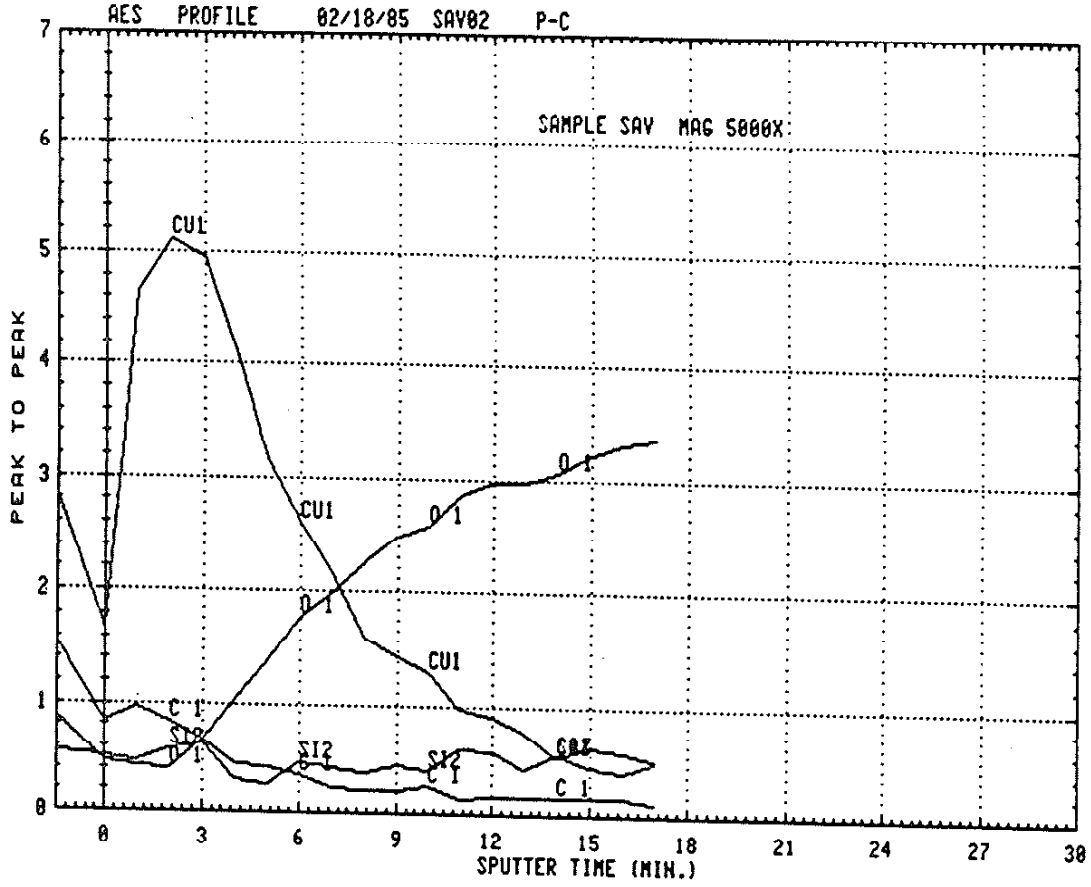

Fig. 44. AES depth profile of a film deposited with sputter cleaning and 5 kV bias during evaporation.

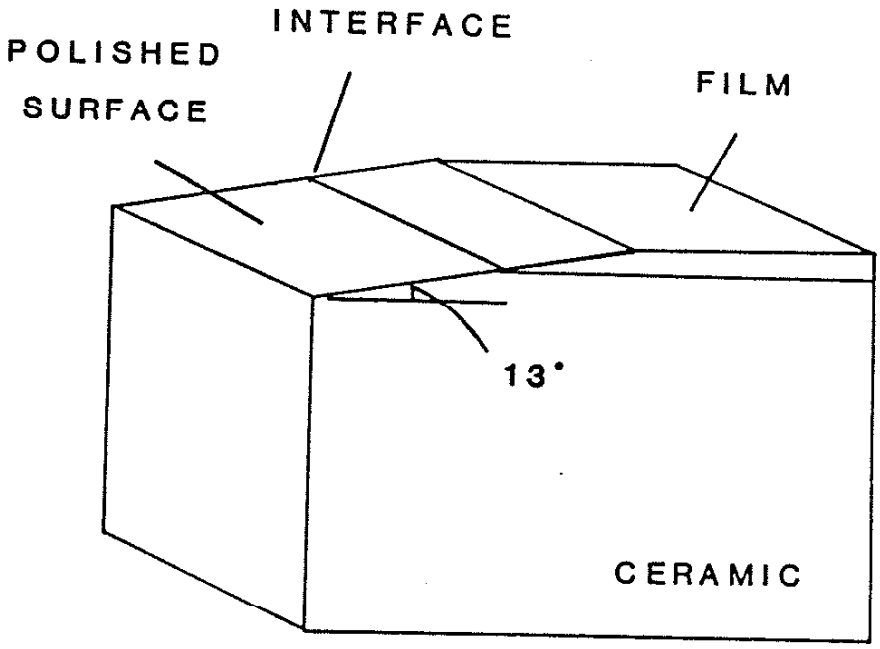

Fig. 45. Schematic of a sample prepared for AES line profile across the metal/ceramic interface.

Problems with the technique involve smearing and tearing of the film. To be successful, a very finely polished section is necessary without grossly distorted regions in the film. This, however, was not achieved as is shown in a low magnification SEM micrograph taken in the 595 (see Fig. 46). The Cu is the lighter colored region in the micrograph, and the ceramic is the darker region. Clearly shown are large patches of ceramic present where the Cu has been torn free of the substrate due to the polishing procedure. A line profile of this region is useless as the probe size is too large.

Secondary ion mass spectroscopy was employed in depth profile mode also with the goal of observing varying interface characteristics with different ion plating process parameters. A typical depth profile is shown in Fig. 47. What was generally determined for these Cu/cordierite samples is that the interface region is rich in oxygen. This is evidenced by the sharp peak for all elements shown in Fig. 47. Quite often an oxygen rich environment will enhance the secondary ion yield of sputtered material. SIMS data are quite difficult to interpret when many elements are present in the sample. The sputter yield of one particular species is influenced by the concentration of the other elements present in the material, the secondary ion yield for the elements varies by as much as 5 orders of magnitude making quantitation difficult, and spectral interferences as from hydride formation and other effects[124] further complicate the scenario. Charging is observed in this spectrum as the ion current for each species rapidly drops off upon interface penetration. This is due to deflection of the incident ion beam such

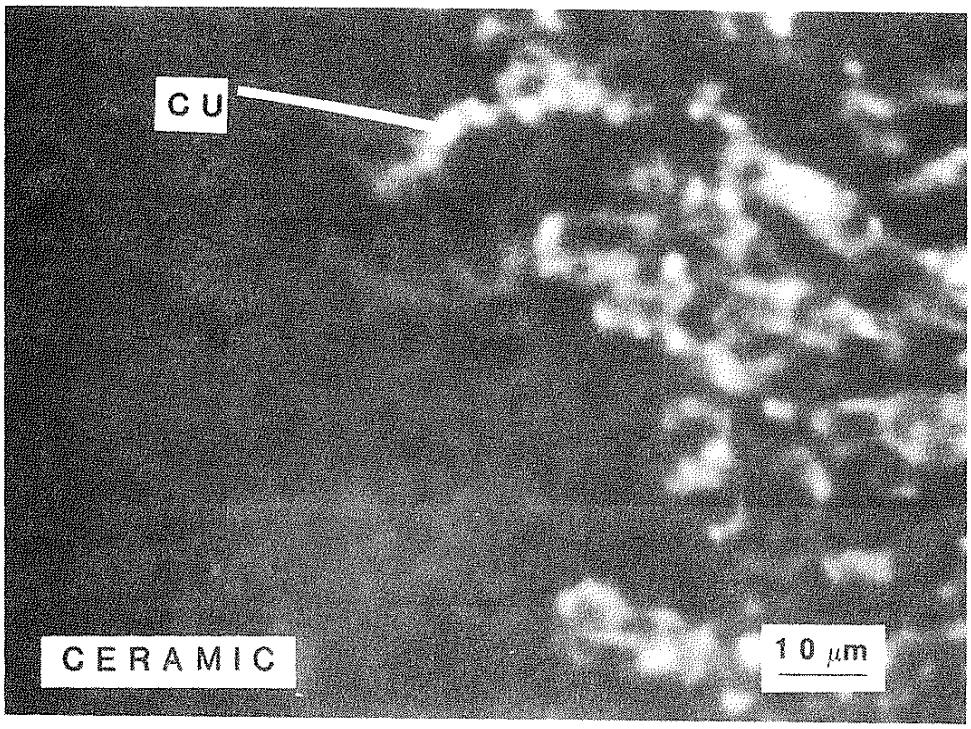

Fig. 46. SEM micrograph of the polished metal/ceramic transition shown in Fig. 45. Large patches of Cu have torn free exposing the ceramic.

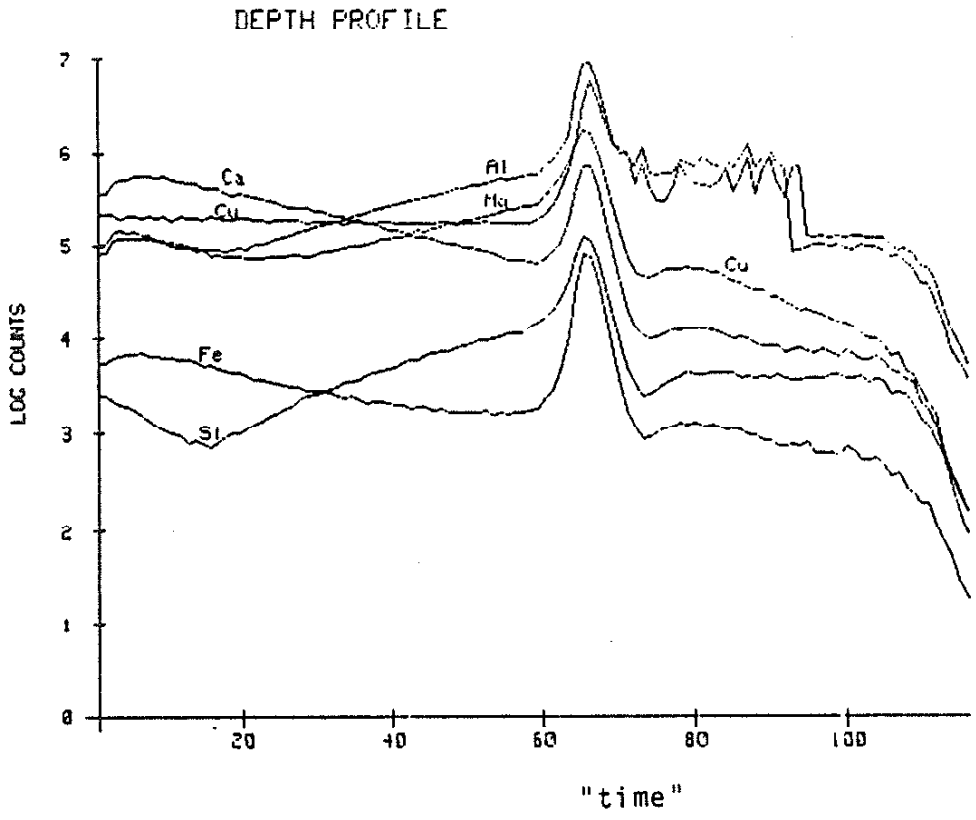

Fig. 47. Depth profile using secondary ion mass spectroscopy (SIMS) of a Cu film deposited with 3 kV applied substrate bias.

that it is no longer in proper alignment with the ion optical system. An electron flood gun on the Cameca may alleviate this problem to some extent.

It was observed during an x-ray diffraction experiment that the cordierite surface becomes discolored by the x-rays. This is likely due to the formation of color centers, charged vacancies, in the ceramic.[125] To determine if large amounts of Mg, Al, or Si were being removed from the ceramic, a sample was analyzed in the 595. The spectrum was not significantly different from a more typical piece of cordierite. The x-ray beam probably displaces atoms up to several microns deep in the ceramic while AES probes the top 3 nanometers or so of the sample. The situation is further complicated by the fact that the electron beam may be causing substantial heating, atomic migration, and damage to the cordierite. Some studies of electron beam effects are available in the literature.[126] Depth profiling of bare cordierite in the 595 is not feasible due to charging effects. Charging causes the electron beam impingement area to shift position, thus effectively misaligning the sample with respect to the Auger electron cylindrical mirror analyzer.

V. SUMMARY AND CONCLUSIONS

This research has investigated the mechanical and microstructural properties of the ion plated Cu/cordierite interface. Several conclusions have been determined as a result of this work:

1) Increasing the mean impinging particle energy via applied substrate bias results in a shift in film morphology from open boundary columnar growth at low voltages to a fully dense equiaxed/columnar structure at 5 kV. This could be due to increased adatom mobility, film heating, and high strain energy defects. These events all occur as a result of the energetic particle flux. Mixing of the film and substrate was observed to positively correlate with increasing substrate bias using TEM analysis. This is most clearly manifested in the 5 kV film which has an approximately 250 Å thick, amorphous, interfacial layer. Mixing processes important in the production of this interface layer include recoil events, cascade mixing, and probably the sputter contamination described in the results section. While vacancies are undoubtedly produced in the ceramic, ion-enhanced diffusion is not considered to be particularly important here since diffusion coefficients in ceramics are typically much less than metals. Thus, Cu seems unlikely to diffuse a great distance into the cordierite under these conditions.

2) A definite improvement in Cu/cordierite interface mechanical strength is positively correlated with the appearance

of the chemically mixed interface layers of the 3 and 5 kV samples. Thus, mechanical properties of the interface are enhanced by a mixing of the material, observed in these samples, as well as perhaps chemical bonding of the two materials which seems present in the 3 kV sample. The 5 kV sample, which had an amorphous interface layer, failed by a mode of ceramic fracture; clearly evidenced by macroscopic chunks of the ceramic tearing out upon failure. This is likely due to crack formation near failure initiation sites in the vicinity of the interface layer, which propagate into the substrate upon loading. The 3 kV crystalline interface exhibited no failure, denoting excellent mechanical properties.

3) Fabrication of mechanically stable Cu films on cordierite substrates requires consideration of several variables. The first is the temperature which the component will achieve in processing and in service. It was clearly observed in this study that 5 kV ion plated Cu films failed by complete metal/ceramic interface failure following a short anneal to T = 600 K. There are several possible reasons for this. One is that the amorphous layer transforms to a product in which Cu is neither bonded chemically nor physically mixed. By considering the compounds Cu_2O, MgO, SiO_2, and Al_2O_3, it is observed that Cu has the lowest bond enthalpy of formation. Thus, from a chemical standpoint, Cu should have poor adhesion. From a physically mixed interface layer standpoint, the mixing does not appear extensive as the interface layer is of the order of

only a few hundred angstroms. The components, particular oxygen, may have sufficient mobility at the chosen annealing T to cause separation of the film, as a more thermodynamically stable state is achieved. Careful in-situ hot stage TEM analysis of the interface layer should be performed to monitor the state of the interface during a heat treatment. Ion beam mixed samples (see Appendix C) did not fail following a similar heat treatment. This could be due to a much more extensive interface zone which requires a great deal more diffusion for easy removal of the Cu film. It has been suggested that mixing Cu into the near surface region of the ceramic with high energy particles, followed by depositing a bulk film, is a reasonable process procedure for producing mechanically stable coatings. Many more experiments are required in this area.

VI. REFERENCES

1. Huntsberger, J.R. "Contact Angle, Wettability, and Adhesion", J. Am. Chem. Soc., Advances in Chemistry Series, 43, Chap. 11 (1964).

2. Kinloch, A.J. "The Science of Adhesion", J. Mat. Sci., 15, 2141 (1980).

3. Kingery, W.D.; Bowen, H.K.; and Uhlman, D.R. Introduction to Ceramics, John Wiley and Sons (1976).

4. Murr, L.E. Interfacial Phenomena In Metals and Alloys, Addison Wesley (1975).

5. Adamson, A.W. Physical Chemistry of Surfaces (4th Ed.), John Wiley and Sons (1982).

6. Smith, G.C. and Lea, C. "Wetting and Spreading of Liquid Metals: The Role of Surface Composition", Surface and Interface Analysis, 9, 145 (1986).

7. Nicholas, M.G.; Valentine, T.M.; and Waite, M.J. "The Wetting of Alumina By Copper Alloyed with Ti and Other Elements", J. Mat. Sci., 15, 2197 (1980).

8. Wake, W.C. Adhesion and the Formulation of Adhesives, Chap. 5, Applied Science Publishers (1976).

9. Perrins, L.E. and Pettit, K. "Mechanism for the Adhesion of Electroplated Copper to Polyethylene", Plastics and Polymers, 39 (144), 391 (1971).

10. Evans, J.R.G. and Packham, D.E. "Adhesion of Polyethylene to Copper: Importance of Substrate Topography", J. of Adhesion, 10, 39 (1979).

11. Voyutskii, S.S. Autohesion and Adhesion of High Polymers, Interscience Publishers (1963).

12. Mattox, D.M. "Interface Formation and the Adhesion of Deposited Thin Films", presented to the 1964 Gordon Research Conference on Adhesion and published as Sandia Laboratories Report No. SC-R-65-852, January 1965.

13. Stoddart, C.T.H.; Clark, D.R.; and Robbie, C.J. "On the Mechanism of the Effect of Glow Discharge Treatment of the Substrate on Thin Film Adhesion", Proceedings of the Conference on the Physics of Adhesion, p. 124 (1969).

14. Cole, M.W. and Klein, J.R. "The Interaction Between Noble Gases and The Basal Plane Surface of Graphite", Surface Science, 124, 547 (1963).

15. Papp, H. "The Chemisorption of Carbon Monoxide on a Co (0001) Single Crystal Surface; Studied By LEED, UPS, EELS, AES, and Work Function Measurements", Surface Science, 129, 204 (1983).

16. Diffusion Bonding of Materials, ed. Kazakov, N.F., Pergamon Press (1985).

17. Economos, G. and Kingery, W.D. "Metal-Ceramic Interactions: II. Metal-Oxide Interfacial Reactions at Elevated Temperatures", J. Am. Cer. Soc., 36 (12), 403 (1953).

18. Petzow, G.; Suga, T.; Elssner, G. and Turwitt, M. "Nature and Structure of Metal-Ceramic Interfaces", Sintered Metal-Ceramic Composites, ed. Upadhyaya, G.S., Elsevier (1984).

19. Stuart, R.V. Vacuum Technology, Thin Films, and Sputtering, An Introduction, Academic Press (1983).

20. Glang, R. "Vacuum Evaporation", Handbook of Thin Film Technology, Chap. 1, ed. Maissel, L.E. and Glang, R., McGraw-Hill (1970).

21. Maissel, L.E. "Application of Sputtering to the Deposition of Films", Handbook of Thin Film Technology, Chap. 4, ed. Maissel, L.E. and Glang, R., McGraw-Hill (1970).

22. Buckley, D.H. Surface Effects in Adhesion, Friction, Wear, and Lubrication, Elsevier (1981).

23. De Bruin, H.J.; Moodie, A.F. and Warble, C.E. "Ceramic-Metal Reaction Welding", J. Mat. Sci., 7, 909 (1972).

24. Bailey, F.P. and Black, K.J.T. "Gold to Alumina Solid State Reaction Bonding", J. Mat. Sci, 13, 1045 (1978).

25. Hirose, Y.; Doi, H. and Kamigaito, O. "Thermal Expansion of Hot Pressed Cordierite Glass Ceramics", J. Mat. Sci., Letters, 3, 153 (1984).

26. McMillan, P.W. Glass Ceramics, Academic Press (1979).

27. Pincus, A.G. "Applications of Glass Ceramics", Advances in Nucleation and Crystallization in Glasses, (Symposium of the Glass Division of the American Ceramic Society), p. 210 (1971).

28. Partridge, G. and Elyard, C.A. "Glass Ceramic Bonds to Metals", Proceedings of the British Ceramic Society, 34, 219 (1984).

29. Kleiner, R.M. and Buljan, S.T. in Phase Diagrams: Materials Science and Technology, Academic Press (1978)

30. Buchanon, R.C. Ceramic Materials for Electronics, Marcel Dekker (1986).

31. Evans, D.L.; Fischer, G.R.; Geiger, J.E. and Martin, F.W. "Thermal Expansions and Chemical Modifications of Cordierite", J. Am. Chem. Soc., 63 (11-12), 629 (1980).

32. Karkhanavala, M.D. and Hummel, F.A. "The Polymorphism of Cordierite", J. Am. Cer. Soc., 36 (12), 389 (1953).

33. Smart, R.H. and Glaser, F.P. "Stable Cordierite Solid Solutions in the $MgO-Al_2O_3-SiO_2$ System: Composition, Polymorphism, and Thermal Expansion", Science of Ceramics, 9, (1977).

34. Bragg, L.; Claringbull, G.F. and Taylor, W.H. Crystal Structure of Minerals, Vol. 4, Cornell University Press (1965).

35. Putnis, A. "The Distortion Index in Anhydrous Mg-Cordierite", Contributions to Minerology and Petrology, 74, 135 (1980).

36. De Vekey, R.C. and Jajumder, A.J. "The Effect of Fabrication Variables on the Properties of Cordierite-Based Glass Ceramics. Part 1. The Effect of Variations in Heat Treatment", Glass Technology, 14 (5), 125 (1973).

37. Allen, G.D. "Characterization and Properties of a Copper Containing Magnesium Aluminosilicate", Masters Thesis, Department of Ceramic Engineering, University of Illinois (1985).

38. Thakur, R.L. "Determining the Suitability of Nucleating Agents for Glass Ceramics", Advances in Nucleation and Crystallization in Glasses (Symposium of the Glass Division of the American Chemical Society), p. 166 (1971).

39. Tomozawa, M. "Effects of Oxide Nucleating Agents on Phase Separation of Simple Glass Systems", Advances in Nucleation and Crystallization in Glasses (Symposium of the Glass Division of the American Chemical Society), p. 41 (1971).

40. Plumat, E. "Surface and Bulk Nucleation and Phase Separation in Some Vitreous Systems", Silicates Industrials, 38, 97 (1973).

41. DeVekey, R.C. and Majumdar, A.J. "The Effect of Fabrication Variables on the Properties of Cordierite Based Glass Ceramics. Part 2. The Effect of Composition", Glass Technology, 15 (3), 71 (1974).

42. Poetzinger, J.E. "Analysis of Copper-Ceramic Reactions During Firing", Masters Thesis, Department of Ceramic Engineering, University of Illinois (1984).

43. Kriven, W.H. and Risbud, S.H. "Electron Diffraction of Precipitates at Copper-Cordierite Interfaces", Mat. Let., 3 (12), 471 (1985).

44. Chapman, B. Glow Discharge Processes, John Wiley and Sons (1980).

45. Chen, F.F. "Electric Probes", in Plasma Diagnostic Techniques, ed. Huddlestone, R. H. and Leonard, S.L., Academic Press (1965).

46. Swift, J.D. and Schwar, M.J.R. Electric Probes for Plasma Diagnostics, ILIFFE Books (1971).

47. Chung, P.M.; Talbot, L. and Touryan, K.S.J. Electric Probes in Stationary and Flowing Plasmas: Theory and Applications, Springer-Verlag (1975).

48. Thornton, J.A. "Diagnostic Methods for Sputtering Plasmas", J. Vacuum Sci. and Tech., 15 (2), 188 (1978).

49. Cherrington, B.E. Gaseous Electronics and Gas Lasers, Pergamon Press (1980).

50. Thornton, J.A. "Plasma Assisted Deposition Processes: Theory, Mechanisms and Applications", Thin Solid Films, 107, 3 (1983).

51. Thornton, J.A. in Deposition Technologies for Films and Coatings, Noyes Publications, p. 19 (1982).

52. Thornton, J.A. "The Use of Low Pressure Plasmas in Materials Processing, Part 1 - Fundamental Considerations", AIAA 13th Fluid and Plasma Dynamics Conference, July 14-16 1980.

53. Davis, W.D. and Vanderslice, T.A. "Ion Energies at the Cathode of a Glow Discharge", Phys. Rev., 131 (1), 219 (1963).

54. Armour, D.G.; Valisadeh, H; Solimon, F.A.H. and Carter, G. "The Characteristics of the Ion and Neutral Fluxes Incident on the Substrate in an Ion Plating Discharge", Vacuum, 34 (1-2), 295 (1984).

55. Teer, D.G. "Adhesion of Ion Plated Films and Energies of Deposition", J. of Adhesion, 8, 289 (1977).

56. Hagstrum, H.D. "Low Energy De-excitation and Neutralization Processes Near Surfaces", in Inelastic Ion Surface Collisions, eds. Tolk, N.H.; Tully, J.C.; Heiland, W. and White, C.W., Academic Press (1977).

57. Eisberg, R. and Resnick, R. Quantum Physics of Atoms, Molecules, Solids, Nuclei, and Particles, 2nd ed., John Wiley and Sons (1985).

58. Rossnagel, S.M.; Robinson, R.S. and Kaufman, H.R. "Impact Enhanced Surface Diffusion During Impurity Induced Sputter Cone Formation", Surface Science, 123, 89 (1982).

59. Caville, J.Y. and Dreschler, M. "Surface Self Diffusion By Ion Impact", Surface Science, 75, 342 (1978).

60. Lewis, G.W.; Krikiakides, G.; Carter, G. and Noves, M.J. "Ion Modification of Clean and Contaminated Single Crystal Cu and Si", Surface and Interface Analysis, 4 (4), 141 (1982).

61. Marinov, M. "Effect of Ion Bombardment on the Initial Stages of Thin Film Growth", Thin Solid Films, 46, 267 (1977).

62. Sigmund, P. "Theory of Sputtering. I. Sputtering Yield of Amorphous and Polycrystalline Targets", Phys. Rev., 184 (2), 383 (1969).

63. Greene, J.E. "Epitaxial Crystal Growth By Sputter Deposition: Applications to Semiconductors. Part 1", CRC Critical Rev. in Solid State and Mat. Sci., 11 (1), 43 (1983).

64. Oeschner, H. "Sputtering - A Review of Some Recent Experimental and Theoretical Aspects", Appl. Phys., 8, 185 (1975).

65. Townshend, P. in Ion Implantation, Sputtering, and Their Applications, Chap. 6, Academic Press (1976).

66. Winters, H.F. "Physical Sputtering: A Discussion of Experiment and Theory", in Radiation Effects on Solid Surfaces, ed. Gould, R.F., American Chemical Society (1976).

67. Sigmund, P. "Sputtering Processes: Collision Cascades and Spikes", in Inelastic Ion Surface Collisions, ed., Tolk, N.H.; Tully, C.; Heiland, W. and White, C.W., Academic Press (1977).

68. Greene, J.E. and Barnett, S.A. "Ion Surface Interactions During Vapor Phase Crystal Growth By Sputtering, MBE, and Plasma Enhanced CVD: Applications to Semiconductors", J. Vacuum Sci. and Tech., 21 (2), 265 (1982).

69. Vossen, J.L. and Cuomo, J.J. Thin Film Processes, Sec. 1, Chap. 2, p. 11, Academic Press (1978).

70. Wiedersich, H. "Kinetic Processes During Ion Bombardment", Nuclear Instruments and Methods in Physics Research, B7/8, 1 (1985).

71. Carter, G. and Armour, D.G. "The Interaction of Low Energy Ion Beams With Surfaces", Thin Solid Films, 80, 13 (1981).

72. Littmark, U. and Hofer, W.D. "Recoil Mixing In Solids By Energetic Ion Beams", Nuclear Instruments, 168, 329 (1980).

73. Carter, G; Armour, D.G.; Ingram, D.C.; Webb, R. and Newcombe, R. "Diffusion Approximations to Cascade Mixing", Radiation Effects Letters, 43, 233 (1979).

74. Kelly, R. and Sanders, J.B. "On the Role of Recoil Implantation In Altering the Stoichiometry of a Bombarded Solid", Nuclear Instruments and Methods, 132, 335 (1976).

75. Nelson, R.S. "The Theory of Recoil Implantation", Radiation Effects, 2, 47 (1969).

76. Moline, R.A. "Recoil Implantation", Ion Implantation in Semiconductors 1976, eds. Chernow, F; Borders, J.A. and Brice, D.K., Plenum Press (1976).

77. Tsaur, B.Y. "Ion Beam Induced Interface Mixing and Thin Film Reactions", in Proceedings of the Symposium on Thin Film Interfaces and Interactions, Princeton (1980).

78. Poate, J.M. "Ion Beam Modification of Thin Films", Chap. 6 in Treatise on Materials Science and Technology, 24, eds. Tu, K.N. and Rosenberg, R., Academic Press (1982).

79. Campisano, S.V.; Techang, C; Cannavo, S. and Rimini, E. "Energy Dependence of Compound Growth in Au-Al and Cu-Al Bilayer Systems During Beam Mixing", Materials Research Society Symposia Proceedings, 27, 97 (1984).

80. Ghandi, S.K. VLSI Fabrication Principles, Chap. 6, John Wiley and Sons (1983).

81. Shimizu, H.; Ono, M.; Koyama, N. and Ishida, Y. "Sputter Enhanced Diffusion Phenomena in Cu:Ni Alloys at Elevated Temperatures", J. Appl. Phys., 53 (4), 3044 (1982).

82. Eltoukhy, A.H. and Greene J.E. "Diffusion Enhancement Due to Low Energy Ion Bombardment During Sputter Etching and Deposition", J. Appl. Phys., 51 (8), 4444 (1980).

83. Rivaud, L; Ward, I.D.; Eltoukhy, A.H. and Greene, J.E. "Enhanced Diffusion and Precipitation in Cu:In Alloys Due to Low Energy Ion Bombardment", Surface Science, 102, 610 (1981).

84. Kelly, R. and Lam, N.Q. "The Sputtering of Oxides - Part 1: A Survey of the Experimental Results", Proceedings of the Conference on Ion Surface Interaction, Sputtering, and Related Phenomena, p. 37, Gordon and Breach (1973).

85. Kelly, R. "On the Problem of Whether Mass or Chemical Bonding Is More Important - Induced Compositional Changes in Alloys and Oxides", Surface Science, 100, 85 (1980).

86. Kelly, R. "Thermal Effects in Sputtering", Surface Science, 90, 280 (1979).

87. Williams, F.L. and Nason, D. "Binary Alloy Compositions From Bulk Alloy Thermodynamic Data", Surface Science, 45, 377 (1974).

88. Wiedersich, H. and Lam, N.Q. "Theory of Radiation Induced Segregation", in Phase Transformations During Irradiation, ed. Nolfi, F.V., Applied Science Publishers (1983).

89. Rehn, L.E.; Lam, N.Q. and Wiedersich, H. "Modification of Micron Thick Surface Layers Using Kev Ion Energies", Materials Research Society Symposia Proceedings, 27, 37 (1983).

90. Lam, N.Q. and Wiedersich, H. "Modifications of Subsurface Alloy Composition During High Temperature Sputtering", J. Nuc. Mat., 103/104, 433 (1981).

91. Cauvin, R. and Martin, G. "Radiation Induced Homogeneous Precipitation In Undersaturated Solid Solutions", J. Nuc. Mat., 83, 67 (1979).

92. d'Heurle, F; Baglin, J.E. and Clark, G.J. "Correlation Between Chemistry and the Amount of Mixing in Bilayers Submitted to Ion Bombardment", J. Appl. Phys., 57, 1426 (1985).

93. Tan, T.A.N.; Azizan, M.; Cinti, R.C. and Chauvet, G. "Interfaces Formed By Evaporation of Si on Ni and Mo Surfaces", Surface Science, 162, 651 (1985).

94. Shawki, G.S.A.; ElOShirbiny, M.G. and Salem, F.B. "Nucleation and Interface Formation in Thin Films", Thin Solid Films, 75, 29 (1981).

95. Babaev, V.O.; Bykov, J.V. and Guseva, M.B. "Effect of Ion Irradiation on the Formation, Structure, and Properties of Thin Metal Films:, Thin Solid Films, 38, 1 (1976).

96. Stroud, P.T. "Preferential Deposition of Silver Induced By Low Energy Gold Ion Implantation", Thin Solid Films, 9, 273 (1972).

97. Pilyankevich, A.N.; Kulykovski, V.Y. and Shaginyan, L.R. "The Influence of Ion Bombardment on the Structure of Ion Plated Indium Films:, Thin Solid Films, 137, 215 (1986).

98. Carter, G; Nobes, M.J.; Lewis, G.W. and Whitton, J.L. "The Kinetics and Energetics of Sputtering Induced Topography on Solids", Radiation Effects Letters, 50, 97 (1980).

99. Kelly, R. and Auciello, O. "On the Origins of Pyramids and Cones on Ion Bombarded Cu Surfaces", Surface Science, 100, 135 (1980).

100. Nelson, R.S.; and Mazey D.J. "Surface Damage and Topography Changes Produced During Sputtering", Proceedings of the Con-

ference on Ion Surface Interaction, Sputtering, and Related Phenomena, p. 199, Gordon and Breach (1973).

101. Movchan, B.A. and Demchishin, A.V. "Study of the Structure and Properties of Thick Vacuum Condensates of Ni, Ti, W, Al_2O_3, and ZrO_2", The Physics of Metals and Metallography, 28 (4), 83 (1969).

102. Thornton, J.A. "High Rate Thick Film Growth", Ann. Rev. of Mat. Sci., 7, 239 (1977).

103. Messier, R.; Giri, A.P. and Roy, R.A. "Revised Structure Zone Model for Thin Film Physical Structure", J. Vacuum Sci. and Tech., A2 (2), 500 (1984).

104. Bunshah, R.F. Deposition Technologies For Films and Coatings, Chap. 4, Noyes Publications (1982).

105. Hertz, H. Ann. Physik. Z., 17, 177 (1882).

106. Knudsen, M. Ann. Physik. Z, 47, 697 (1915).

107. Airco Temescal, Instruction Manual #0101-8011-3 (1979).

108. Beale, H.A.; Weiler, F. and Bunshah, R.F. "Evaporation Variables in Gas Scattering Plating Processes", in Proceedings of the Fourth International Conference on Vacuum Metallurgy, p. 238, Iron and Steel Institute of Japan (1974).

109. Bauer, R.W.; Schwartzman, A. M. and Antonio, C.P. "The Structure of Vapor Deposited Cu", Thin Solid Films, 2, 539 (1968).

110. Belous, M.V. and Wayman, C.M. "Temperature Changes in Thin Metal Films During Vapor Deposition", J. Appl. Phys., 38, 5119 (1967).

111. Thornton, J.A. "Coating Deposition By Sputtering", in Deposition Technologies For Films and Coatings, ed. R.F. Bunshah, Noyes Publications (1982).

112. Thornton, J.A. "High Rate Sputtering Techniques", Thin Solid Films, 80, 1 (1980).

113. Thornton, J.A. "The Influence of Bias Sputter Parameters on Thick Cu Coatings Deposited Using a Hollow Cathode", Thin Solid Films, 40, 335 (1977).

114. Craig, S. and Harding, G.L. "Effects of Ar Pressure and Sputtering Temperature on the Structure and Properties of Sputtered Cu Coatings", J. Vacuum Sci. and Tech., 10 (1), 47 (1973).

115. Mattox, D.M. "Fundamentals of Ion Plating", J. Vacuum Sci. and Tech., 10 (1), 47 (1973).

116. Nelson, R.S. "Ion Plating-Atomic Processes Occurring Within the Surface Layers", in IPAT, 77, 32 (1977).

117. Nelson, R.S. "Ion Implantation", Chap. 3, North Holland Publishing (1973).

118. Armour, D.G.; Carter, G.; Webb, R.P.; Ingram, D.C. and Newcombe, R. "Interface Broadening During Ion Plating", Radiation Effects Letters, 50, 45 (1980).

119. Teer, D.G. and Delcea, B.L. "Grain Structure of Ion Plated Coatings", Thin Solid Films, 54, 295 (1978).

120. Miyoshi, K.; Spalvins, T. and Buckley, D.H. "Tribological Characteristics of Gold Films Deposited on Metals By Ion Plating and Vapor Deposition", Wear, 108, 169 (1986).

121. Leet, D.M. "Microstructure and Interface Studies of Evaporated and Ion Plated Titanium Coatings", Masters Thesis, Department of Metallurgy and Mining, University of Illinois (1985).

122. Necombe, S.B.; Boothroyd, C.B. and Stobbs, W.M. "Specimen Preparation Methods For the Examination of Surfaces and Interfaces in the Transmission Electron Microscope", J. Electron Microscopy, 140 (2), 195 (1985).

123. Holloway, P.H. and Bhattacharya, R.S., "Limitations of Ion Etching For Interface Analusis", Surface and Interface Analysis, 3, 118 (1981).

124. Colby, B.N. and Evans, C.A., Jr., "Spectral Interferences In Secondary Ion Mass Spectrometry", J. Appl Spectroscopy, 27 (4), 274 (1973).

125. Copperthwaite, R.G. "The Study of Radiation-Induced Chemical Damage At Solid Surfaces Using Photoelectron Spectroscopy: A Review", Surface and Interface Analysis, 2, 17 (1980).

126. Pignatel, G.U. and Queirolo, G. "Electron and Ion Beam Effects In Auger Electron Spectroscopy On Insulating Materials", Radiation Effects, 79, 291, (1983).

127. Mittal, K.L. "Adhesion Measurement: Recent Progress, Unsolved Problems, and Prospects", Adhesion Measurement of Thin Films, Thick Films, and Bulk Coatings, ASTM STP 640, ed. Mittal, K.L., American Society for Testing and Materials (1978).

128. Campbell, D.S. "Mechanical Properties of Thin Films", Handbook of Thin Film Technology, ed. Maissel, L.E. and Gland, R., McGraw-Hill Chap. 12 (1970).

129. Mittal, K.L. "Adhesion Measurement of Thin Films", Electrocomponent Science and Technology, 3, 21 (1976).

130. Jacobsson, R. "Measurement of the Adhesion of Thin Films", Thin Solid Films, 34, 191 (1976).

131. Hobbs, L.W. "Radiation Damage in Electron Microscopy of Inorganic Solids", Ultramicroscopy, 3 381 (1979).

VII. APPENDIX

This appendix represents some relevant topics of discussion to this thesis as well as additional experiments to be followed up. The results in Section VII.C. are referenced in the conclusions.

VII.A. ADHESION TESTING

Many methods have been devised for measurement of the "adhesion" of films on substrates.[127,128] These include the peel test, topple test, ultracentrifugal test, and direct pull off test.[129] These tests are all mechanical in nature. Mittal[129] divides the term adhesion into three categories: basic, thermodynamic, and experimental. Basic adhesion refers to specific adhesion forces such as Van der Waals. Practically speaking, it is quite difficult to measure these. Thermodynamic adhesion refers to the Dupree equation (see equation (2)). This is not useful for the practical case of thin films as the various parameters are unknown. Practical adhesion may be defined as the maximum force per unit area to separate two bodies or as the energy expended in separating two bodies. Mittal[129] relates bond strength to basic adhesion by the expression:

Bond Strength = f(basic adhesion, other extraneous factors)

Other factors influencing adhesion results include internal stresses in the film substrate system and the particular test technique used.

The pull test technique[130] used in this study of the Cu/cordierite system yields data in the form of force per unit area. Mittal[129] sites several problems with this technique which include:

1) a mixture of tensile and shear forces at the interface;

2) nonuniform loading across the interface;

3) limited strength of the epoxy or other adhesive;

4) possibility of this adhesive penetrating the film and contaminating the interface; and

5) introduction of stresses during glue curing.

With all these limitations it is clear that qualitative results are the best that the pull test may offer, even though quantitative data are produced. In defense of the pull test, it is not clear that any of the other test approaches would be more quantitative for this study.

VII.B. CORDIERITE AMORPHOUS TRANSFORMATION

It has been observed on numerous occasions that the cordierite transforms from a crystalline to an amorphous state during analysis in the TEM. The time interval for complete transformation of an electron irradiated zone is on the scale of minutes. Figs. 48a and 48b are time lapsed micrographs showing the growth of amorphous zones. Hobbs[131] indicates that amrophous transformations in quartz and related silicate structures are possible through severing of Si-O bonds. The transformation for these materials under electron irradiation conditions is known as metamictization. This is a radiolysis process, which is the permanent re-arrangement of

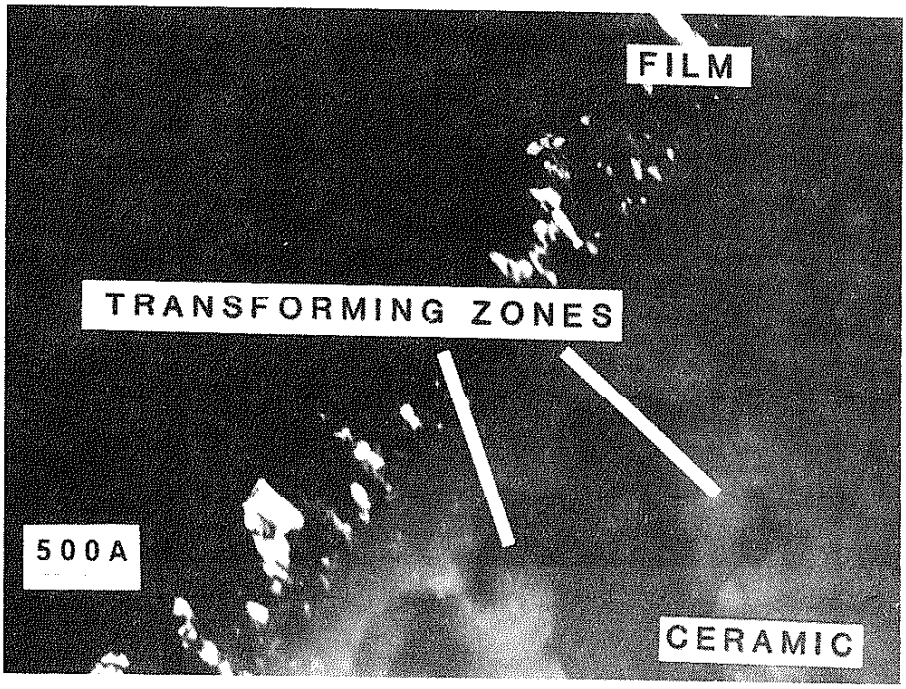

Fig. 48a. Dark field TEM micrograph of cordierite showing circular amorphous zones. First of 3 in time lapsed series.

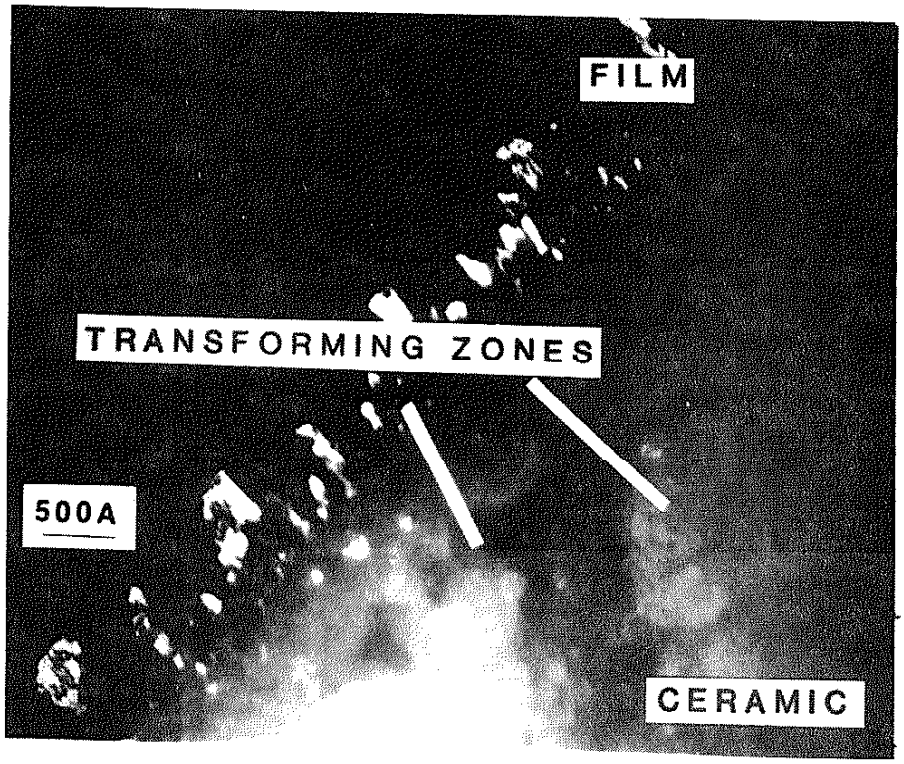

Fig. 48b. Dark field TEM micrograph of the same area in Fig. 47a a few seconds later. The amorphous zones are larger. Third of 3.

atomic nuclei due to localized excited electronic states in an insulator or semiconductor associated with bonding instabilities.[131] Direct displacement of atoms due to electron-nucleus collisions is also possible in these systems. Radiolysis processes occur also in polar crystals.[125,131]

VII.C. ION BEAM MIXING OF THE CU/CORDIERITE SYSTEM

This portion of the interfacial studies was initiated as an alternative to the ion plating process for producing stable, strong interfaces. In some applications where thermal cycling of a part is required, the mechanical strength of the interface may be degraded. This is clearly observed by the adhesion test results following an inert or reducing atmosphere heat treatment.

Ion beam mixing of a film on a substrate generally involves depositing the film onto the substrate in some fashion, evaporation for example, followed by radiating the film surface with high energy massive ions. Massive and high energy are somewhat subjective terms though the incident ion should be massive enough to efficiently transfer energy to the lattice atoms of the Cu film and of sufficient energy to pass through the film and into the substrate. This would effectively mix the film and substrate atoms near the interface region.

Very thin films of Cu (< 1000 Å) which have been ion beam mixed with Kr^+ ions at various energies exhibit good mechanical integrity in the as-implanted condition (see Table 4). Ion beam processed samples retained significant mechanical integrity following intert and reducing gas heat treatment. The ion beam mixed

TABLE 4

Adhesion Failure Stress Values
of Ion Beam Mixed Cu/Cordierite (MPa)

Dose of 100 keV Kr^+ ($ions/cm^2$)	Polished	H_2 Heat Treated
1×10^{13}	47.0 27.8	38.1 ± 17.7
5×10^{13}	60 (60%)*	67.9 (80%)*
1×10^{14}	30.1 (60%)*	30.1 (60%)*

*The percentage indicates the percentage of test specimens which did not fail at the maximum applied stress of the test device, 73 MPa.

failure stresses may be contrasted with the ion plated samples with a short anneal in a reducing gas atmosphere. Table 4 clearly shows that the ion beam mixed samples retain interfacial strength while the ion plated samples are severely degraded (Table 3, Section IV.B.). This is likely due to a more extensively mixed interface region in the ion beam mixed case. Thus, more extensive diffusional processes would be required to cause interface degradation. From a manufacturing standpoint, it may serve the process procedure well to first ion beam mix thin Cu layers on cordierite followed by depositing thicker layers via sputtering or ion plating techniques. The subsequent thicker film would probably bond well to the 'Cu stabilized' surface region in the ceramic, proving to be a feasible scenario for manufacturing considerations.

VII.D. X-RAY PHOTOELECTRON SPECTROSCOPY OF CU ON CORDIERITE

X-ray photoelectron spectroscopy (XPS) is a surface sensitive analytical technique. It is quite useful due to its ability to detect shifts in electron energy spectra which give an indication of the chemical binding state of near surface species. This portion of the investigation of the Cu/cordierite bond is still in a preliminary state.

The initial section of this study will determine if a chemical shift of some type is noted between evaporated films, which have poor adhesion, and films deposited with 5 kV, which have relatively good adhesion. This will be carried out for thin films deposited in the CERL ion plating system. Assuming that a shift is detected, an in-depth follow up study will be initiated that involves evaporating thin layers of Cu in a UHV chamber that may be attached to

the XPS system. An evaporator has already been constructed which will facilitate this experiment. Another topic to be investigated early on in this part of the project is any form of sample degradation which results due to exposure from an x-ray beam. As noted in Section IV.D., x-rays tend to produce a discoloration of the ceramic surface. Presumeably this is due to color center formation.